Parameter Estimation of a Computational Cardiovascular Model Using Echocardiographic Data – Investigating the Changes Associated with Age

Master's Thesis

Submitted in partial fulfillment of the requirements for the degree
M.Sc. Mechanical Engineering
at the Department of Mechanical Engineering of the Technical University of Munich.

Supervised by	Prof. Dr.-Ing. Steffen Marburg
	Chair of Vibroacoustics of Vehicles and Machines
Submitted by	Janina Datz
	Student ID: 03647056
Submitted on	Munich, 28 February 2020

Declaration

Hereby I confirm that this is my own work and I referenced all sources and auxiliary means used and acknowledged any help that I have received from others as appropriate.

Garching bei München, 28 February 2020, Signature

Abstract

Healthcare strives more and more towards personalized medicine. Since knowledge about biomedical processes in the human body advances, as well as imaging technologies get more precise and versatile, opportunities for patient-specific diagnostics arise. With CircAdapt, this biomedical knowledge has been transformed into a realistic, closed-loop computational cardiovascular model. A recent echocardiographic study has collected data from a large cohort of healthy, adult subjects of different age, sex, nationality and ethnicity. This work aims to take a step towards the creation of a personalized simulation model based on a parameter estimation to population-specific data from this study. The focus lies on defined age groups in order to assess changes in the cardiovascular system due to age. The developed framework shall adapt to echocardiographic data and hence provide a model, which could in future be used for clinical health assessments and causative explanations of diseases like heart failure.

Keywords Biomedical Modeling; Cardiovascular; Echocardiography; Precision Diagnosis; Parameter Calibration

Acknowledgements

Herewith I wish to acknowledge those who were involved and provided support throughout this thesis project. Firstly, I would like to thank the Clinical Innovations department of TOMTEC Imaging Systems for welcoming me as a part of the team during my thesis project: Georg Schummers, who provided valuable supervision and assistance throughout the whole project, Marcus Schreckenberg, with whom I had regular discussions helpful for the targeted direction of the study, as well as everyone being involved in the editing of data. Secondly, I wish to express my deepest gratitude to the team of Maastricht University, Tim van Loon and Joost Lumens, for providing incredible support on the CircAdapt model and helping me with all questions about the physiologic correlations. They also welcomed me warmly at their department in the Netherlands in order to discuss things in person. I also would like to pay special regards to Professor Steffen Marburg and Marcus Mäder, who provided supervision on the university-side, enabling me to do this thesis project. The latter provided me with precious support regarding the underlying maths and scientific writing. I am indebted to my proofreaders Tobias Frey and Alexandra Datz for their effort in giving me helpful recommendations. Lastly, to my family and friends for keeping me motivated and especially to Lukas Steigerwald for many encouraging words, thank you!

Contents

List of Figures

List of Tables

List of Abbreviations

ASE	American Society of Echocardiography
AV	Aortic valve
BSA	Body surface area
CO	Cardiac output
CT	Computer tomography
EACVI	European Association of Cardiovascular Imaging
ECG	Electrocardiogram
EDV, ESV	End-diastolic, end-systolic volume
EF	Ejection fraction
ET	Ejection time
HR	Heart rate
IVCT, IVRT	Isovolumetric contraction, relaxation time
IVS	Intervenricular septum
LA, RA	Left and right atrium/atrial
LV, RV	Left and right ventricle/ventricular
LVOT	Left ventricular outflow tract
MAP	Mean arterial pressure
MPI	Myocardial performance index
MRI	Magnetic resonance imaging
MSRS	Metric stochastic response surface
MV	Mitral valve
P	Patient structure array
PCWP	Pulmonary capillary wedge pressure
RBF	Radial basis function
SV	Stroke volume
SBP, DBP	Systolic, diastolic blood pressure
TTE	Transthoracic echocardiogram
TV	Tricuspid valve
VTI	Velocity time integral
WASE	World Alliance of Societies of Echocardiography Normal Values

List of Symbols

Symbol	Unit	Definition
c_h	m/s	Velocity of sound in human tissue
C		Contractility
ch_i		Curve characteristics
$d(\mathbf{x})$		Function value of adaptive samples
e_i		Error value of i
e_{tot}		Total error
f_0	Hz	Transmitted ultrasound transducer frequency
F_d	Hz	Frequency shift at ultrasound transducer
f_{merit}		Merit function of surrogate
k		Vascular stiffness parameter
L_{si}	μm	Sarcomere length
N_i		Number of fitting values, model parameter or function evaluations
p	Pa	Pressure
p_0	Pa	Mean arterial pressure
ϕ	rad	Angle of ultrasound beam
q	ml/s	Blood flow velocity
q_0	ml/s	Cardiac output
$s(\mathbf{x})$		Surrogate function
$\sigma_{f,act}$	Pa	Active stiffness
$\sigma_{f,pas}$	Pa	Passive stiffness
t	s	Time variable
t_{cycle}	ms	Cycle time
t_D	s	Decay time
t_{decel}	s	Deceleration time after E-wave
t_R	s	Rise time
$t_{resampled}$		Resampled time measure [0,1000]
$TimeFac$		Time factor systolic/diastolic time
τ_{av}	s	Atrioventricular delay
$d\tau_{av}$	s	Shift of atrioventricular delay
V	ml	Volume
$V_{m,SW}$	ml	Midwall volume of IVS
w_i		Weighting of fitting values
y_m	m	Radius of TriSeg module

1 Introduction

Cardiovascular diseases are the world's leading cause of death [66]. Many diseases or malfunctions, however, can be treated efficiently when they are detected early. A basis for a reliable diagnosis is medical imaging. In recent times, acquisition of cardiac images improved with regards to quality, time and new methods, opening up more possibilities for accurate monitoring of the cardiac function of individuals and thus, decisions can be made considering their personal physiological properties. Physiological and functional properties do not only differ from person to person, they also change over the lifespan and hence require differentiated diagnoses. For the cardiovascular system, magnetic resonance imaging (MRI), computer tomography (CT) or echocardiography, i.e. cardiac ultrasound, are the most common imaging methods. To analyze the acquired data, cardiologists and radiologists can be supported by software based on intelligent algorithms. Under the keyword 'personalized medicine', new technologies aim to deliver support for a precise, patient-specific diagnosis. In order to achieve this, in recent years, models have been developed, mimicking the physiology or function of the cardiovascular system. By creating a personalized model including the unique features of an individual, these models can help to make diagnoses, monitor changes, plan, and even simulate the effects of treatments.

In this work, an existing computational cardiovascular model, the CircAdapt model [17], is used to adapt to real subject data by employing a parameter estimation based on a multi-step optimization. The resulting model shall resemble the properties of the cardiovascular system of the examined subject. CircAdapt functions as a forward problem, i.e. it computes the phenotypic effects that result from a specific physiologic situation [33]. This means the user proposes a set of model parameters defining structural, mechanical and functional properties like for example the heart rate or the mechanics of heart walls. As a result, time-dependent traces of volume, pressure and flow velocities are retrieved from the model. However, in a clinical setting, the problem is vice versa: a phenotype is given in the form of time-dependent echocardiographic waveforms and geometrical measurements, from which the original physiology shall be inversely determined. For this inverse analysis, the agreement of the volume and flow velocity waveforms of the simulation model and the respective individual or population group is evaluated. Characteristic points of these curves are determined and criteria are defined to quantify the deviation of the measured and simulated curves. Some changes in structure or hemodynamics, i.e. the dynamics of blood flow, cannot be recognized by only scalar values, hence the curve shape is taken into account. In order to match the shape of these curves, the model parameters are altered in such a way, that the deviation based on the criteria minimizes. To facilitate this, a multiple-step optimization algorithm is developed.

As input data serves a recent clinical norm study including a vast number of echocardiographic data from subjects of different age, sex and ethnicity [6, 7]. First, the focus lies on mean values of population groups, namely individuals within the same age group of a decade, later the developed algorithm is applied to individual

subjects. In this study, only healthy adult individuals are considered. The resulting optimized model is investigated considering consistency and conformity of properties and features within the model and in comparison with measured parameters. The degrees of freedom of the optimization are selected as a set of model parameters that sufficiently define the physiology. Electrical information on the conduction sequence in accordance with an electrocardiogram (ECG) acquired simultaneously to the echocardiography is used to achieve an alignment of the signals along the time axis.

The development of this framework has stood under the following requirements. First, the framework shall be usable for a wide range of data, either from population groups or single subjects. As both forms of data vary in their quality, i.e. population functions lack of subject-specific features and change in general form due to the averaging, whereas single-subject data is more difficult to fit, as subject-specific characteristics have to be taken into account. The handling shall be universal and simple, without the need to make extensive adjustments when using different data. Secondly, results are handled critically and are therefore undergone several tests and analysis after the computation. Also, documentation and a helpful presentation of the result is an important part of the development of the framework, this includes logging the computed data along with representative figures and annotations. Especially in prospect of future clinical use of this kind of framework, the results must be comprehensible for clinicians to build up trust against a new technology and keep doctors liable for decisions rather than operating as a blackbox machine [57]. Fast computation time is normally desirable in a clinical context, though, this shall not be the focus of this work, as the framework is not aimed to be used for time-critical clinical assessments, but rather for a post-measurement analysis of the acquired data.

The inverse analysis of the data through iterative simulations with CircAdapt decodes a complete set of structural and functional properties of the respective group or individual. This offers the opportunity to retrieve parameters that are difficult to determine via conventional, non-invasive imaging methods, such as the stiffness of certain patches of the cardiac tissue. Cognitive biases, that occur often in medical imaging, can be reduced [51]. Also, not only cardiac, but also vascular parameters are considered.This also provides information that could not be retrieved before, like physiologic changes that do not affect the hemodynamical outputs. For diseases like heart failure, this might be a step towards a causative therapy rather than the treatment of symptoms.

By applying the framework to data of different age groups, the effects of aging on cardiac mechanics and hemodynamics are evaluated. An estimation of normal physiological changes the heart undergoes in the different decades of life without the presence of cardiovascular diseases or conduction disorders is derived. In consideration of future projects, diagnoses shall be made age-related. Often, changes in cardiac mechanics do not necessarily imply a disease or dysfunction but could rather just stem from cellular changes that naturally occur during the aging process. On the other hand, if those changes do not comply with the chronological age of the individual, it might be concluded that they have a different origin. Some of these

changes cannot be perceived manually, an intelligent algorithm could, therefore, potentially improve diagnostics significantly. As a long-term goal, CircAdapt shall not only be used to improve diagnostics, but also to simulate therapeutic effects [3]. This could crucially improve decision making in dealing with subject-specific circumstances.

The following work presents the developed algorithm and the results found in this study. Section 2 examines the state of the art in both cardiovascular modeling and echocardiographic imaging. Relevant literature is reviewed and presented. Section 3 contains the methodology used and developed as a part of this work. Pre-processing of the data and the different steps of the optimization are derived as well as the handling of the simulation model. Results of the optimization are presented in Section 4. The optimized solution is validated based on different criteria in order to show the success of the developed framework. Age-dependent changes in the cardiovascular system are derived and discussed in Section 4.3. Section 5 discusses the results, makes comparisons to expected outcomes and proposes limitations of this approach. Section 6 closes this work with a summary of the framework and its achievements.

2 State of the art

This section compiles the basics of the research field, as well as already existing academic work relating to this work. Background information is given and literature reviewed and presented. Both the underlying computer model and data is demonstrated.

2.1 Medical background

The physiological background and correlations crucial for the understanding of the methodology are given in the following section. In prospect of the investigation of cardiac aging, recent studies investigating this topic are reviewed.

2.1.1 Properties of the cardiovascular system

The cardiovascular system consists of two major circulations: the systemic circulation supplying the organism with oxygen-enriched blood and the pulmonary circulation, in which the blood passes the lungs to get oxygenated. Blood is transported by a pressure gradient which is generated by contraction and relaxation of the myocardium, the cardiac muscle tissue. To ensure unidirectional flow, valves connect the cavities and the outflow tracts. In this work, the focus lies on the left heart, since measurements are easier to obtain for the left ventricle (LV) and left atrium (LA) than for the right side [52]. Within one cardiac cycle, the heart goes through the following actions, which can also be tracked in the pressure-volume diagram of the LV displayed in Figure 1.

Systole The LV is full of blood and the mitral valve (MV) is closed. The LV pressure has exceeded aortic pressure due to myocardial contraction. The aortic valve (AV) opens, blood is pumped into the aorta and subsequently the systemic circulation. After the ejection, the AV closes. In the following isovolumetric phase, the pressure in the cavity sinks due to myocardial relaxation. During the systole, the LA is filled with blood from the pulmonary circulation.

Diastole As soon as the pressure in the LA is higher than in the LV, the MV opens. Blood fills the ventricle due to the pressure gradient resulting from ventricular relaxation and later due to atrial contraction. When the pressure in the LV exceeds the pressure in the LA, the MV is forced to close. After the closure of the MV, ventricular pressure raises in the isovolumetric contraction phase and systole starts again.

The area inside the pressure-volume loop represents the total myocardial work of one beat. The shape of the pressure-volume loop depends on the mechanical properties of the myocardium [27]. Basic parameters for the description of the cardiac cycle are the following.

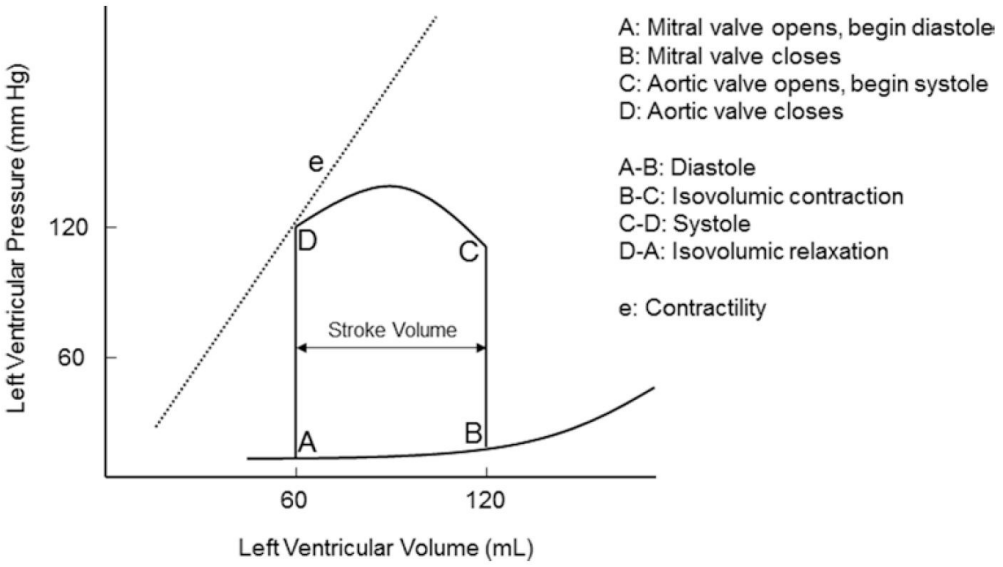

Figure 1: Pressure-volume diagram of one normal cardiac cycle. Source: [27]

Heart rate The heart rate (HR) is the frequency of beats measured in beats per minute, the inverse to the cycle time t_{cycle}.

Stroke volume Stroke volume (SV) is the total volume of blood that the heart ejects in one beat. It is calculated as $SV = EDV - ESV$, where EDV and ESV are the end-diastolic and end-systolic volumes, respectively. In the pressure-volume loop, it is represented by the volume-axis extension.

Cardiac output Cardiac output (CO or q_0) is calculated as $CO = SV \cdot HR$, i.e. it quantifies the amount of blood ejected during a unit of time.

Ejection Fraction The ejection fraction (EF) is the fraction of the EDV that is ejected in one beat and is a measure for a chamber's pumping efficiency.

Furthermore, the volume changes of the cavities and blood flow velocities through the valves over time are examined. Figure 2 shows the curves of the LA (Figure 2a) and LV volume (Figure 2b), as well as flow velocity through MV and AV (Figure 2c) over the time of one heart beat. Throughout this work, the opening of the AV, i.e. the start of the systole, is defined as the start of one beat. The curves are resampled along the time-axis to be within $t_{resampled} = [0, 1000]$, that means the time t(ms) is multiplied by a resampling factor $t_{resampled} = t(\text{ms}) \cdot 1000/t_{cycle}(\text{ms})$. Therefore, the time axes of most plots in this work are unitless.

The first part of the curve is the ejection of blood through the AV; LV volume falls to its minimum value. In the transaortic valve flow, the area under the ejection curve is the SV. It follows the isovolumetric relaxation, where both valves are closed and the LV volume has a plateau. As mentioned before, the diastole is composed

of two phases. First, relaxation of the ventricular tissue draws blood through the MV, resulting in the so-called early injection wave (E-wave). The following phase is called the diastasis, in which the LV inflow is net-zero due to pressure-equilibration after the E-wave. Then, the atrial kick ejects more blood from the atrium into the ventricle, causing the atrial injection wave (A-wave). LA volume gets to its lowest point, while the ventricle is filled. It follows another isovolumetric phase, where the ventricle contracts with both valves closed [27].

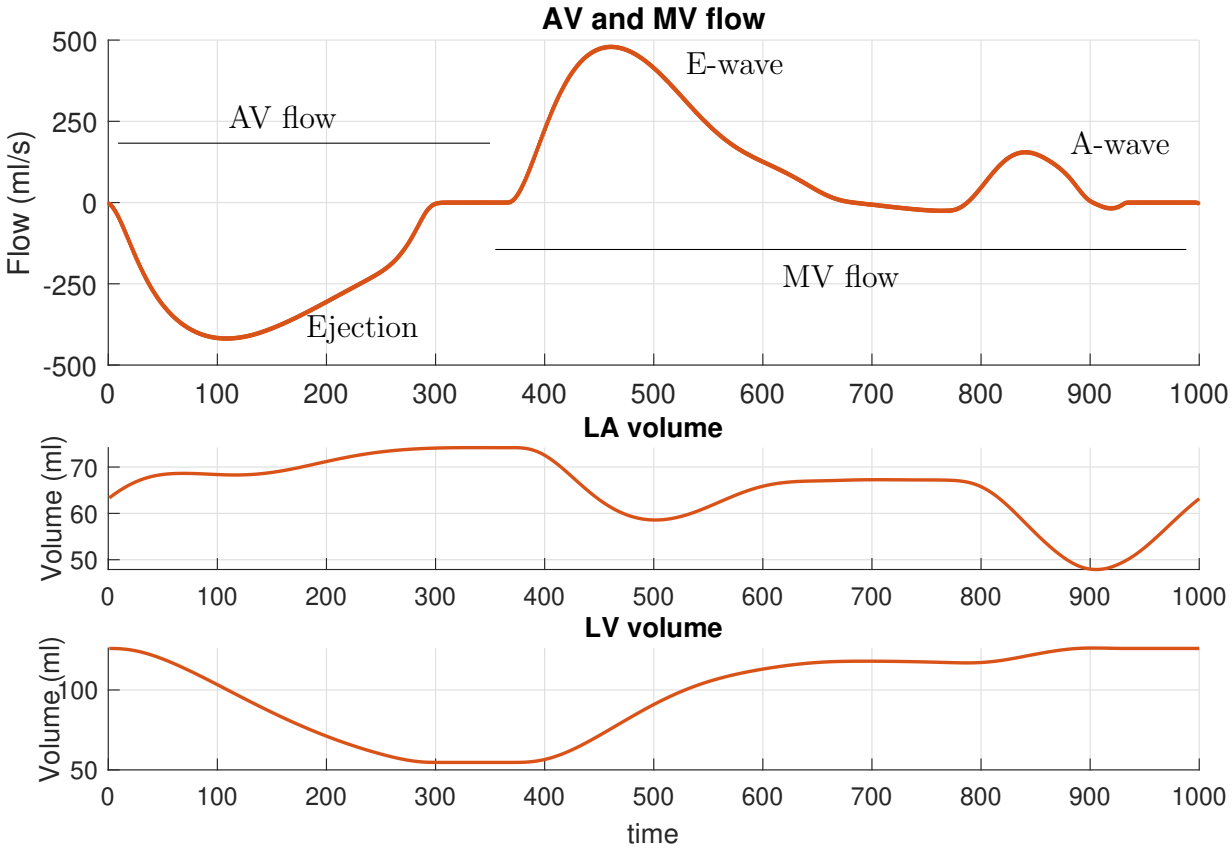

Figure 2: Volume and flow curves; picture generated with CircAdapt [16]

Within one person, this standard curve shape can change with different exercise conditions, as well as with age. For example, exercise increases HR and CO, to supply the body sufficiently with the higher metabolic demand for oxygenated blood. As a result, the E-wave is pushed closer to the A-wave, causing them to eventually join. In some individuals, a third so-called L-wave is occurrent during diastasis. This can be an indication for LV diastolic dysfunction [30] or an elevated LV preload, which is the LV wall stress at end-diastole. L-waves can be caused by delayed active relaxation, larger LA volume, increased LV stiffness and shorter LV isovolumetric relaxation time, long-term resulting in heart failure [29, 34]. However, it is also found in otherwise healthy individuals, being reported to be connected with relatively low HR [29]. Correlated age-dependent changes are discussed in more detail in Section 2.1.2. Also, the curves differ from person to person, depending on mechanical

and hemodynamical properties. Some important CircAdapt model parameters are depicted in the following [40].

Passive stiffness $\sigma_{f,pas}$ determines the stiffness of the myocardial tissue. The stiffer a ventricle is, the more restrictive it becomes to being filled with blood. Therefore, it is common that preload increases in order to keep up the SV. This results in a right shift of the pressure-volume loop [27]. Passive ventricular filling during diastole and hence the slope of the end-diastolic pressure-volume relationship is proportional to ventricular stiffness [27]. Passive stiffness is often given as the inverse term compliance, which equals elasticity.

Active stiffness $\sigma_{f,act}$ is the contractility of the myocardium, i.e. its ability to generate active myofiber stress. Higher contractility in the atrium results in a higher A-wave, as the atrial kick is stronger. Ventricular contractility determines the slope of the contractility line of the end-systolic pressure-volume relationship. For example, with increased contractility and maintained preload, the pressure-volume loop is shifted to the left, increasing the SV.

Rise time and decay time The rise time t_R in the model scales the rate of force-generation increase, i.e. how quickly the myocardium contracts. The decay time t_D describes the opposite, as it scales the rate of force-relieve in the myocardium. Acceleration and deceleration are driven by the atrioventricular pressure difference [10, 28]. Both time frames can be influenced by changes in mitral resistance, myocardial stiffness and peak filling rates. For example, if the LV stiffness is low, LV pressure rises slowly with filling, resulting in a longer decay time. As against a high LV stiffness can cause a negative atrioventricular pressure gradient, which abruptly decelerates the filling [28].

Conduction timings The timing parameters $TimeFac$ and $d\tau_{av}$ influence the flow velocity curve with respect to the time axis. $TimeFac$ is the ratio of the time of systole over the time of diastole. The reference ratio is 1, which means time for systole equals diastole. Atrioventricular delay time τ_{av} is the time difference between the trigger for the contraction of the atrium to the ventricle as controlled by the electrical conduction system of the heart. An additional shift of the contraction trigger is given as $d\tau_{av}$. For the transmitral flow pattern, this means a shift of the E-wave into or away from the A-wave.

2.1.2 Age-dependent changes

Information on the characterization of age-dependent changes is gathered from medical literature, amongst others [13, 14, 32, 45, 55]. In these publications, changes in the healthy heart without comorbid conditions like hypertension, coronary artery disease or obesity are investigated.

In general, the above-mentioned studies show that there is no noticeable age-dependency in total body mass or body surface area (BSA). BSA is used for indexing

measures making them comparable among individuals of different body sizes. As HR and indexed SV decrease, CO values also fall. Blood pressure levels generally increase. While indexed EDV and ESV are smaller in older subjects, EF increases. No changes were observed in the indexed LV mass and LV pressures.

In the arteries, thickening and stiffening can be observed, which causes changes in pressure profiles, a higher afterload and higher end-systolic wall stress. For the myocardium itself, with higher age, the relative wall thickness increases, which is the ratio of wall thickness to chamber radius. However, the indexed wall thickness remains mostly steady. The geometry of the LV outflow tract changes with age, especially the angle between the aorta and interventricular septum. As a result, with higher age, the outflow tract flow measurements are more susceptible to errors.

Phenotypic changes in functional parameters mostly originate from physiological or cellular changes. Biochemical changes from adaptation mechanisms arise from a reduction in intracellular Ca^{2+}. Progressive collagen deposition from the fifth decade of life is reported by [20]. Due to those cellular changes, isovolumetric relaxation time is prolonged, as well as the time of the isovolumetric pressure decay in the LV. Prominently, a slowing of active relaxation and diastolic suction, i.e. early mitral inflow, is observed.

Systolic function is preserved in most older individuals. LV ejection fraction, cardiac output and stroke volume are not affected by aging. Only longitudinal- and short axis shortening is shown to be reduced. Diastolic function, on the other hand, is highly susceptible to changes during the aging process and is a major cause of heart failure in older individuals. Hence it is important to distinguish between pathological and healthy changes. The LV becomes stiffer; hence the MV flow shows a different pattern over time. As the early filling peak velocity reduces, late filling increases due to a stronger atrial kick to keep up the amount of transferred blood. The stiffening of the LV also increases the deceleration time of the early filling wave.

Functional changes in the resting heart dealing with the effects of aging often cause functional deficits with exercise. Changes in the cardiovascular function during exercise, therefore, show the effect of aging rather than being separate alternations. Exercise condition is not covered in the echocardiography study and hence not part of this work.

2.2 Cardiac modeling and precision medicine

The idea of the 'digital twin' has been around for many years and used in different industries. Emerging from analog twins, i.e. a physical model of a device, digital twins represent an entity digitally, enabling to monitor its status based on data from sensors at the real device, diagnose issues and test solutions [25]. For example, intelligent maintenance is achieved for machinery by digitally replicating the entity, simulating its function and predicting failure before it occurs. Digital twins are also used for optimizing the performance of an existing system [68]. Simulations on digital models are especially useful when access to the device is difficult (for example spaceships), dangerous (nuclear power plants) or costly (large scale plants in operation). However, this concept can also be applied to the human body [24],

with the goal to predict potential health risks before they occur or simulate a therapy or operation. Data is acquired by conventional clinical measurements, like taking blood pressure values or measuring body temperature, oxygen levels, etc., but also from medical imaging, which is lately enhancing in terms of quality, simplicity and acquisition time. With this information, models of the anatomy and physiology of body parts or organs can be established. The focus lies on the cardiovascular system, as its failure is responsible for almost one third of deaths worldwide [24]. Since there are many tailored imaging techniques like MRI, CT and ultrasound, personalized models of the patients' hearts can be created and malfunctions detected before they cause a life-threatening disease. Making a step towards this goal, Philips launched a dynamic heart model [46], which automatically creates trackable three-dimensional image of the LA and the LV over the full cardiac cycle based on 3D echocardiographic images combined with the scientifically proven knowledge about the anatomy of the heart. The pumping function is calculated based on this data. The retrieved model allows cardiologists to assess the unique cardiac functions of the individual fast in order to improve diagnosis and treatment [24].

Other approaches of personalized cardiac models have been reported in the last years. Niederer et al. [43, 44] presented an overview over computational models in cardiology. These range from models on a micro level including proteins and biochemical reactions within the sarcomeres, to whole heart subject-specific models. For example, Wang et al. [62] proposed the calculation of passive material properties by creating a customized finite-element model, based on in-vivo MRI data with ex-vivo diffusion tensor MRI data to estimate the myofiber orientation within the myocardial walls. Xi et al. [67] developed a finite-element model describing ventricular mechanics. The geometry and myofiber architecture was also based on MRI data; mechanical properties were fitted to acquired pressure-volume loops, in order to obtain a model parameter set matching subject data. Cardiac mechanics were incorporated with several simplifications. The model was used to study pulmonary arterial hypertension in men.

A cardiovascular model focusing on the mathematical correlations within cardiac structures on multiple levels rather than the exact geometrical shape, namely the CircAdapt model, is presented in the following Section 2.3.

2.3 CircAdapt model basics

CircAdapt is a mathematical model of the human heart and circulation, that has been developed at the Department of Biomedical Engineering at the Maastricht University Medical Center. The MATLAB source code and relevant documentation is available open-source [16]. This section outlines the basics and underlying physical correlations of the model, as well as the organization of its data structure.

2.3.1 Basic principles

Based on a system of partial differential equations, hemodynamics and mechanical parameters of a cardiac system are real-time simulated and provide insight into

different physiologic or pathophysiological situations. The background of cardiac mechanics and the basic correlations between the parameters are found in [27, 38]. As an output, the pressure in cardiac chambers and large blood vessels, volumes of ventricles and atria and the blood flow rates through valves or shunts are computed. These values are presented as functions of time, displaying separate heartbeats. The model holds a modular design that can be adapted to the research interest. The modules and their dependencies are shown in Figure 3.

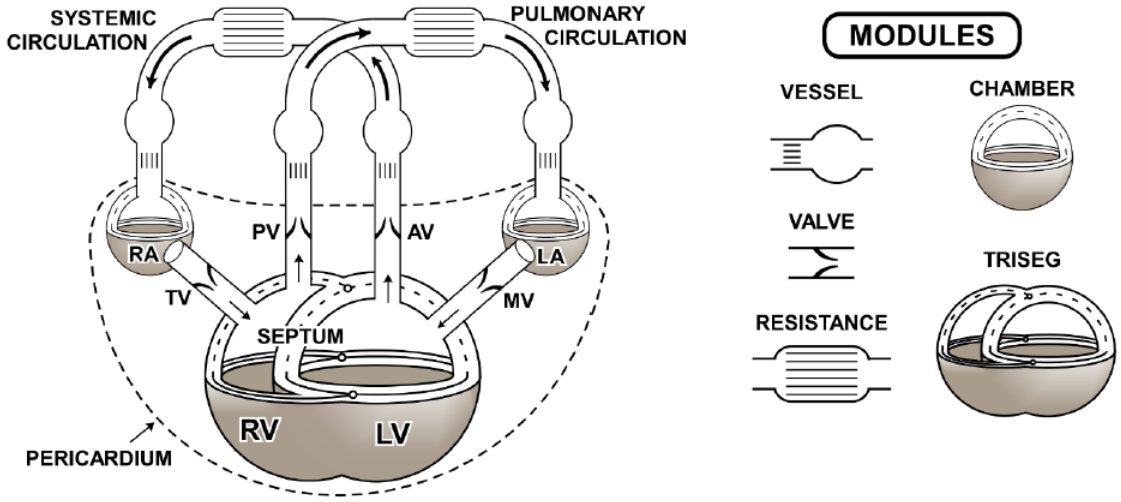

Figure 3: Schematic drawing of the CircAdapt model. Source: [59]

As a multiscale model, global pump mechanisms and local behavior of myocardial tissue are anatomically coupled. Physical and physiological principles are incorporated in terms of conservation of energy, i.e. contractile work equals hydraulic pump energy, and a dependency of both ventricles via direct anatomical coupling as well as hemodynamic interaction. Additionally, structural adaptation of cardiac and vascular wall to mechanical load of tissue is implemented [3, 4, 5, 37].

CircAdapt is used for clinical education and research in the form of an interactive simulator, that can also be retrieved free of charge from the homepage [17]. Since the simulations closely resemble the human cardiovascular hemodynamics and mechanics, as well as flexible and easy to adjust, the model is also successfully used for fundamental research in pathophysiology and physiology [17]. However, so far, most research is based on a fundamental level, in which basic characteristics of a certain pathology is investigated using artificial subject data. Details on the applications of the CircAdapt model are given in Section 2.3.3.

It is aimed to apply the simulations subject-specifically and thus use CircAdapt as a diagnostic tool in clinical practice. The team at Maastricht University is currently investigating the subject-specific use of CircAdapt to determine the hemodynamic status of individuals with regard to heart failure.

Adaptation A unique feature of the CircAdapt model is its ability to adapt tissue properties to mechanical load [3]. This simulates chronic changes over a long period

of time, in which the heart needs to adapt to a difference in loading conditions in order to preserve an appropriate pump function. There are three adaptation protocols that are used in the model. Firstly, pressure-flow control is performed throughout the whole circulation system in order to maintain the pressure-volume relationship. This is implemented by an adaptation of the reference pressure drop of the systemic capillary network after each simulated cardiac cycle in order to match the CO, MAP and systemic vessel pressure-flow relation [58]. A second and a third adaptation mechanism alter vessel and wall properties with regards to the load. To simulate a physiologic state adapted to chronic changes, the cardiac load is altered between resting and exercise condition, while the adaptation protocols are employed, until the simulation reaches a steady state. Adaptations are modeled as realistic as possible, therefore, pathological alterations of the physiology tend to be compensated for by changing blood vessel and tissue properties. To simulate acute changes of structural parameters, adaptation rules are switched off in order to review the effect of those short-term interventions, but pressure-flow control is enabled. Due to this establishment of dependencies, the number of required input parameters is reduced drastically and enables easier employment of the model to subject-specific data [3].

2.3.2 Data structure

The core of a CircAdapt simulation is a MATLAB structure array P ('patient'), where all information about the simulated model is stored and simulation results can be retrieved from. P is handed over as a global variable throughout the majority of the code. The fields of P contain structures based on modules and functionalities. The first level of structures contains amongst others the fields displayed in Table 1. The model heart is composed of four chambers, the atria are described by a cavity and a wall each. Between the ventricles, the chambers are connected by the interventricular septum (IVS) and are surrounded by a bag, the pericardium. The composition of both ventricles and the ventricular free walls and septal wall is modeled mathematically as the TriSeg model [38]. Here, mechanical interaction of the LV and RV free walls and the IVS is modeled, as well as the pump mechanics of both ventricles in relation to respective myofiber mechanics. The interaction is based on the principle of conservation of energy at the common junction [1, 38].

To model the complexity of geometry and structure of the heart, the following underlying assumption is made: the normal heart myofiber structure and geometry adapts so that the load is evenly distributed. This allows for the modeling of the atria as spheres and the ventricles as a set of interpenetrating spheres [1]. By making this simplification, the average computation time of the model can be significantly reduced compared to a geometrically detailed finite-element model [31]. As stated before, the parameter correlations within the model are mounted in a system of partial differential equations. The state variables are listed in Table 2. In total, there are 30 state variables. Every state variable provides information about the respective parameter at each step of time t during a cardiac cycle. The system of state variables, their derivatives and time parameters are also stored within P.

P struct field	Description
General	General data
ArtVen	ArtVen elements, 2 cavities
Chamber	Chamber elements, 1 cavity and 1 wall
TriSeg	TriSeg element, 2 cavities and 3 walls
Cavity	indexed by ArtVen, Chamber and TriSeg
Wall	indexed by Chamber and TriSeg
Patch	indexed by walls
Node	connecting cavities and other elements
Bag	passive eleastic bag like pericardium
Valve	Valve, connecting nodes

Table 1: First level of structure array P. Modified from [2]

Symbol	No.	Description
t	1	Time variable
V	8	Volume of each cavity (atria, ventricles and blood vessels)
q	9	Blood flow through the valves (including atrial inflow and, if present, shunts)
C	5	Overall contractility of the myocardium in the respective wall patches
L_{si}	5	Intrinsic length of the sarcomeres, i.e. the smallest unit within a myofiber, in a wall patch
$V_{m,SW}$	1	Midwall volume of the IVS wall
y_m	1	Radius of the circular sphere intersection of the TriSeg module, i.e. geometry information about ventricules

Table 2: State variable used in the CircAdapt model. Modified from [58]

2.3.3 Applications

CircAdapt has been used for teaching purposes in medical education, as well as for medical research. Recently, the process of correction of MV and tricuspid valve (TV) regurgitation, i.e. a backflow due to insufficient valve closing, was studied by Walmsley et al. [61]. By simulating the intervention with the CircAdapt model, they found that a gradual correction improves the outcome. Heusinkveld et al. [23] used the CircAdapt model for investigations on the augmentation index, stating the correlation between LV stroke work and wave reflection due to artery stiffening. Combining experimental findings with CircAdapt modeling, Willemen et al. [64] assessed cardiac resynchronization therapy responses of the LV and RV. Canine hearts were used to perform a pacing protocol with different atrioventricular pacing delays. Electrical activation times were measured in the animal subjects. The acquired electrical mapping data was then used as an input for the CircAdapt simulation, reproducing the protocol. Huntjens et al. [26] as well investigated the response to

cardiac resynchronization therapy in a combined clinical-computational evaluation. A comparison of output patterns computed with different model parameters was presented by Kirn et al. [31]. Local activation time and contractility was aimed to be estimated by retrieving the strain patterns for different combinations of these model parameters. The strain patterns were rated based on the sum of least-squared differences error to non-invasively measured myocardial deformation patterns from patients with the same global pathology. They discovered that the strain patterns are unique for the underlying model parameters. Walmsley et al. [60] studied how modeling the RV pump function through a CircAdapt simulation can help to understand cardiac imaging of the respective parts. They also present key issues of comparing model outcomes with clinical data. Lumens et al. [39] presented the use of CircAdapt for patient-specific cardiovascular modeling of pulmonary hypertension. In this study, the aortic and pulmonary arterial pressures of 21 patients with pulmonary arterial hypertension were assessed using arm-cuff measurements and right-heart catheterization, respectively. A patient-specific fitting was performed to fit the CircAdapt model to this data.

2.4 Echocardiographic data

As a resource for echocardiographic measurement data, the World Alliance of Societies of Echocardiography Normal Values (WASE) Study [6, 7] is referenced, that was conducted between September 2016 and January 2019. The selection of the study cohort, measurement and analysis methods are discussed in the following section.

2.4.1 WASE study

The WASE study [6, 7] is a study of healthy adult individuals from multiple countries, races and ethnicities with an equal distribution between genders and age groups. For each individual, basic demographic information was collected, which includes age, gender, race, ethnicity, nationality, height, weight, and blood pressure. BSA was derived from height and weight using the Mosteller formula [42]. A comprehensive transthoracic echocardiogram (TTE) was acquired by a physician or sonographer of international societies participating in the study, following a standardized acquisition protocol based on American Society of Echocardiography (ASE) [35, 41] and European Association of Cardiovascular Imaging (EACVI) guidelines. This also includes minimum requirements for the used ultrasound machine and its settings. The performed measurements include dimensions and function information gathered from 2D, 3D, Doppler, and longitudinal strain parameters. Some measurements are indexed, i.e. they are given in relation to BSA. The recorded data was transferred to central and independent echocardiographic core laboratories in the United States. Image analysis was performed using Image Arena^{TM} (TOMTEC Imaging Systems GmbH, Unterschleißheim, Germany), following standard protocols. By following these strictly standardized protocols ensuring uniform measurements, the WASE study presents a unique opportunity to define norm values for cardiac geometry,

morphology, function and hemodynamics based on a widely diverse population of individuals. All subjects are all considered as healthy, 'normal' individuals without heart, lung or kidney diseases. Excluded were also individuals with a history of hypertension, dyslipidemia, diabetes, abnormal BMIs, pregnant women, competitive athletes and alcoholics. For individuals older than 65 years, a history of hypertension or hyperlipidemia was allowed if it is medically controlled, due to the difficulty to find subjects in this age without this condition.

In total, 2,008 subjects were involved in 15 countries, 1,033 were males and slightly fewer females, namely 975. For some subjects, parts of the LV data analysis was not feasible and were therefore excluded in this work, in order to make sure to have a complete data set of each individual available. For this work, the cohort is divided into six age groups: One group of under 30-year-old individuals, groups of 30 to 40 years, 40 to 50, 50 to 60, 60 to 70 and people over the age of 70 years. Total numbers and gender distribution in the age groups are summarized in Table 3. Individuals enrolled in the study are mainly Asian (41.8%) or White (30.1%), but also Hispanic/Latino (10.1%), African/African American (9.7%) and Middle Eastern/North African (8.1%) backgrounds are included. The remaining subjects have a different or mixed ethnicity. 7% of the individuals older than 65 years had comorbid conditions, that were exclusion criteria for the younger subjects, i.e. hypertension or hyperlipidemia.

Age Group	Range (y)	Males	Females	Total
1	<30	177	206	383
2	30-39	235	194	429
3	40-49	175	139	314
4	50-59	130	135	265
5	60-69	182	179	361
6	>70	134	122	256

Table 3: Selected statistics of the WASE study

2.4.2 Data acquisition and analysis

TTE is a common, non-invasive method for cardiac imaging [27]. In two-dimensional imaging, an arc of ultrasound beams provides cross-sectional views of the heart. The echocardiogram is performed from standard views on the chest: the parasternal window, apical window, subcostal region, and suprasternal notch. For the apical view, the ultrasound transducer is positioned in extension to the cardiac long-axis; hence all four chambers, as well as MV and TV are visible in this view in two-dimensional imaging. LV volumes and LV EF are measured in apical views using the biplane Simpson rule. In Simpson's rule, the volume of a cavity is calculated by summing up the cross-sectional areas measured in each slice, multiplied by the slice thickness [22]. This is a very common and reliable method for estimating

ventricular function. As part of the WASE study, LV dimensions are given as a time-dependent function from B-mode measurements. In B-mode, amplitudes sent by the ultrasound transducer are returned as grey values, providing a two-dimensional greyscale image. The targeted LV or LA cavity area is selected in an initial view, the Image Arena$^{\text{TM}}$ software follows this contour through the cycle. Volumes are calculated considering the shape of the cavities. A time-volume function is provided from these calculations. The first derivative of the time-volume curve serves as a representation of the flows into and out of the LV, approximating the flow through the MV and AV, respectively. These curves serve as the main basis for the parameter estimation derived in this work. LA and RV volume curves are acquired as well, though they are of a lower quality due to their irregular shape and inaccessibility. For most of the time-dependent images, an ECG is collected in parallel to simplify the time orientation within the cardiac cycle.

The two-dimensional images are used to guide the Doppler ultrasound [48]. For Doppler imaging, a single beam of ultrasound waves is positioned in the direction of the blood flow in the vasculature. The waves are reflected off the moving red blood cells, inducing a frequency shift that is measured by the transducer. Blood flow velocity q can then be derived using the correlation

$$F_d = \frac{2 \cdot f_0 \cdot q \cdot \cos\phi}{c_h} \,, \tag{1}$$

where F_d is the frequency shift measured at the transducer, f_0 is the transmitted frequency, c_h the velocity of sound in human tissue at body temperature (37°C) and ϕ the angle between the ultrasound beam and the blood flow direction. Due to the difficulty of precisely determining ϕ, as well of artifacts by valve leaflets or other disturbances, Doppler imaging is not always accurate. Another drawback of Doppler ultrasound is that the acquisition is often prone to biases [65]. Additionally, for this work, the availability of analyzed Doppler images from the WASE was delayed and hence they were only used for a comprehensive analysis of the data.

3 Methodology

This section describes the methodology of the framework developed in this work. Based on the echocardiography study population groups are formed, for which the algorithm is ought to find a model that produces cardiovascular hemodynamics whose output accords with this data.

As described in Section 2.3, the CircAdapt model is used as a basis for the cardiovascular model. The first step visualizes and dissects the available data from the WASE study. Next, the existing model is analyzed in terms of the implemented model parameters and output data. The underlying principles of CircAdapt are retraced in order to evaluate the capacity and possible limitations of the model. In accordance with the clinical requirements on the framework, i.e. which model parameters are useful to retrieve, parameters of interest are chosen. The criteria to judge the quality of the fitting is explained in Section 3.3. Frame conditions, such as the computational effort and data formats are retrieved and conclusions are drawn for the requirements of the implemented optimization. The development of the optimization methodology is derived for this problem and the choice and functionality of the underlying algorithm is lined out.

3.1 Data pre-processing

The LV volume and therefrom derived flow curves of all subjects are averaged over the defined age groups. A comparison of the curves of the age groups is shown in Figure 4.

The averaged curves are much smoother than the single measurements and show a clear dependence on age. However, by averaging, subject-specific features are omitted and changes occur in the general shape. For instance, in the isovolumetric phases, the measurement of the non-moving walls is less reliable and those times are smoothed out and hence not recognizable. Also, asymmetry in the peaks can arise from combining differently located, but symmetric peaks. Nonetheless, averaged curves are used to find age-related patterns in changes of the model parameters, that apply to specific populations, here age groups, rather than individuals. Volume and flow curves of single subjects from the respective age groups are shown in Figure 23 in Appendix B. Curves of individuals hold subject-specific characteristics, as well as they can contain irregularities from the image analysis, for example, the resampling or smoothing. LA dimensions are also available, but underdetermined. For the RV, the volume cannot reliably be derived from the two-dimensional image, since its shape is very irregular.

Doppler images of the respective flows are processed by indicating the characteristic points, which are the beginning of the diastole, the peak of the E-wave, the minimum value of the diastasis, A-wave and the end of the diastole. A shape-preserving piecewise cubic interpolation is deployed between those points using MATLAB. In order to retrieve population-averaged curves, the mean isovolumetric time is calculated; the remaining curve is averaged over all curves belonging to the respective

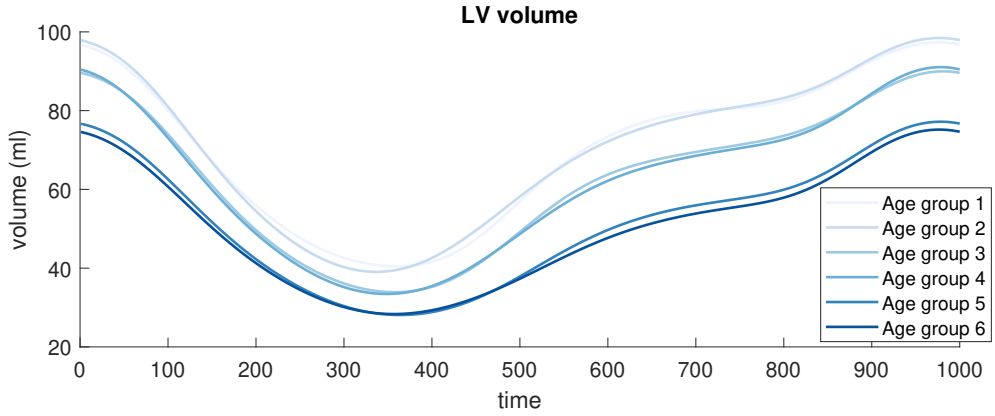

(a) Tracings of the LV volume flow

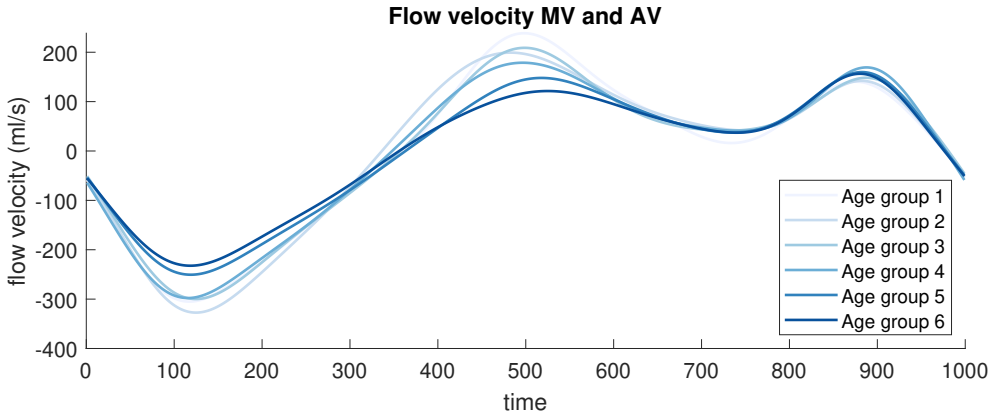

(b) Flow velocity tracings

Figure 4: Subject data from WASE study, volume and flow curves of different age groups

population. The resulting curve is smooth while retaining the average time of the systole. Doppler imaging is also performed on the LV outflow tract (LVOT), the blood vessel attached to the LV. An LVOT velocity time integral (VTI) provides information about the systolic function and the CO. The LVOT flow velocity curves are also averaged within the age groups. As ECG information for the LVOT curves is not available, the position within the cardiac cycle is estimated. Figure 5 shows a comparison of the flow velocity patterns retrieved from the derivative of the volume measurements and the Doppler curve. In Figure 5a, the averaged curves of the first age group are presented, whereas a single subject of age group 1 is examined in Figure 5b. Since the Doppler ultrasound measurements always provide an absolute blood flow velocity, while the derivative of the volume measurements is given as volume flow, the AV and MV areas are used to compare the curves. Due to the irregular shape of those valves, a direct measure of the valve area is difficult and prone to errors. Hence, the valve areas are determined based on a comparison of the absolute values of Doppler and volume flow as $3.3\,\mathrm{cm}^2$ for the averaged tracing and $2.8\,\mathrm{cm}^2$ for the individual subject.

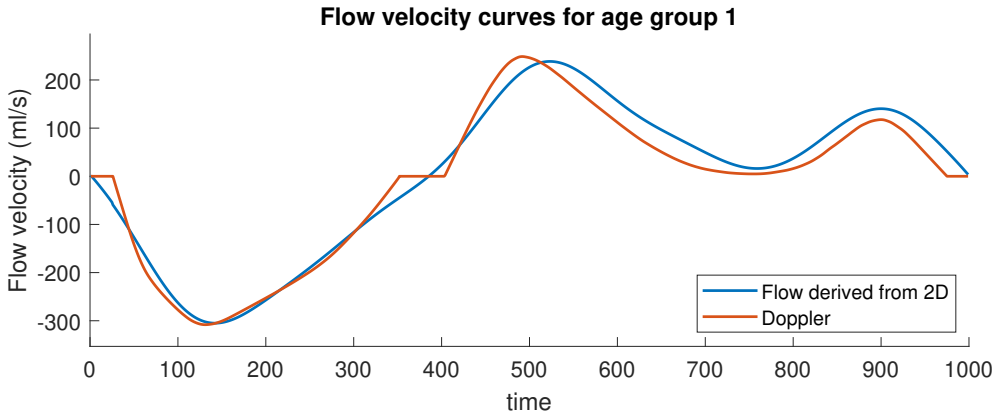

(a) MV flow velocity curve derived from volume curve in comparison with Doppler curve, age group 1

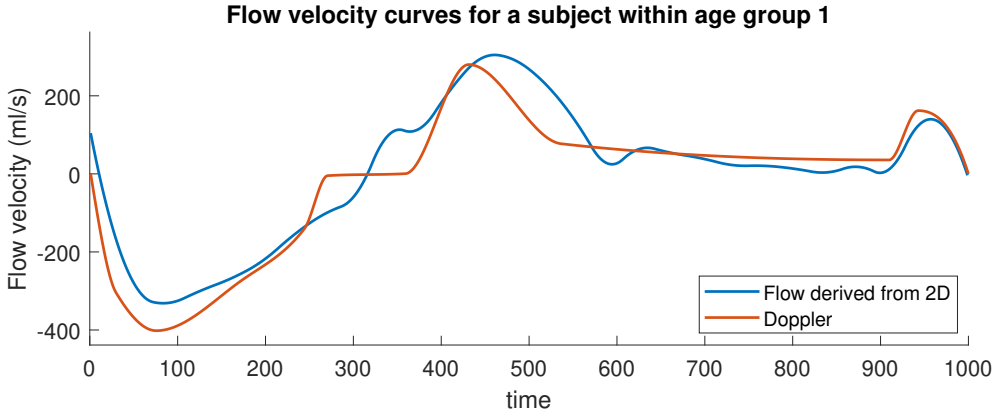

(b) MV and AV flow velocity derived from volume curve and Doppler curve, subject from age group 1

Figure 5: Age group averaged and subject-specific data

Furthermore, the standard deviations of the averaged LV volume curves are investigated, as they indicate how precise the input data is. Figure 6 shows the mean curve of the LV volume for the first age group, along with the upper and lower bounds of the standard deviation. A comparison of the standard deviation between the different age groups is presented in Figure 7. Table 4 shows the mean values and standard deviations for the LV volume averaged over a full cycle for each age group. The variation coefficient provides a measure for the dispersion of the distribution. It varies between 28% and 31%, implying that the standard deviation is almost one-third of the mean value, which is rather high. It can be noted that the standard deviation of the older age groups is lower. Given the high variation of the input data, the accuracy of the output results is expected to be limited.

Some phenotypic age-related changes can be observed in the dataset directly. LV EF, CO and SV hardly show an age-dependency. The peak velocity of the early filling wave in comparison with the atrial kick decreases significantly over age.

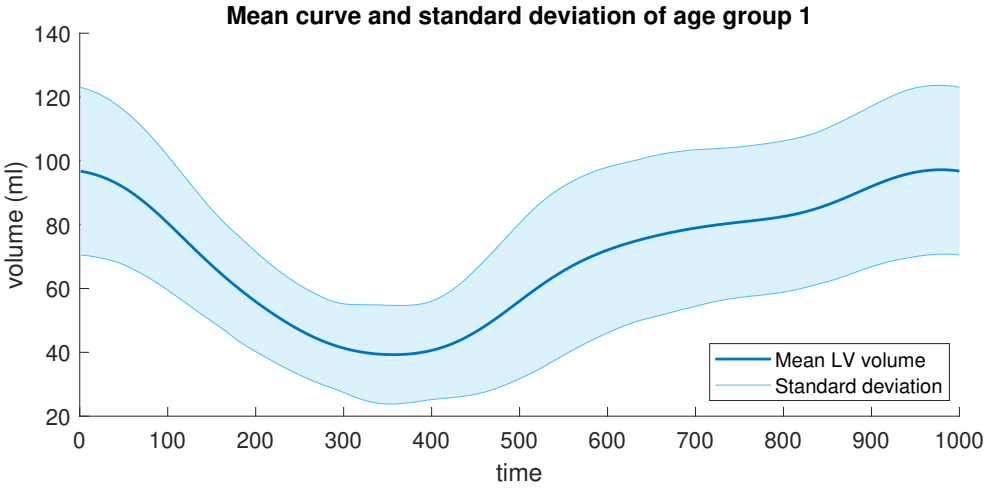

Figure 6: LV volume for age group 1: Mean curve and standard deviation

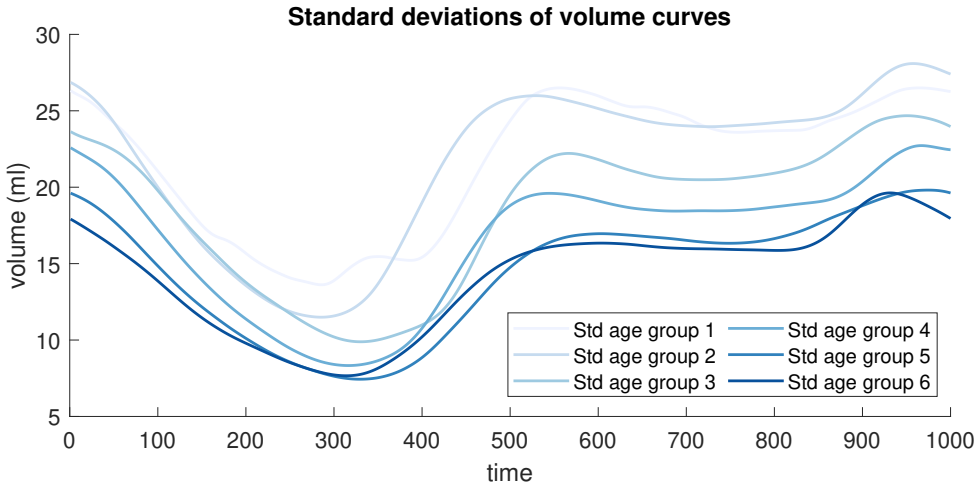

Figure 7: Standard deviation of LV volume for all age groups

3.2 Model parameter assessment

Model parameters are the model-describing parameters, that are altered in the process of the optimization. The behavior of the model output to different input conditions by performing a grid search is analyzed. For this, one or two model parameters are bounded and discretized within the parameter field [15]. The parameter field is chosen vastly, but with respect to physiologically realistic values. For example, the influence of passive stiffness and the LV relaxation duration on the MV flow pattern is analyzed. The discrete parameter spaces are defined as

$$t_D \in \{-60t_{D,0}, -33.3t_{D,0}, -6.7t_{D,0}, 20t_{D,0}\} \tag{2}$$

$$\sigma_{f,pas} \in \{-30\sigma_{f,pas,0}, -3.3\sigma_{f,pas,0}, 23.3\sigma_{f,pas,0}, 50\sigma_{f,pas,0}\}\ , \tag{3}$$

where $t_{D,0}$ and $\sigma_{f,pas,0}$ are the initial values of the relaxation duration and the passive stiffness as given in the reference model, respectively. For every parameter

Age group	1	2	3	4	5	6
Mean value	69.68	69.69	62.00	61.40	51.13	49.87
Standard deviation	21.64	21.66	18.50	16.59	14.47	14.17
Variation coefficient	0.31	0.31	0.30	0.27	0.28	0.28

Table 4: Mean values and standard deviations over a full cycle

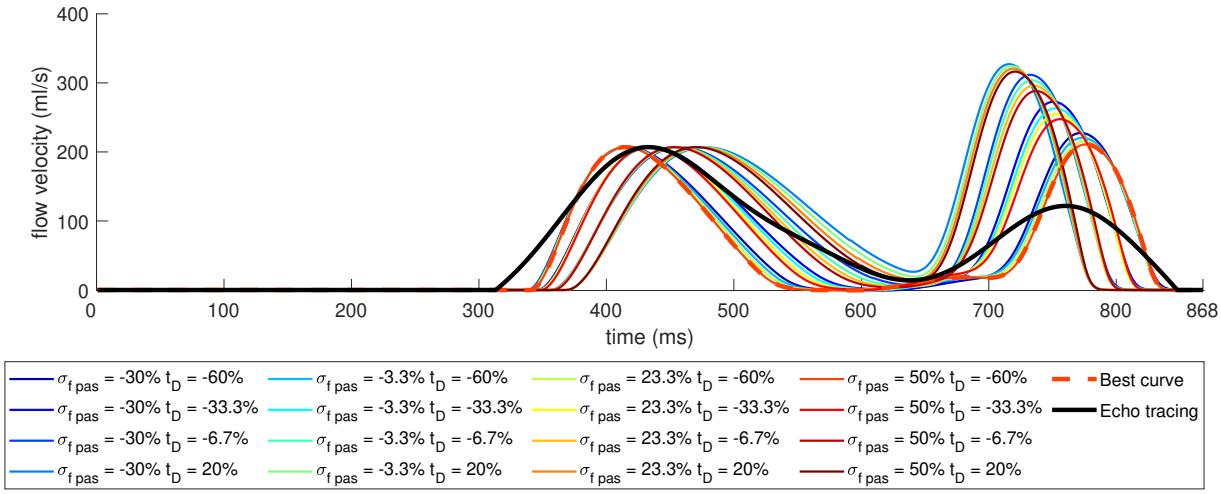

Figure 8: Grid search for passive stiffness and relaxation duration

combination, the model is evaluated and the resulting MV flow pattern retrieved. Results are shown in Figure 8. The curve shapes of every parameter combination are compared to the pattern of the measurement tracing, plotted as a black line. Based on manual or defined criteria, the best curve is chosen and highlighted in the plot with a dashed line. More details on the choosing of the best curve are given in Section 3.3. The objective of this grid search is to find parameter ranges, that have the potential to resemble the target curve. In the shown example, the curve with the highest stiffness and lowest relaxation duration value comes closest to the echocardiography tracing. However, extending those parameters beyond these values causes the curve to develop other unwanted features like in this case an L-wave. It is concluded that the exact shape of the tracing cannot be resembled using only these two parameters; more parameters have to be taken into account. Obviously, a higher-dimensional grid search would exponentially increase the computational effort. Also, the discretization of the parameter space would reduce the resolution and accuracy of the solution. Therefore, a directed optimization is employed, which is explained in the remainder of this chapter.

Another useful resource for the validation of parameters based on the interrelations among each other and relations with the output curves is the CircAdapt teaching tool. The implemented model parameters that can be altered are limited in the teaching tool, however, it provides a simple handling and meaningful rep-

resentation of results [33]. Hence it is used to run test simulations, alter different parameters and assess the output.

3.3 Assessment of the quality of fit

The deviation of a simulated curve from the targeted measurement curve is quantified by the definition of fitting values. Both curves have different sources and are hence not entirely comparable. Since the echocardiography flow velocity curves are based on a 2D volume measurement, the values are based on the total variation of the volume of a chamber. On the other hand, the flow velocity curves retrieved from the simulation model represent the total flow on a point within the cardiac valves. The averaging of different curves within one age group as described in Section 3.1 also influences the shape of the curve. For the curves of single individuals, subject-specific characteristics and irregularities are relevant.

Nevertheless, the defined criteria are retrievable for any of these curves to make them comparable. The total deviation of the matching is computed by errors of characteristic points of the curves multiplied by a factor weighting the respective characteristic.

3.3.1 Determination of characteristic points

For a reliable comparison of the fitting values, the characteristic points of the curves must be determined in the same, steady way for every possible shape. During the optimization, combinations of the model parameters can occur, where the characteristic points cannot be unambiguously determined. It is assumed that those combinations do not apply for candidates of the best fit, therefore those cases will be actively omitted in the optimization. This is explained in more detail in Section 3.5. Figure 9 and 10 visualize the definitions of the characteristic points exemplary for the averaged echocardiography curve of the first age group. Dealing with irregularities in data from single subjects, those points are less intuitively calculated. In Appendix B, Figure 24 shows those points exemplary for the first three age groups.

E-wave The E-wave marks the first diastolic flow, i.e. after the MV opens. To get the coordinates, all peaks of the transmitral flow are determined, sorted by descending heights. The two highest peaks are most likely the peaks of the E- and A-wave; the L-wave and measurement artifacts are usually lower in value. The time at which the MV opens is determined as described in Section 3.3.2. The E-wave is the peak closest to and timewise after the valve opening. The width of the E-wave is determined as follows: the prominence of the peak marks the height counted from the highest point to the higher turning point of either side. Halfway on this prominence line, the width of the curve is measured.

A-wave The A-wave is the last peak of the diastole. Independently from the number of peaks in total, the one caused by atrial contraction is ought to be chosen. Therefore, the time of the maximum contraction of the atrium is determined by

referring to the contractility level over time. It is concluded that the A-wave is the peak which is closest to the maximum contraction peak. The width is calculated the same way as described for the E-wave. For the measured curve, there is a lack of information about the contractility of the LA. Therefore, the A-peak is defined as the one of the two highest peaks, that is closest to the end of the diastole. The E/A ratio is computed from the two maximum velocities; the time difference between the E- and A-peak by subtracting the time values.

Ejection peak The ejection peak is the maximum velocity of the systole, i.e. the maximum flow velocity through the aortic valve. This can easily be determined by choosing the highest peak of the aortic flow.

Deceleration time The time of the deceleration of blood flow after the E-wave is included in the fitting values. For this, a first step computes the angle of deceleration. As the shape can differ between the simulations, a working point is defined at the highest deceleration between E- and A-wave. From the point of the highest deceleration, a section of the curve set to this point is included and the deceleration averaged in this section. As boundaries, the starting point is defined to be 30% of the distance to the E-peak and the end-point 30% of the distance to the minimum between E- and A-wave. This allows for stability when E- and A-wave are almost joined or when an L-wave is present. Deceleration t_{decel} time is then defined by

$$t_{decel} = \frac{x_E}{\dot{x}_{E,decel}} \,, \tag{4}$$

where x_E is the maximum amplitude of the E-wave and $\dot{x}_{E,decel}$ is the mean slope of the E-wave deceleration. The highlighted part of the curves in Figure 24 expresses which part of the E-wave deceleration slope has been taken into account when calculating the deceleration time.

Volume curves The LV and LA volume over time is considered in order to direct the solver to find a physiologically correct solution. The end-systolic and end-diastolic volumes of the LV are determined by finding the minimum and maximum value of the volume curve, respectively. For the LA volume, absolute values do not meet the expected values from literature as presented by Aune et al. [8]. In their study, LA volumes are found to be 19 ml/m^2 to 41 ml/m^2 indexed by BSA, which in this study was an average of 1.91 m^2. Thus, only the ratio between the maximum and minimum values of the LA volume is included, not the absolute values.

3.3.2 Alignment of the curves

In order to match the curves, both the measured and the simulated curve are analyzed with regard to the timing within a cardiac cycle. This enables to compare the characteristics described in Section 3.3.1. The assessment is based on the time events happening during a cardiac cycle, such as active contraction and passive valve

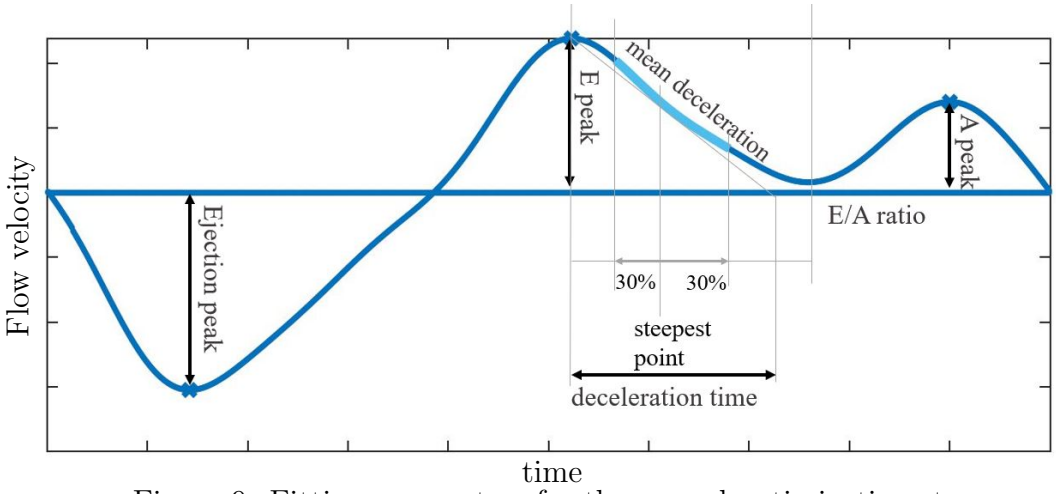

Figure 9: Fitting parameters for the second optimization step

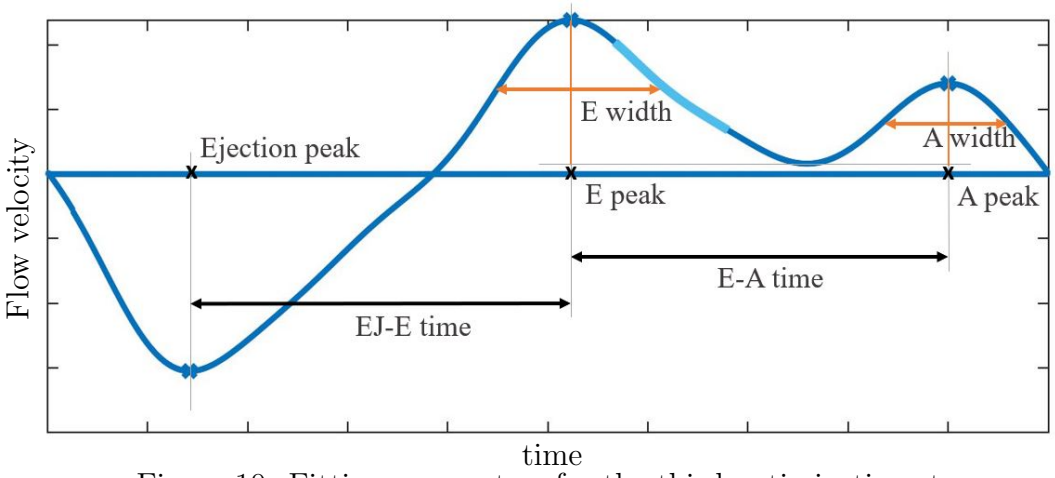

Figure 10: Fitting parameters for the third optimization step

events. Here, the cycle start is defined as the time of the opening of the aortic valve, i.e. the start of the systole.

The contraction of the myocardium is triggered by electrical signals. Depolarization of the sinoatrial node, which is located near the atria, marks the start of a normal cardiac cycle. As the signal is conducted through the LA and RA, their tissue is depolarized and this consequently lets the atria contract. Further conduction of the signal leads to depolarization of the ventricular tissue, which results in a major deflection of the potential, clearly detectable in an ECG by the so-called QRS complex. With the end of the QRS complex, the ventricles are completely depolarized and contract. In the resulting curve of the atrioventricular valve flow velocity, this is marked by the event of the closure of the valve, i.e. the start of the ventricular systole. Since the QRS complex is rather prominent on an ECG because the electrical impulse is directly proportional to the total amount of myocardial cells that are depolarized at once, it is easily detectable even on a low-quality ECG and is hence used as an indication for the cycle start. In CircAdapt, these activation times

are implemented phenomenologically, hence, the times can be retrieved directly.

Valve events, i.e. valve opening and closing, are determined based on the output pressure curves from CircAdapt. The valve opens, when the pressure in the proximal chamber is greater than in the distal chamber. Thus, the MV opens when the pressure in the LA exceeds the pressure in the LV, and the AV opens with LV pressure exceeding the pressure in the aorta.

Closing times are dependent on the pressure changes in the distal chamber and can be determined using its third derivative. For example for the MV in Figure 25 (Appendix B), the valve closing is at the local maximum of the third derivative of the LV pressure that is located near the significant LV pressure rise at the beginning of the cycle. For the aortic valve in Figure 26, it is sought for the cusp of the aortic pressure into linearity. This can be derived from the minimum of the third derivative of the pressure curve, which is closest to the end of the systole. In clinical practice, the closing of the valve can be determined via a recording of the heart sounds.

Figure 11 valve opening and closing events with respect to the left heart's pressures, volumes and valve flows.

3.4 Optimization

As a reference model for the optimization, the reference P structure provided in the CircAdapt source code [16] is used. The initial output of this model can be reviewed in Figure 12, compared to the echocardiographic data for the first age group as a comparison. It is clearly visible that both the flow and the volume profile deviate significantly from the targeted function. Hence, the first step is to generate a new reference model that is closer to the measurement data.

Once this new reference model is established, it is used to fit the model to the rest of the data sets. This iterative procedure aims to minimize the search space and hence reduces the risk of convergence towards a local minimum.

Within this optimization process, different parameter spaces of the model are defined. Parameters that can be confidently measured in the subject are considered as fixed parameters and directly altered in the model for each age group. Model parameters are altered dynamically in the process of the optimization. These parameters aim to define the nature of the model and also serve as insight into cardiovascular parameters that cannot be measured directly. Hence it is aimed to include as many model parameters as possible to get the closest representation of the human cardiovascular system. The deviation between the output values is quantified by a composition of the fitting values, which define the differences in certain characteristics of the curves. Hence the fitting procedure is as follows, as it is shown in Figure 13[1]: The reference model is altered by the set of fixed parameters. Its output is compared with the measurement data by calculating an error based on the fitting values. If this error exceeds the tolerance, model parameters of the simulation model are changed, aiming to reduce the error. This is repeated until the error is sufficiently small.

[1]Icons made by Eucalyp from www.flaticon.com

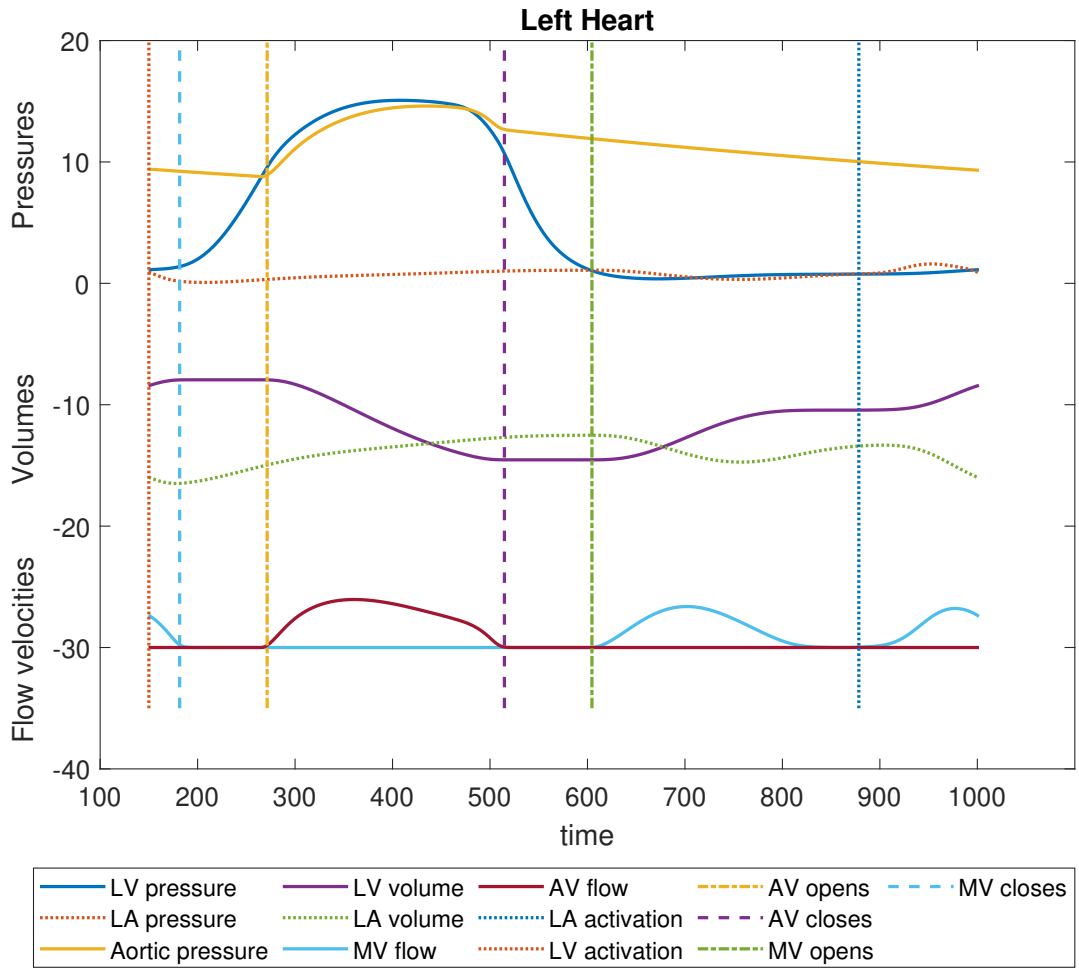

Figure 11: Valve opening and closing events of the left heart on qualitative curves of pressures, volumes and flow velocities

It is aimed to fit multiple parameters of which one cannot exclusively state that they are independent. In order to avoid over-fitting, the optimization process is executed in three steps. In Optimization 1, only the blood pressure levels are fitted by altering vascular and pressure-related parameters. Optimization 2 covers more parameters concerning the myocardial properties, fitting absolute values of flow and volume curves. In Optimization 3, model parameters are added aiming for the optimal fit of the whole curve.

Since only parameters and function of the left heart are considered, the respective parameters of the right heart are kept in a physiologic range by altering them simultaneously to the left heart parameters.

3.4.1 Initialization of the model

As a starting point, a reference simulation model of a normal, healthy cardiovascular system is altered by general parameters according to those measured in a subject

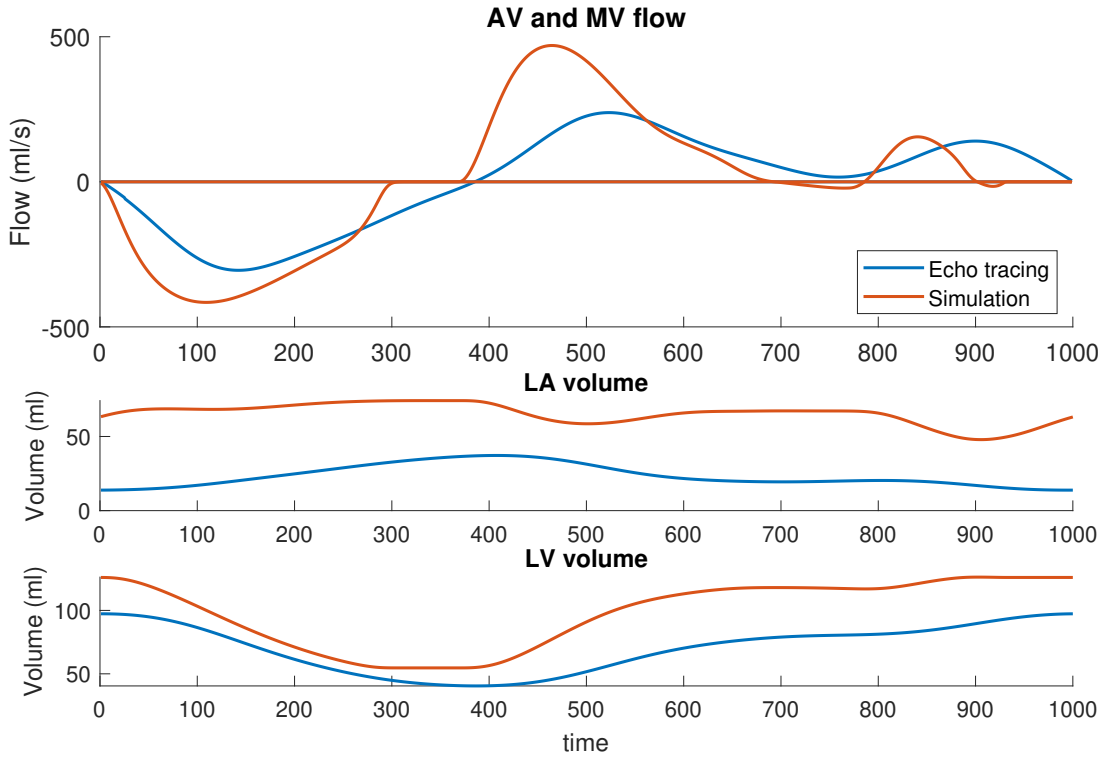

Figure 12: Flow velocity and volume curves of the reference P structure

cohort. These parameters serve as an input for the simulation and are considered as fixed. The following fixed parameters are defined.

Cycle time t_{cycle}, calculated from the heart rate.

Cardiac output The value for the cardiac output q_0 is available through different measurement methods, i.e. directly measured in a Doppler measurement, as well as calculated from a biplane or triplane view. The methods differ in accuracy. It is necessary to be consistent in the method that is used to determine cardiac output and values for volume and flow to prevent comparing values that are prone to different uncertainty sources. In this study, we used the CO calculated from the triplane view.

Mean arterial pressure Mean arterial pressure (MAP) p_0 cannot be retrieved directly from an echocardiographic assessment. However, from the peak values, i.e. systolic and diastolic blood pressure, a good estimation can be provided for the initialization of the model. As the blood pressure levels are highly dependent on vascular stiffness, the mean arterial stiffness is updated after a first optimization (explained in Section 3.4.2).

After initializing the model, a simulation is run to carry out as many heartbeats as it requires for the pressure-flow regulation to induce a steady solution. This is

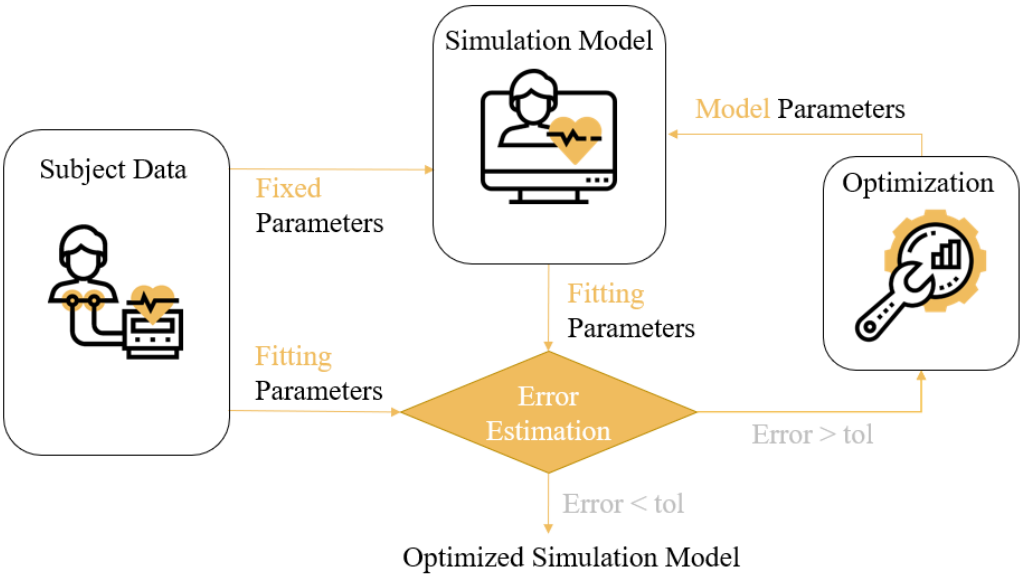

Figure 13: Parameter fitting procedure

necessary to claim that the reference model is hemodynamically stable. An adaptation of the model using different exercise states as described in Section 2.3.1 would be advisable if only one age group was considered. Cardiac and vascular wall thickness, area and passive stiffness adapt to the altered initial conditions when facing different loading conditions, which is the case in reality. However, the adaptation protocol is not used here, since it is aimed to compare the models of different population groups. An adaptation of the wall parameters would lead to a different starting model for each age group, making it difficult to compare the results from the optimization process. In order to validate the choice of the fixed parameters, a sensitivity analysis is performed to see their influence on the result and to assess if they can confidently be considered as fixed. It is aimed to investigate the relation between the uncertainty of values used as fixed parameters in terms of measurement errors compared to their impact on the resulting output. The sensitivity analysis is performed for this initial state of the model, providing information about in what manner the fitting parameters change with small changes in the input parameters in Section 4.2.2.

3.4.2 Optimization regarding blood pressure

Systolic and diastolic blood pressure (SBP and DBP) are available for all subjects within the measurement data. CircAdapt bases its simulations on the general parameters pressure, flow and time of one beat. The MAP p_0 defines the average blood pressure during a full cycle. MAP is calculated from the systemic arteries pressure curve over one heartbeat. Pressure levels are dependent on the transmural pressure within the vessel walls and the wall fiber stiffness in arteries and veins. This is a consequence of Laplace's law [27], which states that the tension in the myocardial

fibers equals the ventricular pressure multiplied by the volume divided by the wall thickness. The blood pressure levels in the model are in a first optimization aimed to be fitted to systolic and diastolic blood pressure retrieved from the population group or individual.

As displayed in Table 5, the model parameters p_0 and k are varied, i.e. mean arterial pressure and the stiffness coefficient of the vasculature, respectively. The error between the measured and simulated blood pressure values is aimed to be minimized. The stiffness coefficient is altered simultaneously for both arteries and veins. MAP has been approximated in the initialization step and shall be enhanced by this optimization.

Model parameters		**Fitting values**
p_0 (Pa)	Mean arterial pressure	Systolic blood pressure
k	Vessel stiffness	Diastolic blood pressure

Table 5: Model parameters and fitting values of Optimization 1

The respective objective function retrieves the P structure with the modified fix parameters of each age group and modifies the values for vessel stiffness and MAP. It generates a steady solution for the model and compares the arterial pressure peak values to the measured blood pressure values. For the comparison, the absolute error is computed

$$\mathrm{e}_{SBP} = \|SBP_{sim} - SBP_{tr}\| \tag{5}$$

for the systolic blood pressure and likewise for the diastolic blood pressure. The total error that is aimed to be minimized is then

$$\mathrm{e}_{tot} = \mathrm{e}_{SBP} + \mathrm{e}_{DBP} \ . \tag{6}$$

As an optimization algorithm, the surrogate optimization from MATLAB's Global Optimization Toolbox is used as it is able to find a global optimum with a relatively small number of executions of the objective function. This is explained in detail in Section 3.5. An error tolerance of $e_{tot} \leq 0.01\,\mathrm{Pa}$ is defined. The minimum number of random sample points is kept at the default value of 20.

The resulting updated model is used as a context for the next optimization step.

3.4.3 Optimization regarding model parameters

In the next step, the MV flow velocity curve is investigated, along with the volume curves of the LA and LV. In order to fit these model outputs to the echocardiography curves, parameters involved in the patterns are used as degrees of freedom. Table 6 provides an overview of both fitting and model parameters.

The model parameters represent the degrees of freedom of the problem, whereas the fitting values represent constraints that restrict the degrees of freedom. In this problem, the number of fitting values $N_{fit} = 8$ exceeds the number of model parameters $N_{mod} = 7$, therefore the system is overdetermined and in theory is inconsistent,

Model parameters		Fitting values
$\sigma_{f,pas}$ (Pa)	Passive stiffness of LV, LA	Peak values of E-wave, A-wave
$\sigma_{f,act}$ (Pa)	Active stiffness of LV, LA	Peak value of ejection wave
t_D (s)	Decay time of LV	Ratio E/A
A (m^2)	Opening areas of MV and AV	Deceleration time of E-wave
		Max, min. LV volume
		Ratio max./min. LA volume

Table 6: Model parameters and fitting values of Optimization 2

i.e. it has no solution. However as it is an optimization problem, the lowest value of the objective function represents a global solution. Also, because of the underlying biomechanical model, the model parameters have cross-correlating effects that practically reduce the constraints, i.e. the targeted fitting values.

The objective function retrieves the previously created heart model, where the model parameters passive and active stiffness ($\sigma_{f,pas}$ and $\sigma_{f,act}$) of LA and LV, decay time t_D of the ventricular contraction and the areas of MV and AV are set as free input parameters. Boundaries are set according to physiologic levels retrieved from literature [8, 32, 53]. For example, the average MV area ranges between $4 \cdot 10^{-4}\,m^2$ and $6 \cdot 10^{-4}\,m^2$ [21, 50], therefore the boundary are set loosely around this range. To avoid overfitting, this rather limited set of model parameters is used to fit characteristic values of the flow and volume patterns. The resulting optimized model serves as an initial context for another optimization which aims to fit more curve characteristics. The fitting parameters for this second optimization are explained in detail and visualized in Section 3.3.

Note that the model parameters regard the left heart, since the comparison of the data uses displays of the function of the left heart. However, it is not expected to have major functional differences between the patches of the left and right myocardial walls as this would cause a mechanical disequilibrium in the coupling of the walls as well as the hemodynamics. Therefore, assume that properties of the patches of the right heart change relative to those of the left heart by copying the properties between the respective sides.

For the comparison of the blood flow, the total volume flow is considered rather than a flow velocity. The reason for this is the relatively inaccurate measurement data of the valve areas and can be improved with additional information. Therefore, the absolute values of the peaks are given in ml/s. Additionally to the peak values, the E/A ratio is considered as it provides insight into the diastolic function [3]. The pattern of the decay of the ventricular contraction is of interest as well, since physiological information about the behavior of ventricular tissue in diastole can be retrieved.

Since the MV flow mostly contains information about the interaction between the LA and LV, independent information about the two chambers provided by the volume curves is used to restrict the cohort of possible solutions. For the left ventricle, end-systolic and end-diastolic volume are used as comparison characteristics.

Since for the LA the reliability of the measurements is restricted, only the ratio between the maximum and minimum value is taken into consideration.

These comparison characteristics have different units and values, therefore a total error combines the relative error of each of the characteristics in the objective function. The total error expresses, to which the characteristics of the simulated model $ch_{i,sim}$ differ from the ones retrieved from the measured tracings $ch_{i,tr}$

$$\mathrm{e}_i = \left\| \frac{ch_{i,sim} - ch_{i,tr}}{ch_{i,tr}} \right\| , \qquad \mathrm{e}_{tot} = \sum_{i=1}^{N_{fit}} \mathrm{e}_i w_i , \tag{7}$$

where N_{fit} is the number of fitting parameters. This calculation also includes a weighting of the single errors w_i, which is dependent on how important they are to fit the whole curve and how reliable they can be computed or compared. The total error is then aimed to be minimized by an optimization algorithm. As in the last section, surrogate optimization is used to obtain the best solution. As the number of degrees of freedom is significantly higher and the error function more complex, the maximum number of evaluations is raised to $N_{max} = 350$. Hence, the optimization is aborted after 350 function evaluations and the best parameter set is declared as the optimal solution. The computation time is reduced by using parallel computing.

3.4.4 Expansion of the model parameter set

Having optimized the model parameters of Section 3.4.3, the resulting model is used as an initial context for the next optimization step. This means, the optimal values of the model parameters are used as a starting point and are more tightly bounded. New parameters are added to fit more characteristics of the curve. In this step, timing parameters are aimed to be fitted. Since a change of related model parameters will also influence the fitting parameters of Section 3.4.3, the model parameters are added and not replaced. Table 7 shows the parameter sets. Overdetermination is even more prominent for this optimization step, since there are $N_{fit} = 15$ fitting values, but only $N_{mod} = 11$ model parameters. However, the correlations within the fitting values restrict the constraints and enable the optimization to a global solution.

Model parameters		**Fitting values**
t_R (s)	Rise time of LV, LA	Time positions E-wave, A-wave
$TimeFac$	Time factor	Time position ejection wave
$d\tau_{av}$ (s)	Atrioventricular activation delay	Width E-wave, A-wave
	+ parameter from Optimization 2	Time difference ejection-E and E-A
		+ values from Optimization 2

Table 7: Model parameters and fitting values of Optimization 3

The total error is calculated in the same way as described in Section 3.4.3 with one exception: the absolute time values are not ought to be dependent on their

occurrence within one cycle, therefore the error is divided by the total cycle time instead of the position of the tracing time point

$$\mathrm{e}_i = \left\| \frac{ch_{i,sim} - ch_{i,tr}}{t_{cycle}} \right\| . \tag{8}$$

Since this generally makes these time errors smaller in comparison to normal relative errors, their weighting is increased accordingly. The surrogate optimization increases in computational effort as more free parameters are involved. Maximum number of function evaluations is set to $N_{max} = 550$.

3.4.5 Quantification of the fitting

As described in Section 3.4.3 and 3.4.4, the quality of the fit is quantified by the sum of the error of the fitting values e_i, multiplied by weighting factors w_i. In Optimization 2, the total error expands to the following

$$\mathrm{e}_{tot} = \sum_{i=1}^{N_{fit}} \mathrm{e}_i w_i = \sum_{i=1}^{10} \mathrm{e}_i w_i \ . \tag{9}$$

The fitting values and respective weightings are determined based on the following regards. First, they are chosen so that the overall fit of the curves is optimal. Correlations with other fitting values are taken into account. For instance, a fitting parameter having negative interference on other values, i.e. worsening the fit significantly for other parts of the curves, is used with a lower weighting. Also, the comparability of the respective characteristics between the curves is accounted for. Lastly, a sensitivity analysis like in Section 4.2.2 is performed in order to track the influence of different model parameters on the single fitting values. The following fitting values and weights are used in Optimization 2:

Height of the E-wave $e_{E,y}$ with $w_{E,y} = 0.17$. The maximum flow velocity in the early filling phase. It carries information about ventricular and atrial properties. This is important for the fitting of the diastolic function, hence it has a relatively high weighting.

Height of the A-wave $e_{A,y}$ with $w_{A,y} = 0.43$. Maximum flow velocity in atrial injection. Influenced by atrial function and ventricular properties. High weighting due to significance for the cardiac function.

Height of the ejection wave $e_{EJ,y}$ with $w_{EJ,y} = 0.04$. Maximum flow during systole. Measure for ventricular function and general systolic function. Low weighting, because the absolute value of ejection peak is influenced by the way the curve is computed, see Section 4.2.1. Due to the known differences of the shape of the ejection curve that makes them less comparable, a higher weighting would cause the curve to overfit to the ejection curve, causing the reduction of the fit of the diastolic function.

E/A ratio $e_{E/A}$ with $w_{E/A} = 0.09$. This is an important measure for the LV function and often used as a clinical indicator of LV filling quality [3]. A relatively low weighting is applied because absolute values are already considered in $e_{E,y}$ and $e_{A,y}$.

Deceleration time of the E wave $e_{E,decel}$ with $w_{E,decel} = 0.04$. This value is directly related to the LV function. It is both influenced by passive and active stiffness of the myocardium and is hence an important indication for the myocardial properties. However, the slope can be influenced by averaging the curves within an age group and is therefore weighted low.

Minimum and maximum value of the LV volume curve $e_{LV,vol,min}$ with $w_{LV,vol,min} = 0.09$, $e_{LV,vol,max}$ with $w_{LV,vol,max} = 0.09$. Both maximum and minimum value are directly proportional to the myocardial stiffness. The stiffer the ventricle is, the higher preload is required in order to keep up the required stroke volume.

Ratio of maximum and minimum value of LA volume $e_{LA,vol,ratio}$ with $w_{LA,vol,r} = 0.04$. Since the LA volume measurement is rather imprecise, the algorithm only uses the ratio rather than absolute values and a low weighting. Therefore, the influence of measurement errors is reduced.

Expanding the problem to $N_{fit} = 15$ in Optimization 3, more fitting values are added; the existing ones are assigned to a reduced weighting. The total weight of the existing values is $w = 0.15$.

Time positions of E-wave, A-wave and ejection peak $e_{E,x}$, $e_{A,x}$ and $e_{EJ,x}$ with weightings $w_{E,x} = 0.22$, $w_{A,x} = 0.22$ and $w_{EJ,x} = 0.17$, respectively. The time positions within one cardiac cycle are assigned to the ventricular relaxation, atrial contraction and ventricular contraction, respectively. For the A-wave and the ejection wave, the timings are dependent on the activation of the patches. The timing of the E-wave is influenced by the mechanical behavior and pressure differences within the chambers. Weightings are chosen high because the matching of the curve shape largely depends on the time-axis position of the characteristics of the curves, which are aimed to fit in this third optimization step.

Time differences E-A and ejection-E Additionally to the absolute timings of the peaks, the time differences between both the E- and A-wave $e_{E-A,x}$ and the ejection and E-wave $e_{EJ-E,x}$ are considered. This is assigned to a lower weighting of $w_{E-A,x} = 0.06$ and $w_{EJ-E,x} = 0.06$.

Widths E-wave and A-wave The widths of the E- and A-wave $e_{E,w}$ and $e_{A,w}$ with $w_{E,w} = 0.06$ and $w_{A,w} = 0.06$ provide information about the mechanical and

elastic behavior of the myocardial tissue, as well as about the valves and interaction between the chambers.

3.5 Surrogate optimization method

In order to fit the resulting time-dependent waveforms from the in silico model to the measurement data, model parameters are altered in a systematic way, guiding the discrepancy between the curves to an achievable minimum. Within the fitting of a waveform, the deviation of characteristic parameters is considered, summarized by a total error value e_{tot}. The assessment of the quality of a fit was discussed in Section 3.3. This total error is aimed to be minimized.

To choose an appropriate optimization algorithm, the nature of the problem is investigated and the requirements on the solution determined. The objective function is composed of the creation of a model with modified parameters, the simulation of a steady solution and the assessment of the output functions with regards to the quality of the fit. Due to the beat-to-beat dynamics in finding a steady solution and the multiple solving of a system of partial differential equations, the evaluation of the objective function is computationally expensive. Performing one evaluation in MATLAB (R2019a) on an Intel(R) Core i7-6700K with 4.00GHz CPU takes approximately 20-30 seconds. At an average, several hundred evaluations are needed to perform an optimization. Since the model is based on biomechanics, its behavior is highly nonlinear and the objective function cannot be considered as smooth. This excludes the option to reliably approximate gradients by finite differences and therefore, gradient-based optimization methods are not suitable. Also, it is expected to have multiple local minima within the working space. In this section, the objective function is considered as a black box and the focus lies on the optimization.

The problem is subdivided into three optimizations as described in Section 3.4. These three optimizations have different properties and requirements, hence they require differentiated handling. For Optimization 1, i.e. optimization of the blood pressures, there are only two degrees of freedom. The objective function returns the absolute error of the difference of systolic and diastolic blood pressures, for which a maximum tolerance of $e_{tot} \leq 0.01$ is defined. A starting point and boundaries are known. In the second optimization, there are seven model parameters, hence the optimization gets more complex. Boundaries are set referring to literature values. Due to vast ranges and therefore a large parameter field, many local minima are expected and multiple starting points are necessary to detect a global one. As a starting point serves the result of Optimization 1, which can be far from the optimal solution. In the third optimization, more model parameters are added as degrees of freedom to a total of eleven. As a starting point, the resulting model from Optimization 2 is employed as it is expected to be close to the overall best model.

Surrogate algorithm

This framework uses a stochastic surrogate based optimization algorithm, as it has been proposed by Wang and Shoemaker [63]. This approach addresses global optimization problems with computationally expensive deterministic objective functions. As an extension to the previously proposed Metric Stochastic Response Surface (MSRS) algorithm by Regis and Shoemaker [49], the input space can be high-dimensional, though the problem must be bounded. It is aimed to find a reasonably satisfying solution using a limited number of function evaluations. The requirements on the objective function are low, i.e. it can be non-convex and without reliable gradient information. Hence, the method is suitable for the parameter calibration in complex computer simulation models. A random search method is used rather than a deterministic algorithm since the latter are generally not able to solve high dimensional problems as efficiently as random methods. In particular with regard to future implementations, where more model parameters are to be fitted, a solution that has a high probability of being correct is accepted, rather than claiming that the solution is exclusively correct.

It follows an explanation of the functionality of the surrogate optimization algorithm. It is implemented in MATLAB within the Global Optimization Toolbox. As an input, the algorithm requires a continuous function f, which is defined in $\mathcal{D} = \mathbb{R}^{N_{mod}}$, where N_{mod} is the number of problem variables. A set of initial evaluation points $\mathcal{I}$ 'random samples' is created from a quasirandom sequence, which is similar to a pseudorandom sequence, but the results are more evenly distributed within the parameter space $\mathcal{D}$. The maximum number of function evaluations is defined as $N_{max} = 50 \cdot N_{mod}$, which comes to $N_{max} = 350$ and $N_{max} = 550$ for Optimization 2 and 3, respectively.

Step 1: Construct Surrogate The costly function is evaluated at the random sample points $\mathcal{I}$. A surrogate (also called response surface or metamodel) is created by interpolating a radial basis function (RBF) through the initial points.

Step 2: Search for Minimum In this step, the algorithm searches for a minimum by analyzing and updating the surrogate. Hence, with every iteration n of this step, the surrogate more and more reflects the information of the black box objective function via adaptive learning. The next point to perform a function evaluation on, a so-called "adaptive sample" is chosen based on a merit function underlying the surrogate. However, if the merit function equals the surrogate and therefore the next adaptive sample is always the minimum of the surrogate, the algorithm might get stuck in a local solution, as the chosen point is likely to be very close to the last evaluation point and the solution already known. In order to prevent this, Wang and Shoemaker [63] proposed a criterion for choosing the next adaptive sample more intelligently. First, a perturbation of the parameters of the current best solution point provides a set of random candidate points within the given boundaries. The probability for each parameter to be perturbed is based on the current learning of the information on the objective function, for example local sensitivity information,

measured on the surrogate surface. More sensitive parameters are more likely to be perturbed, as they are most promising to contribute to a better solution. The probability can lie anywhere between 0 and 1, therefore it is possible that only a subset of the parameters is perturbed. The surrogate is evaluated on each of the random candidate points. This process is computationally cheap given the simplicity of the surrogate. Finally, the next evaluation point is chosen based on the merit function f_{merit}, which is a weighted sum of the surrogate value $s(\mathbf{x})$ of the random candidate point and the distance from the previous adaptive sample $d(\mathbf{x})$

$$f_{merit}(\mathbf{x}) = w_n^S \frac{s(\mathbf{x}) - s_{min}}{s_{max} - s_{min}} + w_n^D \frac{d_{min} - d(\mathbf{x})}{d_{max} - d_{min}} , \tag{10}$$

where the weightings $w_n^S + w_n^D = 1$ control the balance between the surrogate value criteria and the distance criteria. This way, it is aimed to both find the data point with the best value, but also the one providing most new information about the objective function to help the adaptive learning. Then, the original objective function is evaluated at the chosen adaptive sample point and the surrogate updated including information of this point. This step is repeated until the stopping criterion has been met, which can be the maximum number of function evaluations or the objective value has reached the desired tolerance.

The optimization being trapped in a local minimum is caught by performing a "surrogate reset" if the distance of all random candidate points to the previous point falls below the minimum sample distance. Then, the algorithm switches from Step 2 back to Step 1.

Generally, the use of any type of response surface to construct a surrogate is possible. In an RBF, the complex objective function is expressed as a weighted sum of simple functions. According to Gutmann [18] and Buhmann [11], the advantages are, that the interpolation itself, as well as adding data points and evaluating the function on other points is fast and computationally cheap. Also, the interpolated function takes exactly the given values on the evaluated points. MATLAB uses a cubic RBF with a linear tail, which is ought to minimize bumpiness, according to Gutmann [18]. On a machine with more than one core, the optimization can be run on workers (MATLAB computational engines) that run locally. The expensive objective function evaluations are run in parallel, whereas the control of the adaptive points and hence the construction and update of the merit function is consistently performed on one worker as it is computationally cheap. In order to keep the sequence of the adaptive learning, a queue of adaptive points is maintained to be evaluated in a FIFO order. The available machine is able to employ four workers, which reduces the computation time significantly.

Figure 14 shows an exemplar surrogate plot that has been generated in Optimization 1 for age group 4. The light blue triangles represent the initial samples that have been evaluated as a base for the surrogate. The best value is highlighted by a green circle. It follows the phase of searching for a minimum (Step 2): The result of the evaluation of each adaptive sample is marked by a black dot. Its value decreases converging towards a minimum, until the algorithm stops after reaching the tolerance of 0.01. In the presented example it took 82 function evaluations to

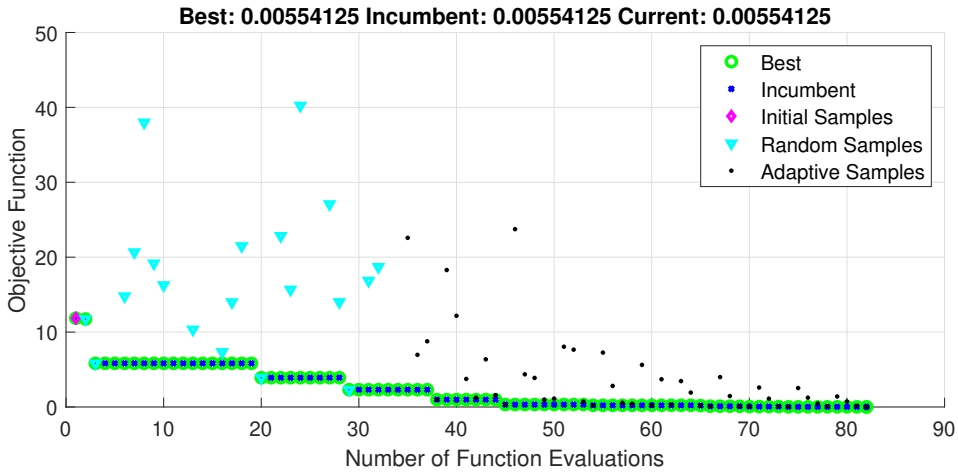

Figure 14: Example for a surrogate plot; Optimization 1 for age group 4

reach a minimum that satisfies the required precision.

Another requirement for the implementation of the optimization in order to make it easier to work with in future projects is, that it should reliably work on low-level hardware. Since one fitting is a series of operations including the optimization, hang-ups are considered by logging every iteration into a separate file to be able to resume the program and not having to restart.

Additionally, errors might occur within the objective function evaluation. First, the success of CircAdapt finding a steady solution for the model is not always granted. For some parameter sets, the algorithm is not able to solve the system of partial differential equations. If the system has been successfully solved, however, the pattern of the output function can take various forms, of which not every curve is realistic or close to the expected waveform. If the deviation is large, some error values might not be computable. For example, if the distance between the E- and the A-wave is very short, the waves become joined. Then, the algorithm is unable to detect the locations of each peak properly, which leads to an error in evaluating the deviation of the peak coordinates to the ones of the measurement data. The optimization algorithm takes such cases into account by employing a penalty function, which sets the error to a given, large value in order to omit this set of parameters as a potential candidate for the best solution.

Subsequent outlier filtering

As the objective function is based on a biomechanical model, which is highly nonlinear, outliers can happen in the objective function evaluation. Sources of these uncertainties can differ: The simulation model itself has limitations, such as the inability of finding a steady solution for every possible model parameter set. This might stem from the physical dependencies that underlie the model. As stated before, the objective function can therefore not be considered as a smooth continuous function. Also, errors can happen in the later calculation of the fitting values. The reason for this could, for instance, be memory allocation issues within the code.

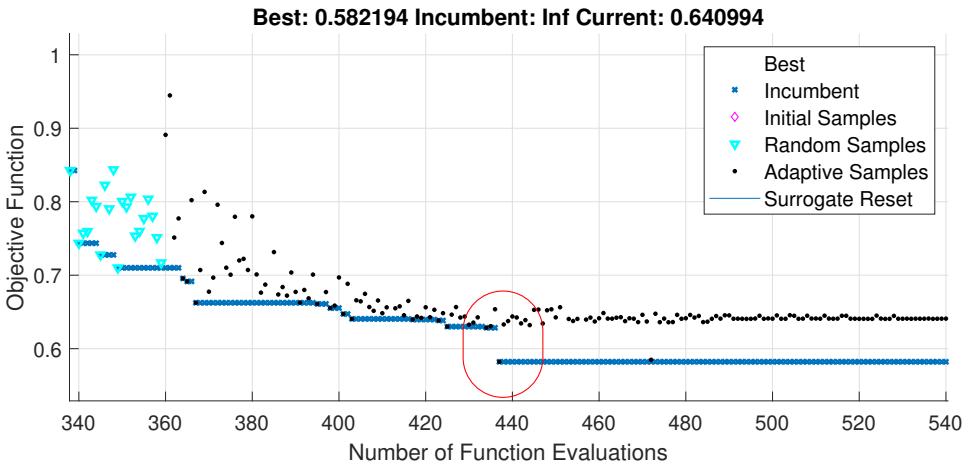

Figure 15: Exemplary surrogate plot with negative outliers

'Positive' outliers, i.e. outliers, for which the total error is unexpectedly high, are normal considering the optimization algorithm. The algorithm makes a guess on the best value without knowing the exact shape of the objective function. This will in most cases not be the global minimum and the surrogate is updated using this sample. However, 'negative' outliers do occur. This means, for one or more instances, the total error is significantly lower than for similar model parameter sets. This is most likely due to a computational error. Figure 15 shows a surrogate plot, where negative outliers exist. At the 437^{th} function evaluation (red oval), the function value is extremely low compared to previous evaluations and also compared to the boundary that the error function is converging to. Re-evaluating the model for

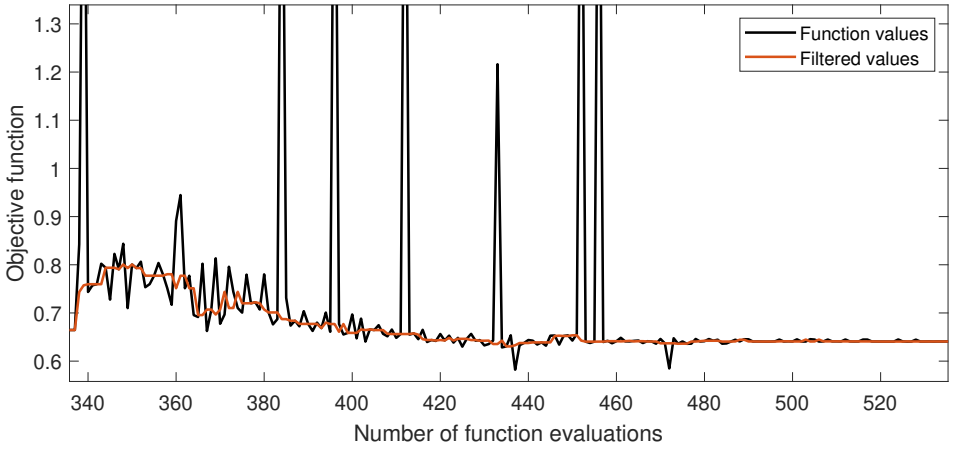

Figure 16: Function values after subsequent error value filtering

this model parameter set delivers a different, higher result. Hence, one can conclude that a computation error is present. The dark blue 'x' indicates that this is the best function value and finally chosen as the optimal solution. In order to avoid

such errors in choosing an outlier as the best solution, the chosen solution is altered for such cases. The model parameter sets with the appropriate function values are saved in a checkpoint file during the optimization. The function values are plotted in Figure16. Subsequently, a filter is applied to remove scattered outliers. A one-dimensional 5^{th} order median filter from MATLAB's Signal Processing Toolbox [47] is employed for this purpose. The filtered signal is shown by the red line in Figure 16. Eventually, the minimum of the filtered signal is determined and the respective model parameter set replaces the best solution chosen by the optimization algorithm.

4 Results

The methodology described in Section 3 is applied to the population-specific data and age-related changes are derived from the results. The optimized models are critically assessed and validated based on various aspects. Finally, a subject-specific data set is used as an input, verifying the applicability of the framework.

4.1 Results of the optimization

The framework has been run five times for each age group in order to review its behavior with different random sample points. The total time of the computation was approximately 4 days, which means, it takes around 18 hours to compute one run.

The total error of the final solution of each age group can be reviewed in Table 13 in Appendix B. For the evaluation of the results, the best runs according to the lowest total error are chosen. After the second optimization, the absolute values, deceleration time and volumes are fitted. Figure 17 shows the resulting curve of this step. The characteristic points and the mean slope that were used to calculate the error values are highlighted in the graph. The final resulting fitted flow and volume curve is presented in Figure 18 for the first age group. Appropriate figures for the other age groups are attached in Figure 27 in Appendix B.

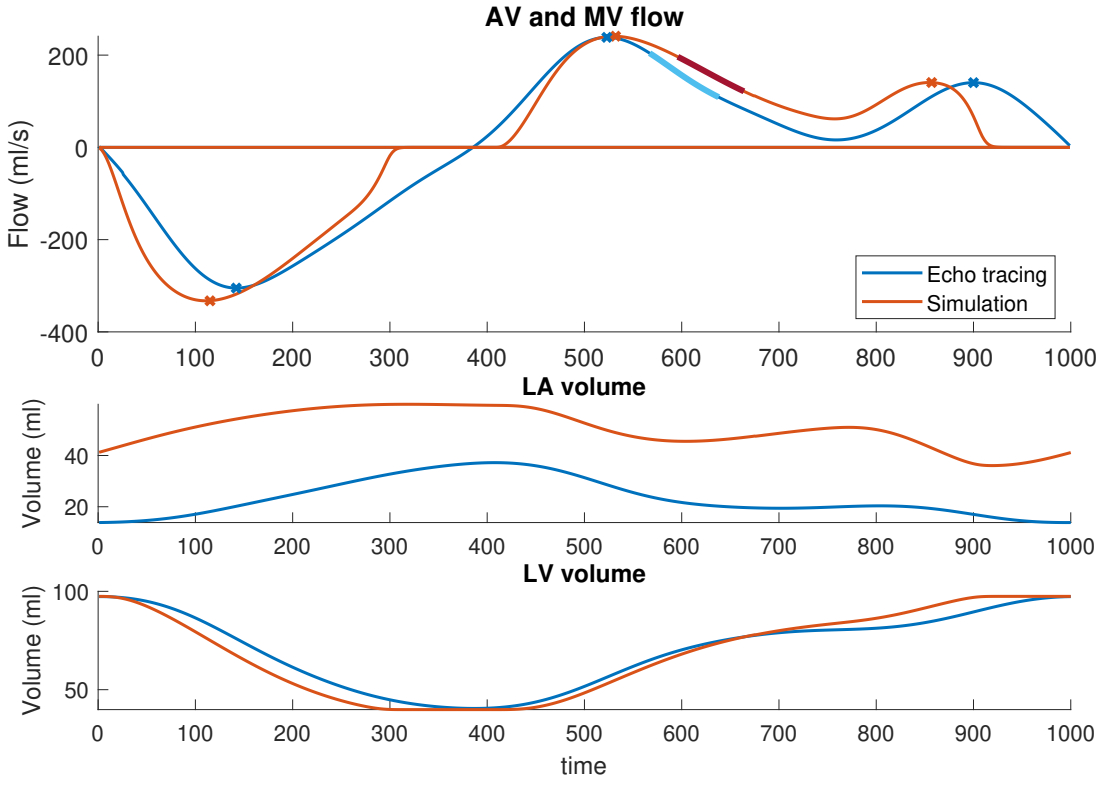

Figure 17: Model for age group 1 after the second optimization step

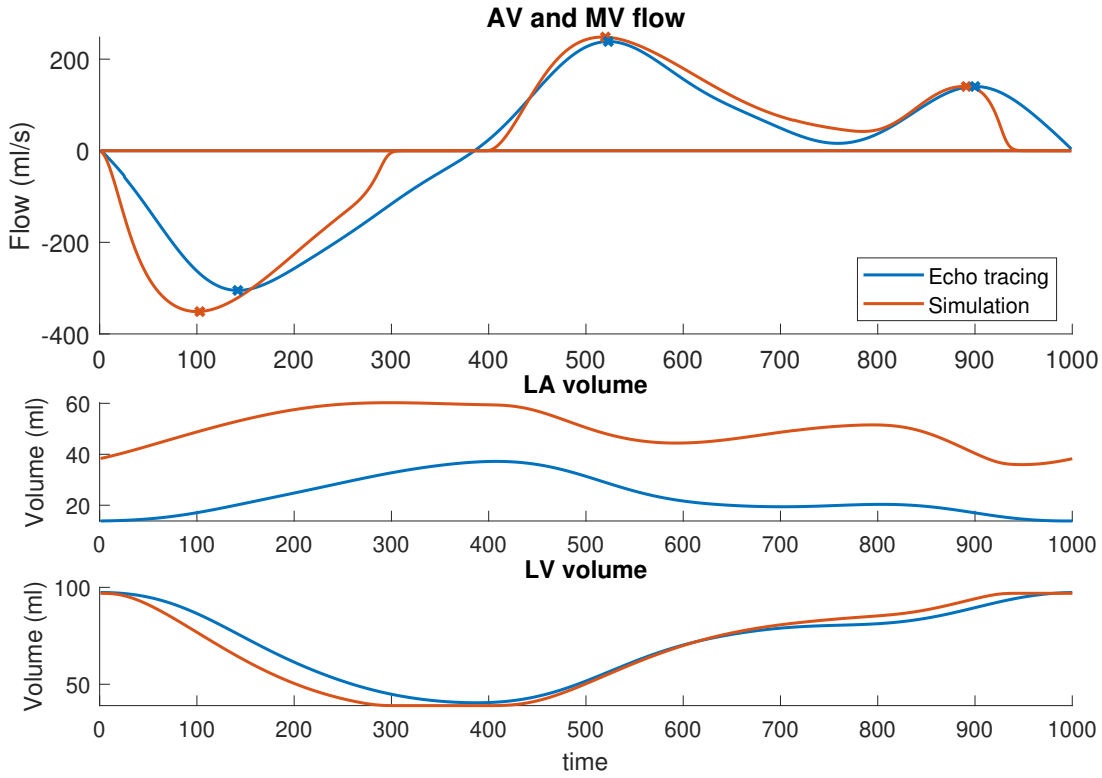

Figure 18: Optimal fit for age group 1

Optimized model parameters for every age group are listed in Tables 15 and 16. The numbers represent the modification of the initial value of the model parameter in percent for every age group. Table 15 shows the results of Optimization 2, whereas Table 16 shows the respective results of Optimization 3. The total change of one model parameter is therefore calculated by adding the values from both tables. The boundaries set for each parameter are stated in the first line. The resulting model parameters of the optimized model are displayed in Table 8.

4.2 Validation of the solution

The optimized solution is validated in terms of feasibility and uniqueness. In prospect of the use in clinical practice, users are to be convinced that the presented solution is sufficient and physiologically correct. To prove the methodology it is shown that the result fulfills basic guidelines of consistency and cardiac properties agree with values found in literature. One should bear in mind that the initial model has not been created based on real data and therefore lacks the level of detail we aim to provide for the fitting. It is rather used as a starting point with valid properties within a physiologic range. Therefore it is abstained from using the reference model for validation or comparisons. In the following section, the validation of the result is explained exemplified by the analysis of the first age group.

$t_{R,LA}$	=	0.395 s
$t_{R,LV}$	=	0.211 s
$TimeFac$	=	1.082
$d\tau_{av}$	=	−0.00932 s
$\sigma_{f,pas,LA}$	=	30989.6 Pa
$\sigma_{f,pas,LV}$	=	6120.9 Pa
$\sigma_{f,act,LA}$	=	25316.9 Pa
$\sigma_{f,act,LV}$	=	168437.7 Pa
$t_{D,LV}$	=	0.207 s
A_{MV}	=	0.000345 m^2
A_{AV}	=	0.000224 m^2

Table 8: Values of model parameters of the optimized model for age group 1

4.2.1 Consistency and physiological correctness

Valve Areas The valve diameters can be estimated from the two-dimensional echocardiographic images in apical view, though the computation of the opening area is only an estimation. The irregular shape of the valve and potentially misaligned view angle increase susceptibility to errors. For the MV, the valve diameter can be determined reliably through volume change and Doppler curves. Since this approach used the MV and AV areas as variable model parameters, the measured or calculated values are used as a validation. However, since the model uses spherical cavities, exact agreement between the valve areas can be diluted. Also, it is assumed that all study subjects had competent valves without leakage. Considering these constraints, the relative errors of the simulated and validation value are calculated and found to be within a range of $< 40\%$ for every valve and age group.

Age group	1		2		3		4		5		6	
	MV	AV	MV	AV	MV	AV	MV	AV	MV	AV	MV	AV
Simulation	3.45	2.24	2.59	2.11	2.70	2.00	3.20	2.15	2.86	2.80	2.75	2.99
Echo	3.98	2.32	4.20	2.46	4.11	2.40	4.02	2.38	3.93	2.29	4.11	2.28
Rel. Error	13.3	3.3	38.5	14.2	34.3	16.9	20.4	9.6	27.3	22.5	33.2	31.2

Table 9: Mitral and aortic valve opening areas resulted by simulation and from the echocardiographic measurements and calculations herefrom; relative error in percent

Total Ejection As stated in Section 4.1, the relative error of the maximum flow velocity in the systole, i.e. the ejection peak, has an offset of about $e_{EJ,y} = 15\%$. To compare the systolic flow of simulation and tracing, the total volume that is ejected during systole, i.e. the stroke volume, is also taken into account. For this comparison, the area under the aortic valve flow velocity curve is computed for both model and measurement. Figure 19 shows both curves, scaled and positioned to start with the opening of the aortic valve.

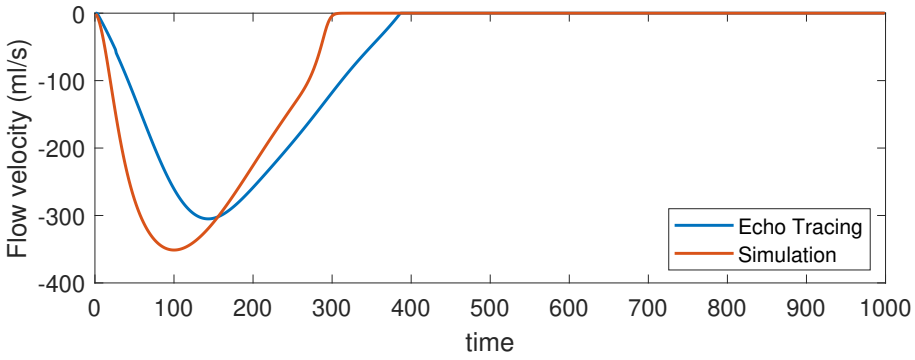

Figure 19: Aortic valve flow curves of simulation and measurement

The absolute area under the curves, which equals the total ejected blood is $SV_{sim} = 76.77\,\text{ml}$ and $SV_{tr} = 75.45\,\text{ml}$, for simulation curve and tracing, respectively. This means an absolute deviation of $e_{SV} = 1.75\%$. Hence it can be concluded that the systolic function in both the averaged population group and the simulated model is very close.

Myocardial performance index By the myocardial performance index (MPI), we investigate the isovolumetric phases which have not been considered in the fitting procedure due to the inability to see them in the flow velocity curves. The MPI is defined as

$$\text{MPI} = \frac{\text{IVCT} + \text{IVRT}}{\text{ET}}\,, \tag{11}$$

where IVCT and IVRT are the isovolumetric contraction and relaxation times, respectively. These are the time frames in which the ventricle contracts or relaxes, but the volume is kept upright by pressure changes. The ejection time (ET) is the time of the systole. The isovolumetric contraction and relaxation times are not displayed in the flow velocity curves derived from the volume curves. This is first due to the consideration of multiple curves, creating one average curve. Therefore, plateaus are evened out. Secondly, the motion of the myocardium ceases at no point in the cardiac cycle. When both valves are shut, contraction or relaxation attenuates until the next valve opens again. A small portion of blood is also pushed in the opposite direction, causing the valve leaflets to close the valve. This small regurgitation is reported as positive flow in the volume curve, but as a negative flow in Doppler echocardiography.

The mean MPI for the first age group in the measurements is 0.2626, whilst the MPI of the optimized solution comes to 0.5191. This means a deviation of 97.67%.

4.2.2 Sensitivity analysis

Data inputs, as well as model simulation results, are prone to uncertainty. To evaluate the impact of uncertainty in single input values, a sensitivity analysis is performed.

Firstly, the effect of uncertainty in the fixed parameters, i.e. the cycle time, CO and MAP, is investigated. As the used data is collected within the WASE study or calculated from values therein, those values are also prone to measurement errors or inaccuracies. These uncertainties propagate through the system, leading to inaccurate results. A one-at-a-time analysis is performed for the fixed parameters using the optimized model for the first age group. For a 10% variation in the fixed parameters, the impact on the result is evaluated and presented as a percentage in Table 10. Colors indicate significantly high (red) or low (blue) values.

	t_{cycle}	q_0	p_0
time pos. E	5.33	0.89	0.89
time pos. A	10.08	0.78	0.26
time pos. EJ	4.65	2.33	2.33
time diff. EA	16.67	3.09	1.85
width E	4.80	2.54	0.70
width A	10.09	1.97	0.28
hight E	7.67	9.77	0.32
hight A	11.03	0.70	1.55
hight EJ	4.65	8.43	0.40
E to A	21.01	10.55	1.21
decel. slope	2.59	4.21	0.09
min LV vol	3.97	3.51	6.11
max LV vol	4.37	4.46	2.48
min LA vol	1.47	2.98	1.31
max LA vol	3.12	3.81	0.91
ratio LA vol	1.63	0.81	0.40

Colors
22.00
20.00
18.00
16.00
14.00
12.00
10.00
8.00
6.00
4.00
2.00
0.00

Table 10: Sensitivity analysis for the fix parameters, sensitivity of the curve characteristics in per cent for a 10% model parameter change

A relatively low impact of changes on the MAP p_0 can be observed, whereas high sensitivity is given for changes on the cycle time t_{cycle}. Especially the correlation of E- and A-peak is significantly dependent on the cycle time. Since the E/A ratio and time difference are important measures in the assessment of age-dependent changes, it is crucial that the quality of the cycle time calculation is sufficient.

Secondly, the impact of small variations in the model parameters on the uncertainty of the output is evaluated. This analysis aims to assure confidence in the model and detect inconsistencies. For example, unexpectedly high influence of a small variation of a model parameter on a part of the output that should not be interrelated can be further investigated. Moreover, model parameters that do not contribute to the achievement of improving the curve fitting at all can be detected and omitted for further runs.

To validate that the found solution is unique, a global sensitivity analysis would deliver appropriate results. However, global methods are computationally costly; additionally, the optimization is performed with a global optimization tool, which reassures that the solution is a global minimum. Also, due to the highly nonlinear

	$t_{R,LA}$	$t_{R,LV}$	TmeFac	dt_{av}	$\sigma_{f,pas,LA}$	$\sigma_{f,pas,LV}$	$\sigma_{f,act,LA}$	$\sigma_{f,act,LV}$	$t_{D,LV}$	A_{MV}	A_{AV}
time pos. E	3.45	4.31	4.74	2.59	2.59	2.59	3.02	3.45	0.43	2.16	2.59
time pos. A	4.01	2.41	2.94	1.60	4.01	4.01	3.21	4.28	4.01	3.74	4.01
time pos. EJ	14.00	6.00	8.00	14.00	10.00	10.00	14.00	14.00	10.00	10.00	12.00
time diff. EA	16.20	13.38	0.00	8.45	14.79	14.79	13.38	16.90	9.86	13.38	14.79
width E	2.99	3.85	0.58	3.69	2.45	4.20	3.50	4.89	0.47	7.90	3.27
width A	9.25	2.46	8.50	3.90	6.93	4.20	3.07	4.24	4.61	2.28	4.33
hight E	4.26	2.20	2.50	1.18	2.94	3.69	1.45	5.02	0.35	6.59	2.72
hight A	7.23	0.57	2.29	3.22	6.48	1.27	5.32	3.00	2.28	2.37	0.36
hight EJ	5.10	3.37	0.16	5.18	5.23	5.10	5.12	7.93	5.27	5.22	6.53
E to A	12.39	1.62	0.21	1.97	10.07	5.03	3.67	8.27	1.88	4.12	3.08
decel. slope	6.89	6.18	5.89	6.81	3.64	8.40	5.86	11.06	2.17	21.38	6.41
min LV vol	2.29	2.01	3.82	2.21	2.27	2.26	2.22	8.37	2.04	2.23	2.36
max LV vol	0.89	0.87	1.54	0.79	0.79	0.88	0.85	3.35	0.77	0.78	0.80
min LA vol	3.66	0.18	1.41	3.18	0.01	0.18	3.56	0.30	0.37	1.20	0.45
max LA vol	0.88	0.62	0.59	0.50	1.64	0.63	0.23	0.39	0.34	0.04	0.28
ratio LA vol	2.68	0.80	0.81	2.77	1.65	0.45	3.45	0.69	0.72	1.25	0.74

Table 11: Results of the sensitivity analysis, sensitivity of the curve characteristics in per cent for a 10% model parameter change

and non-smooth behavior of the CircAdapt model, a global sensitivity analysis is computational expensive and difficult to interpret. Hence a local sensitivity analysis is performed in the location of the global minimum.

With the assumption of local linearity, the sensitivity is computed by the one-at-a-time methodology [12, 19]: variations in model parameters are analyzed independently while the other parameters are held fixed. This allows for a straight-forward evaluation of the single influence, however, it does not provide any information about interactions of model parameters. The sensitivity is then defined as the ratio between the output variation and the input variance. Table 11 shows the influence of a 10% variation of each model parameter from its initial value on the fitting values of the output. The optimized model is investigated for the first age group. Some curve characteristics are not sensitive to certain model parameters, those combinations have a sensitivity close to or equal zero and are color-coded in blue in the table. Significantly high influences are marked in shades of red. It can be noted that especially the volume parameters are little sensitive to changes in the model parameters. This strengthens the approach to consider flow velocity parameters for the model parameter estimation rather than only the volume curves. Time parameters and the deceleration of the E-wave are highly sensitive to most input parameters. The most sensitive correlation is found in the MV area and the E-wave deceleration behavior. This correlation can be explained by the dependency of the shape of the E-wave with the area of the MV. As the flow is induced by the passive suction of the LV, it is decelerated when the LV wall is fully relaxed. The MV area determines how easily blood can still flow from the LA to the LV when the pushing force from the pressure gradient decreases. However, the weighting of the deceleration time is low.

As sensitivity analyses are conducted throughout the development of the framework, the resulting sensitivity of the fitting values to changes on the model param-

eters is used for adjustments on the weightings of the fitting values. Though one can observe a high sensitivity of position and absolute value of the ejection peak, a relatively low weighting is added on it, as the position of the peaks differs due to the data acquisition as shown in Section 4.2. Coordinates and shapes of E- and A-peaks have a significant influence on the fitting and hence the respective fitting values are higher weighted. Values dependent on other fitting values, as time differences and ratios, are provided with a lower weighting to prevent overfitting, even when the sensitivity is high. Volume curves stay mostly unchanged with changes of the model parameters, hence a low weighting of the respective parameters is legitimate.

4.3 Age-dependent changes

This section investigates the changes in the model parameters of the optimal simulation models over the different age groups. Due to the use of averaged curves as an input for the optimization, it is aimed to retrieve information about general developments of CircAdapt model parameters, and therefore cardiovascular system properties, as they occur during aging regardless of inconsistencies or artifacts of single curves. As stated in Section 4.1 and visualized in Table 13, the best achieved total error differs between the runs, hence the optimized models are of different quality. For the assessment of age-dependent changes, the focus lies on the runs providing an acceptable result as defined by a maximum tolerance, which is chosen as $e_{tot} \leq 0.37$ for age groups 1 to 4 and $e_{tot} \leq 0.65$ for age groups 5 and 6. The tolerance for the older age groups is higher because the data of older subjects is less reliable, as it includes subjects with some distinctive features that were exclusion criteria for the other subjects (refer to Section 2.4), i.e. they are more likely to be asymptomatic rather than healthy. Also, the form differs more from the reference model and is thus more difficult to fit with only three optimization steps.

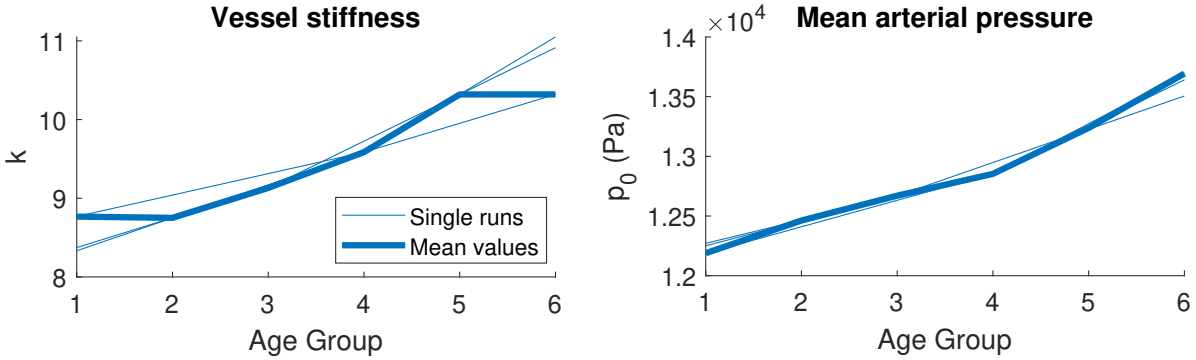

Figure 20: Change of the model parameters of the first optimization step over the age groups

First, the model parameters fitted to the blood pressure values are investigated. Hence, mean arterial pressure and mean vessel stiffness is retrieved from the optimized models of the first optimization step and plotted in Figure 20. The model parameters of the final models achieving results below the tolerance are retrieved

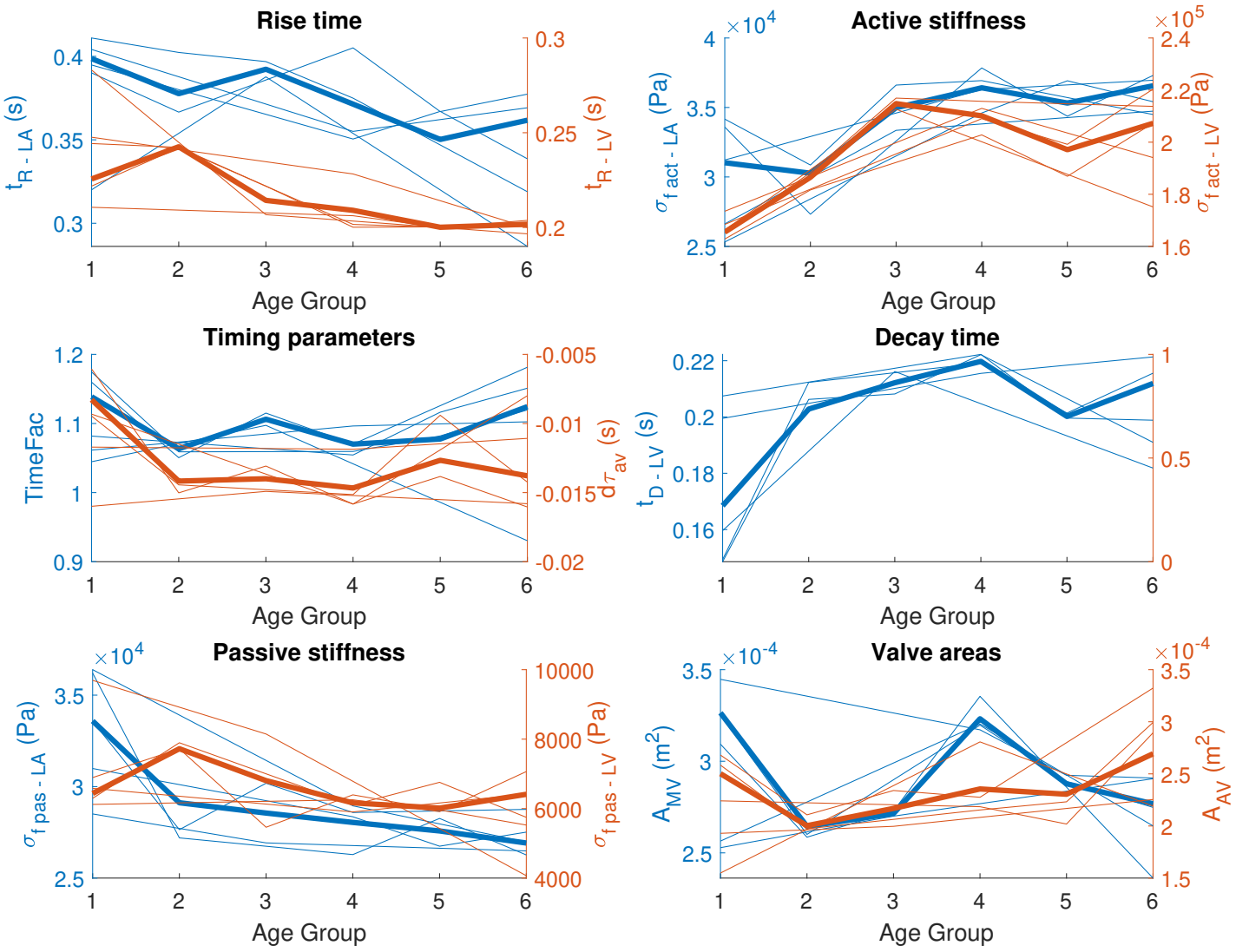

Figure 21: Change of the model parameters over the age groups in the final model

and shown as thin lines in Figure 21. Values between the age groups, as well as the missing values due to an exceeded tolerance are interpolated linearly for the visualization. The mean values of the considered runs are plotted as a thick line, showing the tendency of how the model parameter change with advanced age given by the multiple runs.

4.4 Application to subject-specific data

The framework is applied to subject-specific data in order to validate its feasibility for data of individual subjects. For this, one representative subject is picked out of each age group. For the selection, the focus lies on the availability and quality of the necessary data. Requirements on demographic information are not made since the framework must be applicable for all kinds of data independently from their age,

sex or ethnicity. Like for the population-specific data, the algorithm is run 5 times for each subject, assessing the respectively best result. For an exemplary subject of the first age group, the output of the resulting model is presented in Figure 22. Figure 22a shows the resulting fitting after the second optimization, whereas Figure 22b shows the final result. Fittings of the remaining age groups is presented in Figure 28 in Appendix B. Notably, some of the subject-specific waveforms deviate significantly from the average shape presented in Section 3.1 and hence require large modifications of model parameters.

Model parameter	**Value**	2^{nd} **Optimization**	3^{rd} **Optimization**
$t_{R,LA}$	0.480 s		20 ([-20,20])
$t_{R,LV}$	0.201 s		-19.47 ([-20,20])
$TimeFac$	0.986		-15 ([-15,15])
$d\tau_{av}$	−0.0186 s		-10 ([-10,10])
$\sigma_{f,pas,LA}$	29343.5 Pa	-12.34 ([-20,20])	-3.25 ([-5,5])
$\sigma_{f,pas,LV}$	8629.5 Pa	19.83 ([-20,20])	0.78 ([-5,5])
$\sigma_{f,act,LA}$	25324.6 Pa	-13.09 ([-20,20])	-3.09 ([-5,5])
$\sigma_{f,act,LV}$	218091.3 Pa	20 ([-20,20])	2.30 ([-5,5])
$t_{D,LV}$	0.222 s	20 ([-20,20])	4.84 ([-5,5])
A_{MV}	0.000350 m^2	9.84 ([-20,20])	-5.0 ([-5,5])
A_{AV}	0.000195 m^2	-19.58 ([-20,20])	-5.0 ([-5,5])

Table 12: Values of model parameters of the optimized model for a single subject from age group 1 and relative changes of the parameters

The resulting model parameters for the subjects of the first age group is shown in Table 12. Columns 3 and 4 represent the relative deviation of the parameters after Optimization 2 and 3, respectively, with the set boundaries in parenthesis. Hit or almost (within 5%) hit boundaries are highlighted in red or light red, respectively. A few boundaries are hit in the second optimization, mainly concerning the LV stiffness parameters and the relaxation time, where the upper boundary is reached. In the third optimization, the timing parameters exclusively hit either upper or lower boundary. As visible in Figure 22, one can observe an extraordinary long diastasis, which would require a very short atrioventricular delay, i.e. low $d\tau_{av}$ and a low time factor $TimeFac$. Since these values are restricted by the defined boundaries, the rise time of LA and LV is used additionally to compensate for the high time difference of E- and A-wave, adjusting them to be very high or low, respectively.

A comparison of the optimized models for a subject from the first age group from the five different runs is presented in Table 17. In this table, the model parameters of the optimized models are given for each run, followed by the mean value, standard deviation and the standard deviation in relation to the mean value, i.e. the variation coefficient, given in percent. Since the algorithm uses different random sample points for each of the runs, this is a good indication if the algorithm converges to a local minimum. This enables to track the accuracy of the framework in finding the optimal solution.

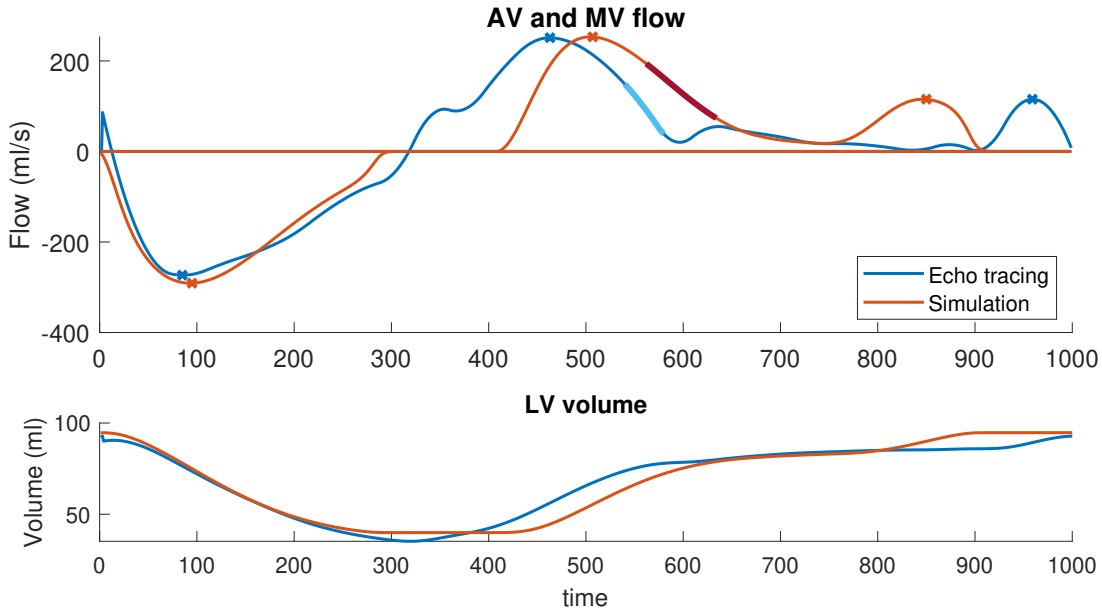

(a) Fitting after the second optimization

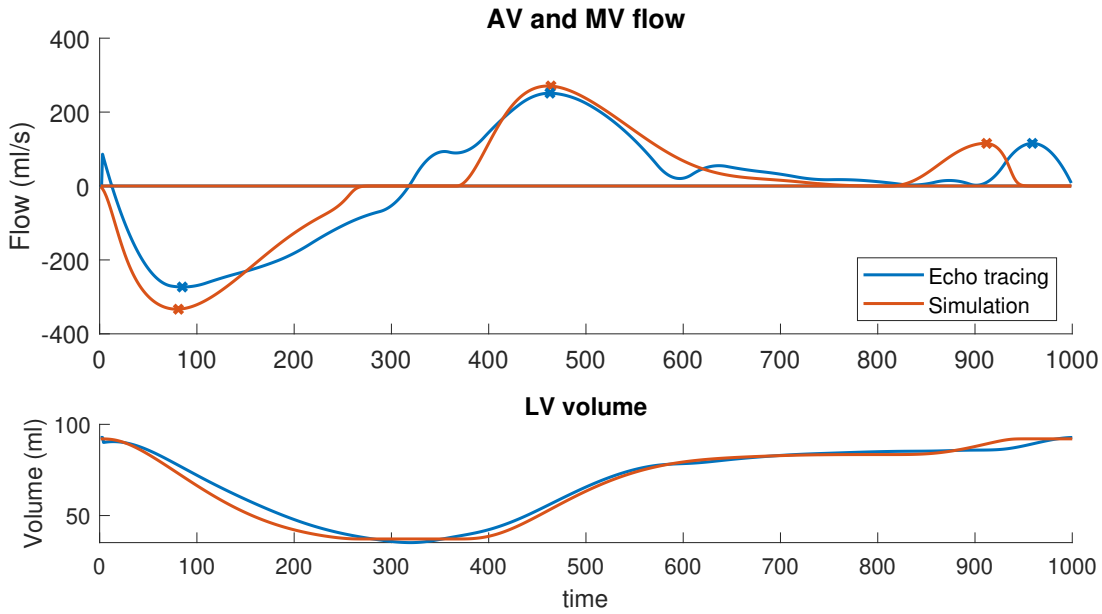

(b) Fitting after the third optimization

Figure 22: Subject-specific fit for a subject of age group 1

5 Discussion

The following pages discuss the results and their meaning and implications in relation to the research question. The results of the optimization are brought into context with regards to the expected outcomes. Limitations of the inputs, i.e. the CircAdapt model, the WASE study data and the used optimization algorithm, as well as the presented algorithm are outlined and discussed. The latter is investigated based on the parameter choice, boundaries and the methodology in general. Recommendation for future research projects are given at the bottom of this section.

The results of the optimization presented in Section 4 are analyzed. The starting model from Figure 12 has some discrepancies from resembling a normal healthy cardiovascular system, i.e. the E-wave deceleration is unsteady and is followed by a regurgitation in the diastasis and another one after the closing of the MV. The following isovolumetric contraction is extremely long. Also, the absolute values of LV volume and the valve flows are differing largely from the measured values, indicating a deviation of geometrical parameters. By the multi-step optimization, it was possible to create a model that mimics normal cardiovascular hemodynamics as observed in clinical measurements. Especially for age group 1 in Figure 18, to which the primary focus lay on in the development of the framework, the volume and flow velocity curves in the optimized model come very close to the shape of the echocardiography measurement. As explained in Section 3.3, main concentration lay on the fitting of those characteristics of the curves, that are actually comparable given the different sources of the curves. Also for the other age groups, the curves near the targeted shape sufficiently. Specifically, the diastolic events and the connection between E-wave and A-wave are modeled very realistically. For the systole, disregarding the exact timing, the pumping function is resembled well. Considering that the targeted shape lacks the isovolumetric contraction and relaxation times, this shape has been neared sufficiently for most instances. The definition of the curve fitting criterion is verified by observing multiple generated curves along with their quantified error value. Based on characteristic points and the general shape of the curves, the criterion is compared with a subjective estimation of the fitting. For a reliable computation, the stable determination of these error values is crucial to avoid fitting to a non-desired pattern. The criterion indicates a less good fitting for the older age groups, which can also be observed in the comparison of the curves 27d and 27e. This implies that the chosen model parameter set is not exclusively responsible for cardiac aging. The optimized models have been further investigated concerning the consistency of the model parameters and physical correctness in Section 4.2, to make sure they display a realistic system. The tests have been positively completed for all of the presented models, demonstrated for the first age group. All in all, this is a good indication for the success of the framework to optimize towards population-specific hemodynamics by using the presented parameters and data. A subsequent one-at-a-time sensitivity analysis shows which parameters are particularly important for the fitting of the curves. Furthermore, even though the objective function containing the model is computationally expensive, the frame-

work runs stable and has low hardware requirements. It can be accelerated if a multiple core machine is available.

The applicability of the framework on data from individual subjects within every age group is tested in Section 4.4. Even though the subject-specific data required a broader range of model parameter space, a fitting could be sufficiently reached for most instances. There is a good agreement of the solutions of the different runs (Table 14). Table 17 indicates, how much the solutions of the different runs deviate. In general, the deviation is low (below 13%), for most model parameters even lower. This multi-start approach leads to conclude that even though the model is highly nonlinear and non-smooth, the optimization to local minima is restricted. Some of the curves deviated significantly from the expected curve shape based on literature, previous simulations and the averaged curves. Thus the framework was not able to mimic those behaviors, as for example in age group 5 28d. Given the relatively low iterations of optimization procedures, a good fit could be achieved for most of the curves.

The age-dependent changes of the model parameters based on the population-specific fittings are presented in Section 4.3. They provide insight into which parts of the cardiovascular system are prone to changes with age and which parameters arbitrarily change in order to provide a good fitting. It has to be noted that the changes in the systolic and diastolic blood pressure values are also dependent on other parameters. In this optimization, the rest of the heart is assumed to have the same properties for every age group. Starting with the indicated changes due to the fitting of the blood pressure levels in Figure 20, a quite unambiguous trend within the different runs is seen. The error tolerance of 0.01 is surpassed in almost every run, which means that the result rather precisely minimizes the fitting values. This can be explained by the chosen model parameters of only vascular stiffness and MAP to determine the blood pressure with enabled pressure-flow control steering the desired output. Vascular stiffness increases with age to an almost 30% higher mean stiffness coefficient with a slight tendency to exponential growth. This complies with the findings of Arts et al. [3]. They state that the effect of aging appears similar to a 42% increase of the vascular stiffness exponent k. The fitted mean arterial pressure also rises with growing age, from a mean value of 1.21 Pa for age group 1 to almost 1.37 Pa in the averaged older subjects. These observations cover expectations based on the literature findings in Section 2.1.2, as vasculature is stiffening with higher age and arterial pressure is slightly increasing [14, 55]. Furthermore, the model parameters altered in optimization steps 2 and 3 are investigated. The deviation of values between the different runs is relatively high in comparison to the absolute value of age-dependent changes. In conclusion, the observed changes are of limited explanatory power and only tendencies can be monitored. The most obvious change can be seen in the change of the active stiffness. For both LV and LA, contractility is observed to increase with age. Even though hypertrophy, i.e. a thickening of the myocardial walls, mostly due to hypertension, has been an exclusion criterion for the participation in the WASE study and was also not included in the model parameters, a slight increase in both mean arterial pressure and thus an

increase of myocytes to keep up the required flow can be observed. This increase is functionally related to the active stiffness. Active stiffness is a phenomenological parameter and does not necessarily address the contractility of one myocyte but rather the global contractile function of the myocardium, hence the contractility increases even though the ability of contraction of a single cell might be impaired. This relation suggests that the increase in the contractility is more likely due to hypertrophy than an actual increase of the single myocyte's contractility. As outlined in Section 2.1.2, a slight thickening of the LV wall can be observed in older subjects, even though it evens out by indexing with BSA. Passive stiffness is observed to slightly decline in the first four decades, though almost plateauing for older age groups. This result is against the expectation, that the elasticity decreases due to dilation at a higher age [56]. However, this dilation is also governed by wall parameters, which are not included in the model parameter set. The rise time refers to the slope into the ejection peak at the beginning of the systole. This slope has not been included in the fitting criteria particularly. As discussed in Section 4.2, fitting of the systole can still be considered as sufficient, since the total ejection is close to the measurement. The deviation in the ejection wave arises to some extent because of the averaging of the measured traces and the accompanied falsification of the shape. The decay time rises relatively continuously with growing age, except for an outlier in age group 5. This complies well with the predication found in literature [13], dealing with the duality of both the active and passive stiffness influencing the deceleration time. The MV and AV opening areas in general greatly influence the flow of blood during diastole and systole, respectively, as they determine how much blood at a time can flow between the chambers. As those values are not necessarily connected to the age, the respective model parameter changes are mainly due to the improvement of the fit. Especially for the peak value of the ejection wave, which depends a lot on the opening area of the AV, the definition of the fitting criterion includes a very low weighting. Therefore, it is comprehensible that the changes show no particular tendency. Despite some limitations, tendencies in the change of some parameters could be observed. The phenomenological nature of the CircAdapt model provides the opportunity to draw such conclusions, given the fact that the provided data is representative of the suspected observations.

Although the framework successfully generated computer models of the respective population group or individual, there are some known limitations of the model and framework that have to be taken into account. In general, it has to be noted that the framework is not fitting patterns by optimizing parameters that directly describe the form of the curves, but rather fitting mechanical behaviors and their interaction to various components of the cardiovascular system, which then produce those patterns. There are discrepancies between which effects are measured by echocardiography and which effects the model is capable of simulating. Since a biophysical model is involved, rules of physics and biology apply, which sets boundaries to the fitting. Most parameters have a natural boundary, for example, stiffness parameters cannot take the value 0, even if that would mean the best fit of a specific pattern. As in all biomechanical models resembling complex physiology and interrelations, many

assumptions are needed in order to transform the complexity into a mathematical model. This always results in a constraint for the quality of the results. Also, in this study, the pulmonary circulation and the right heart are not directly included in the fitting. Through indirect interaction like RV function, manipulations of CO and cycle time or pressure-flow control, its function and influence is included. This is considered in the interpretation of the results, though the pulmonary circulation obviously influences other relations of parameters and hence should be included for the completeness of the study. In the development of the methodology, the first age group is often used as a reference and testing group. Hence, the fitting is best for this group. For a better fitting of the older age groups, more investigation is required on the specific features of these groups.

A restrictive factor was the availability of the data, even though the WASE study offers a great collection of TTE data from a sufficiently large cohort of diverse subjects. Subjects enrolled in the study were asymptomatic, hence it cannot be guaranteed that no pathological conditions are present and the individuals were not necessarily in perfect health condition. As mentioned, the right heart is not used for the fitting due to the lack of sufficient data on this part. Since the right heart is more difficult to access in a normal TTE, which is mainly due to its shape and position, data are not reliable to conclude from. The averaged curves of the left heart are prone to uncertainty and hence have a relatively high standard deviation. As demonstrated in Section 3.1, the relative standard deviation is around 30%, which means the dispersion of the data is relatively high. Thus, one can expect a propagation of the uncertainty through the optimization and the accuracy of the result to be limited. This uncertainty might have influenced the results of retrieving the age changes. Also, the timing of the different events during a cycle is very different from subject to subject. As mentioned before, taking the mean value of all subjects from one age group influences the shape of the curve significantly. To compensate for this, characteristic points of the curve are used as a fitting criterion, however, some of the characteristics were still difficult to resemble using the simulation model. For example, the absence of the isovolumetric contraction and relaxation influences the rest of the curve. With data on the MPI, this is still taken into account in the validation of the results.

The CircAdapt model itself has limitations as well. It is a highly phenomenological contraction model, which makes the comparison to subject data challenging [60]. One limitation is the neglect of the actual geometry of the heart and circulation systems. The approximation of atria and ventricles as spheres rather than ellipsoidals or their actual form and vasculature with valves as round tubes is sufficient for most instances, but not accurate to reality. The model is also not able to find a steady solution for every parameter set. Since it solves a set of partial differential equations for retrieving a steady solution for its closed-loop relations, this solution is not always possible and the computation fails. This could also be due to the desired solution being too far away from the current simulation and hence it would require in-between solutions. The failure of the computation has been taken into account while developing the methodology. It is assumed, that if the model is unable to find a steady solution for a model parameter set, this set is not among

the optimal solution and the model shall resume with another parameter set. One reason for this could arise from not including changes in the right heart parameters. Due to the simultaneous copying of changes of the left heart to the right heart, instabilities in the TriSeg module can arise due to forced dependencies of the patches. Also, of course, not every possible correlation could be included in the model. Every simplification means a change of the results and thus a limitation in mimicking real systems.

Assumptions are also made with defining the boundaries of the presented framework. For the parameters, choices are made based on literature, expected outcomes and practical parameters. The chosen set of model parameters is still a fraction of what would be possible using the CircAdapt model. Some parameters, mainly the timing parameters, are to a high extent subject-specific and are thus prone to uncertainty and unreliability. The boundaries of the parameters are chosen as small as possible to bound the parameter space to a clearly arranged field, leaving less space for local minima and non-physiologic parameter combinations. However, some parameters hit the boundary, which implies that the global minimum was outside the predefined space, or the fitting protocol aims to go towards a value surpassing the boundary. Iterative runs could prevent this issue, though would result in significantly higher computation time. In Table 15 and 16, the values which hit the lower or upper boundary are highlighted in red. Values being close to one of the boundaries – a margin of 5% of the range is defined – are highlighted light red. Therefore it is comprehensible that the minimum error is limited.

Even though the problem has been analyzed carefully in order to find a tailored optimization algorithm, there are still limitations with the use of the surrogate optimization. Because the model is highly nonlinear and non-smooth, the random sampling approach promotes the possibility of skipping the actual global minimum by not performing a function evaluation near this point. A higher number of random sample points can reduce this risk. Another possibility is to multi-start the optimization. This is implemented in the algorithm if it gets stuck in a local minimum, which normally happens one to four times during one optimization. A big issue is that the algorithm is not able to reliably find an optimal solution for every run. As it has been discussed in Section 4.1, the framework is not always able to reduce the total error below a certain tolerance. Therefore for the assessment of the result, a subsequent, higher tolerance is defined for the optimized model and those models are neglected, for which these requirements are not met. As shown in Section 3.5, outliers are present in both directions. As the surrogate optimization algorithm is designed for deterministic objective functions, which is generally the case for the proposed methodology, it cannot handle the outliers observed in some computations. Also, the use of parallel computing does not deliver reproducible results due to the non-reproducibility of the parallel timing leading to different execution paths. This is excusable considering the computation time advantage this offers. In a future work, this could be improved by hard-coding the random sequence and hence making the results more reproducible.

Some of these limitations can provide the base for future research in this field. Tackling the optimization success and computation time could significantly improve the outcome as well as the practicability of the framework in prospect of future use in a clinical setting. It could be considered to use a Bayesian optimization approach [36, 54]. This is an approach specifically tailored and often used for biomedical models, as it covers for the occurrence of outliers and noise in general, which is often the case when dealing with complex biomechanical correlations. The model parameter set could be expanded so that it spreads the focus to the fitting of older age groups, in order to more confidently draw conclusions on cardiac aging. As this algorithm provides additional physiological information to the data gathered in a TTE, an even more powerful big data set can be generated from studies like the WASE study. This data set could be used as a basis for the supervised learning with a neural network. With a machine learning algorithm underlying such a neural network, newly acquired TTE data could be evaluated fast and without the need to run a full parameter optimization, giving causative explanations for diseases or assessing the cardiac age [9, 15]. Combining this approach with finite element models as proposed by Wang et al. [62] or Xi et al. [67] in order to incorporate a subject-specific geometry could offer an even more exact representation of a specific cardiovascular system based on measured data. A general objective for the future should be to combine as much knowledge as possible within one model, representing the physiological and functional features of the individual, as well as their changes over different data acquisitions.

6 Summary and conclusion

This work proposes a framework to generate a population-specific cardiovascular simulation model, that builds on the CircAdapt model and is personalized by a parameter estimation using echocardiographic data. In the pre-processing, population groups were formed and averaged MV and AV flow velocity generated, as well as LV and LA volume curves. These curves were investigated based on their characteristics, representing the age group they are assigned to. From the reference CircAdapt model, the output curves were assessed and compared to the measurement data. Defined model parameters were altered dynamically in order to find a model parameter set that resembles the volume and flow curves of the population data. The generated model was analyzed based on physiology and consistency. A subject-specific analysis was performed with data from individual subjects of different ages. The comparison of the models resembling populations of different age groups led to conclusions about the change of cardiac properties due to age. Such an optimization was performed to subject-specific data in order to assess the performance of the framework.

The presented work serves as a proof of principle towards the development of a subject-specific framework that could in future be integrated into medical devices, like imaging or image analysis devices, to assist decision making in clinical practice by providing the underlying (patho-)physiological understanding. With this model, clinical data can be incorporated into a biophysics model assembling and correlating parameters and functions. This is a crucial step towards the assembly of the digital twin of parts of the human body. This work estimates parameters of the cardiovascular system, which are difficult to access in a clinical setting. Also, active and passive stiffness parameters of certain myocardial patches can easily be retrieved from the personalized model, providing information about the underlying cardiac mechanics of the subject. With the herein retrieved information, diseases like heart failure could be investigated on a causative level. Since heart failure can occur in different pathophysiologic situations and be caused by different malfunctions, the responsible clinicians could be provided with information on what causes the condition. This information can crucially improve the derivation of further treatment plans personalized for the patient. The model also presents parameter correlations, that can be used to assist the acquisition of data by providing context about consistencies. Therefore, measurement errors due to inaccuracies and biases of clinicians during the acquisition of ultrasound images can be reduced. Cognitive biases are prominent in medical image analysis and can influence the correctness of diagnosis significantly. Hence, interrelating different measurements assessing the consistency could reduce this issue. The assessment of age-related changes in the cardiovascular systems adds age information to the normal values and states. It can also eliminate a lot of age related biases. For instance, when reading literature regarding heart failure, all studies mention that stiffness, or LV hypertrophy, are common sightings in elderly patients and could therefore not be considered a malfunction. However, through this work, which investigates what changes in cardiovascular system pa-

rameters can be associated with age, it can then be concluded whether an observed anomaly should be blamed due to age, or due to a yet undiscovered (mal)adaptation. For the planning of further treatments tailored to the individual's age, as the composition of medication, surgery or other interventions, these findings can be very useful.

References

[1] Arts, T ; Bovendeerd, P ; Delhaas, T ; Prinzen, F: Modeling the relation between cardiac pump function and myofiber mechanics. In: *Journal of biomechanics* 36 (2003), Nr. 5, S. 731–736

[2] Arts, T. ; Delhaas, T. ; Prinzen, F. ; Lumens, J.: *The CircAdapt Model*. Universiteitssingel 50, 6200MD Maastricht, The Netherlands: Maastricht University, The Netherlands, 2019

[3] Arts, Theo ; Delhaas, Tammo ; Bovendeerd, Peter ; Verbeek, Xander ; Prinzen, Frits W.: Adaptation to mechanical load determines shape and properties of heart and circulation: the CircAdapt model. In: *American Journal of Physiology-Heart and Circulatory Physiology* 288 (2005), Nr. 4, S. H1943–H1954

[4] Arts, Theo ; Lumens, Joost ; Kroon, Wilco ; Delhaas, Tammo: Control of whole heart geometry by intramyocardial mechano-feedback: a model study. In: *PLoS computational biology* 8 (2012), Nr. 2, S. e1002369

[5] Arts, Theo ; Reesink, Koen ; Kroon, Wilco ; Delhaas, Tammo: Simulation of adaptation of blood vessel geometry to flow and pressure: Implications for arterio-venous impedance. In: *Mechanics Research Communications* 42 (2012), S. 15–21

[6] Asch, Federico M. ; Banchs, Jose ; Price, Rhonda ; Rigolin, Vera ; Thomas, James D. ; Weissman, Neil J. ; Lang, Roberto M.: Need for a Global Definition of Normative Echo Values - Rationale and Design of the World Alliance of Societies of Echocardiography Normal Values Study (WASE). In: *Journal of the American Society of Echocardiography* 32 (2019), Nr. 1, S. 157–162

[7] Asch, Federico M. ; Miyoshi, Tatsuya ; Addetia, Karima ; Citro, Rodolfo ; Daimon, Masao ; Desale, Sameer ; Fajardo, Pedro G. ; Kasliwal, Ravi R. ; Kirkpatrick, James N. ; Monaghan, Mark J. u. a.: Similarities and Differences in Left Ventricular Size and Function among Races and Nationalities: Results of the World Alliance Societies of Echocardiography Normal Values Study. In: *Journal of the American Society of Echocardiography* 32 (2019), Nr. 11, S. 1396–1406

[8] Aune, Erlend ; Baekkevar, Morten ; Roislien, Jo ; Rodevand, Olaf ; Otterstad, Jan E.: Normal reference ranges for left and right atrial volume indexes and ejection fractions obtained with real-time three-dimensional echocardiography. In: *European Journal of Echocardiography* 10 (2009), Nr. 6, S. 738–744

[9] Baldi, Pierre ; Brunak, Søren ; Bach, Francis: *Bioinformatics: the machine learning approach*. MIT press, 2001

[10] Bellhouse, BJ ; Bellhouse, FH: Fluid mechanics of the mitral valve. In: *Nature* 224 (1969), Nr. 5219, S. 615–616

[11] Buhmann, Martin D.: *Radial basis functions: theory and implementations*. Bd. 12. Cambridge university press, 2003

[12] Campolongo, Francesca ; Saltelli, Andrea ; Cariboni, Jessica: From screening to quantitative sensitivity analysis. A unified approach. In: *Computer Physics Communications* 182 (2011), Nr. 4, S. 978–988

[13] Carrick-Ranson, Graeme ; Hastings, Jeffrey L. ; Bhella, Paul S. ; Shibata, Shigeki ; Fujimoto, Naoki ; Palmer, M D. ; Boyd, Kara ; Levine, Benjamin D.: Effect of healthy aging on left ventricular relaxation and diastolic suction. In: *American Journal of Physiology-Heart and Circulatory Physiology* 303 (2012), Nr. 3, S. H315–H322

[14] Chiao, Ying A. ; Rabinovitch, Peter S.: The aging heart. In: *Cold Spring Harbor perspectives in medicine* 5 (2015), Nr. 9, S. a025148

[15] Chicco, Davide: Ten quick tips for machine learning in computational biology. In: *BioData mining* 10 (2017), Nr. 1, S. 35

[16] CircAdapt Research Team: *MATLAB source code of the CircAdapt model*. `http://www.circadapt.org/downloads`, . – Accessed: 2019-01-23

[17] CircAdapt Research Team: *CircAdapt webpage containing source code and documentation as downloads*. `http://www.circadapt.org/downloads`, 2015. – Accessed: 2019-01-23

[18] Gutmann, H-M: A radial basis function method for global optimization. In: *Journal of global optimization* 19 (2001), Nr. 3, S. 201–227

[19] Hamby, DM: A review of techniques for parameter sensitivity analysis of environmental models. In: *Environmental monitoring and assessment* 32 (1994), Nr. 2, S. 135–154

[20] Henein, Michael Y. ; Lindqvist, Per: Assessment of left ventricular diastolic function by Doppler echocardiography. In: *Cardiac failure review* 1 (2015), Nr. 2, S. 87

[21] Henry, WL ; Griffith, JM ; Michaelis, LL ; Mcintosh, Ch L. ; Morrow, AG ; Epstein, St E.: Measurement of mitral orifice area in patients with mitral valve disease by real-time, two-dimensional echocardiography. In: *Circulation* 51 (1975), Nr. 5, S. 827–831

[22] Hergan, Klaus ; Schuster, Antonius ; Frühwald, Julia ; Mair, Michael ; Burger, Ralph ; Töpker, Michael: Comparison of left and right ventricular volume measurement using the Simpson's method and the area length method. In: *European journal of radiology* 65 (2008), Nr. 2, S. 270–278

[23] Heusinkveld, Maarten H. ; Delhaas, Tammo ; Lumens, Joost ; Huberts, Wouter ; Spronck, Bart ; Hughes, Alun D. ; Reesink, Koen D.: Augmentation index is not a proxy for wave reflection magnitude: mechanistic analysis using a computational model. In: *Journal of Applied Physiology* 127 (2019), Nr. 2, S. 491–500

[24] Houten, Henk van: *How a virtual heart could save your real one.* `https://www.philips.com/a-w/about/news/archive/blogs/innovation-matters/20181112-how-a-virtual-heart-could-save-your-real-one.html`, 2018. – Accessed: 2020-01-29

[25] Houten, Henk van: *The rise of the digital twin: how healthcare can benefit.* `https://www.philips.com/a-w/about/news/archive/blogs/innovation-matters/20180830-the-rise-of-the-digital-twin-how-healthcare-can-benefit.html`, 2018. – Accessed: 2020-01-29

[26] Huntjens, Peter R. ; Ploux, Sylvain ; Strik, Marc ; Walmsley, John ; Ritter, Philippe ; Haissaguerre, Michel ; Prinzen, Frits W. ; Delhaas, Tammo ; Lumens, Joost ; Bordachar, Pierre: Electrical substrates driving response to cardiac resynchronization therapy: a combined clinical–computational evaluation. In: *Circulation: Arrhythmia and Electrophysiology* 11 (2018), Nr. 4, S. e005647

[27] Iaizzo, Paul A.: *Handbook of cardiac anatomy, physiology, and devices.* Springer Science & Business Media, 2009

[28] Keren, G ; Meisner, JS ; Sherez, JACK ; Yellin, EL ; Laniado, SHLOMO: Interrelationship of mid-diastolic mitral valve motion, pulmonary venous flow, and transmitral flow. In: *Circulation* 74 (1986), Nr. 1, S. 36–44

[29] Kerut, Edmund K.: The Mitral L-Wave: A Relatively Common but Ignored Useful Finding: CME. In: *Echocardiography* 25 (2008), Nr. 5, S. 548–550

[30] Kim, Sung-Ai ; Son, Jungwoo ; Shim, Chi-Young ; Choi, Eui-Young ; Ha, Jong-Won: Long-term outcome of patients with triphasic mitral flow with a mid-diastolic L wave: prognostic role of left atrial volume and N-terminal pro-brain natriuretic peptide. In: *The international journal of cardiovascular imaging* 33 (2017), Nr. 9, S. 1377–1384

[31] Kirn, Borut ; Walmsley, John ; Lumens, Joost: Uniqueness of local myocardial strain patterns with respect to activation time and contractility of the failing heart: a computational study. In: *Biomedical engineering online* 17 (2018), Nr. 1, S. 182

[32] Kitzman, Dalane W. ; Sheikh, Khalid H. ; Beere, Polly A. ; Philips, Judy L. ; Higginbotham, Michael B.: Age-related alterations of Doppler left ventricular filling indexes in normal subjects are independent of left ventricular mass, heart rate, contractility and loading conditions. In: *Journal of the American College of Cardiology* 18 (1991), Nr. 5, S. 1243–1250

[33] Kuijpers, Nico H. ; Dassen, Willem ; Dam, Peter M. ; Dam, Eelco M. ; Hermeling, Evelien ; Lumens, Joost ; Arts, Theo ; Delhaas, Tammo: CircAdapt: A user-friendly learning environment for (patho) physiology of heart and circulation. In: *2012 Computing in Cardiology* IEEE, 2012, S. 969–972

[34] Lam, Carolyn S. ; Han, Lin ; Ha, Jong-Won ; Oh, Jae K. ; Ling, Lieng H.: The mitral L wave: a marker of pseudonormal filling and predictor of heart failure in patients with left ventricular hypertrophy. In: *Journal of the American Society of Echocardiography* 18 (2005), Nr. 4, S. 336–341

[35] Lang, Roberto M. ; Badano, Luigi P. ; Mor-Avi, Victor ; Afilalo, Jonathan ; Armstrong, Anderson ; Ernande, Laura ; Flachskampf, Frank A. ; Foster, Elyse ; Goldstein, Steven A. ; Kuznetsova, Tatiana u. a.: Recommendations for cardiac chamber quantification by echocardiography in adults: an update from the American Society of Echocardiography and the European Association of Cardiovascular Imaging. In: *European Heart Journal-Cardiovascular Imaging* 16 (2015), Nr. 3, S. 233–271

[36] Liepe, Juliane ; Kirk, Paul ; Filippi, Sarah ; Toni, Tina ; Barnes, Chris P. ; Stumpf, Michael P.: A framework for parameter estimation and model selection from experimental data in systems biology using approximate Bayesian computation. In: *Nature protocols* 9 (2014), Nr. 2, S. 439

[37] Lumens, Joost ; Delhaas, Tammo: Cardiovascular modeling in pulmonary arterial hypertension: focus on mechanisms and treatment of right heart failure using the CircAdapt model. In: *The American journal of cardiology* 110 (2012), Nr. 6, S. S39–S48

[38] Lumens, Joost ; Delhaas, Tammo ; Kirn, Borut ; Arts, Theo: Three-wall segment (TriSeg) model describing mechanics and hemodynamics of ventricular interaction. In: *Annals of biomedical engineering* 37 (2009), Nr. 11, S. 2234–2255

[39] Lumens, Jozef E.: Patient-specific cardiovascular modeling in pulmonary hypertension: assessment of hemodynamic and mechanical ventricular interaction. (2010)

[40] Maastricht University, Department of Biomedical Engineering (BME) (Hrsg.): *Manual CircAdapt Simulator*. Universiteitssingel 50, 6200MD Maastricht, The Netherlands: Maastricht University, Department of Biomedical Engineering (BME), 2019. – http://www.circadapt.org/documentation

[41] Mitchell, Carol ; Rahko, Peter S. ; Blauwet, Lori A. ; Canaday, Barry ; Finstuen, Joshua A. ; Foster, Michael C. ; Horton, Kenneth ; Ogunyankin, Kofo O. ; Palma, Richard A. ; Velazquez, Eric J.: Guidelines for performing a comprehensive transthoracic echocardiographic examination in adults: recommendations from the American Society of Echocardiography.

In: *Journal of the American Society of Echocardiography* 32 (2019), Nr. 1, S. 1–64

[42] Mosteller, RD: Simplified calculation of body surface area. In: *N Engl J Med* 317 (1987), S. 1098

[43] Niederer, Steven A. ; Campbell, Kenneth S. ; Campbell, Stuart G.: A short history of the development of mathematical models of cardiac mechanics. In: *Journal of molecular and cellular cardiology* 127 (2019), S. 11–19

[44] Niederer, Steven A. ; Lumens, Joost ; Trayanova, Natalia A.: Computational models in cardiology. In: *Nature Reviews Cardiology* 16 (2019), Nr. 2, S. 100–111

[45] Oxenham, Helen ; Sharpe, Norman: Cardiovascular aging and heart failure. In: *European journal of heart failure* 5 (2003), Nr. 4, S. 427–434

[46] Philips: *Cardiac 3D chamber quantifications driven by advanced automation*. `https://www.usa.philips.com/healthcare/resources/feature-detail/ultrasound-heartmodel`, 2015. – Accessed: 2020-01-29

[47] Pratt, William K.: *Introduction to digital image processing*. CRC press, 2013

[48] Quiñones, Miguel A. ; Otto, Catherine M. ; Stoddard, Marcus ; Waggoner, Alan ; Zoghbi, William A.: Recommendations for quantification of Doppler echocardiography: a report from the Doppler Quantification Task Force of the Nomenclature and Standards Committee of the American Society of Echocardiography. In: *Journal of the American Society of Echocardiography* 15 (2002), Nr. 2, S. 167–184

[49] Regis, Rommel G. ; Shoemaker, Christine A.: A stochastic radial basis function method for the global optimization of expensive functions. In: *INFORMS Journal on Computing* 19 (2007), Nr. 4, S. 497–509

[50] Reid, CL ; McKay, CR ; Chandraratna, PA ; Kawanishi, DT ; Rahimtoola, SH: Mechanisms of increase in mitral valve area and influence of anatomic features in double-balloon, catheter balloon valvuloplasty in adults with rheumatic mitral stenosis: a Doppler and two-dimensional echocardiographic study. In: *Circulation* 76 (1987), Nr. 3, S. 628–636

[51] Rohman, Melissa: *10 cognitive biases in medical imaging and how to avoid them*. `https://www.healthimaging.com/topics/practice-management/10-cognitive-biases-medical-imaging-and-how-avoid-them`, 2018. – Accessed: 2020-02-18

[52] Rudski, Lawrence G. ; Lai, Wyman W. ; Afilalo, Jonathan ; Hua, Lanqi ; Handschumacher, Mark D. ; Chandrasekaran, Krishnaswamy ; Solomon, Scott D. ; Louie, Eric K. ; Schiller, Nelson B.: Guidelines for the echocardiographic assessment of the right heart in adults: a report from

the American Society of Echocardiography: endorsed by the European Association of Echocardiography, a registered branch of the European Society of Cardiology, and the Canadian Society of Echocardiography. In: *Journal of the American Society of Echocardiography* 23 (2010), Nr. 7, S. 685–713

[53] Salton, Carol J. ; Chuang, Michael L. ; O'Donnell, Christopher J. ; Kupka, Michelle J. ; Larson, Martin G. ; Kissinger, Kraig V. ; Edelman, Robert R. ; Levy, Daniel ; Manning, Warren J.: Gender differences and normal left ventricular anatomy in an adult population free of hypertension: A cardiovascular magnetic resonance study of the Framingham Heart Study Offspring cohort. In: *Journal of the American College of Cardiology* 39 (2002), Nr. 6, S. 1055–1060

[54] Snoek, Jasper ; Larochelle, Hugo ; Adams, Ryan P.: Practical bayesian optimization of machine learning algorithms. In: *Advances in neural information processing systems*, 2012, S. 2951–2959

[55] Steenman, Marja ; Lande, Gilles: Cardiac aging and heart disease in humans. In: *Biophysical reviews* 9 (2017), Nr. 2, S. 131–137

[56] Strait, James B. ; Lakatta, Edward G.: Aging-associated cardiovascular changes and their relationship to heart failure. In: *Heart failure clinics* 8 (2012), Nr. 1, S. 143–164

[57] Topol, Eric: *Deep medicine: how artificial intelligence can make healthcare human again*. Hachette UK, 2019

[58] Törner, Emma: Adaptation of existing cardiovascular simulation model to cardiac pumping physiology. (2017)

[59] Walmsley, John ; Arts, Theo ; Derval, Nicolas ; Bordachar, Pierre ; Cochet, Hubert ; Ploux, Sylvain ; Prinzen, Frits W. ; Delhaas, Tammo ; Lumens, Joost: Fast simulation of mechanical heterogeneity in the electrically asynchronous heart using the multipatch module. In: *PLoS computational biology* 11 (2015), Nr. 7

[60] Walmsley, John ; Everdingen, Wouter van ; Cramer, Maarten J. ; Prinzen, Frits W. ; Delhaas, Tammo ; Lumens, Joost: Combining computer modelling and cardiac imaging to understand right ventricular pump function. In: *Cardiovascular research* 113 (2017), Nr. 12, S. 1486–1498

[61] Walmsley, John ; Squara, Pierre ; Wolfhard, Ulrich ; Cornelussen, Richard ; Lumens, Joost: Impact of abrupt versus gradual correction of mitral and tricuspid regurgitation: a modelling study. In: *EuroIntervention: journal of EuroPCR in collaboration with the Working Group on Interventional Cardiology of the European Society of Cardiology* 15 (2019), Nr. 10, S. 902–911

[62] Wang, Vicky Y. ; Lam, HI ; Ennis, Daniel B. ; Cowan, Brett R. ; Young, Alistair A. ; Nash, Martyn P.: Modelling passive diastolic mechanics with quantitative MRI of cardiac structure and function. In: *Medical image analysis* 13 (2009), Nr. 5, S. 773–784

[63] Wang, Yilun ; Shoemaker, Christine A.: A General Stochastic Algorithmic Framework for Minimizing Expensive Black Box Objective Functions Based on Surrogate Models and Sensitivity Analysis. In: *arXiv preprint arXiv:1410.6271* (2014)

[64] Willemen, Erik ; Schreurs, Rick ; Huntjens, Peter R. ; Strik, Marc ; Plank, Gernot ; Vigmond, Edward ; Walmsley, John ; Vernooy, Kevin ; Delhaas, Tammo ; Prinzen, Frits W. u. a.: The left and right ventricles respond differently to variation of pacing delays in cardiac resynchronization therapy: A combined experimental-computational approach. In: *Frontiers in physiology* 10 (2019), S. 17

[65] Willemetz, JC ; Nowicki, A ; Meister, JJ ; De Palma, F ; Pante, G: Bias and variance in the estimate of the Doppler frequency induced by a wall motion filter. In: *Ultrasonic Imaging* 11 (1989), Nr. 3, S. 215–225

[66] World Health Organization: *The top 10 causes of death.* `https://www.who.int/news-room/fact-sheets/detail/the-top-10-causes-of-death`, 2018. – Accessed: 2020-02-15

[67] Xi, Ce ; Latnie, Candace ; Zhao, Xiaodan ; Tan, Ju L. ; Wall, Samuel T. ; Genet, Martin ; Zhong, Liang ; Lee, Lik C.: Patient-specific computational analysis of ventricular mechanics in pulmonary arterial hypertension. In: *Journal of biomechanical engineering* 138 (2016), Nr. 11

[68] Zhou, Jin ; Chen, Xuefeng: *Intelligent Maintenance Driven by Digital Twin.* `https://www.frontiersin.org/research-topics/11013/intelligent-maintenance-driven-by-digital-twin`, . – Accessed: 2020-01-28

Appendices

A Matlab code structure

All code developed as a part of this work has been written in MATLAB and are attached in the digital appendix (CD). Additionally, codes of the open-source cardiovascular model CircAdapt [17] have been used, as well as built-in functions from MATLAB and its toolboxes. This section provides an overview of the main framework performing the optimizations and retrieving the results. For the full source code, as well as additional codes including the post-processing of the result, it is referred to the digital appendix. It is disclaimed that all code is to be treated confidentially and belongs to TOMTEC Imaging Systems GmbH.

```
MAINopt
├── readParamsTable
├── modifiedFixParams
│   ├── PRefJa
│   │   └── SteadyRunner
├── optBP
│   ├── objFctBP
│   │   └── SteadyRunner
│   ├── surrogateopt
│   └── SteadyRunner
├── optModelParams
│   ├── objFct
│   │   ├── SteadyRunner
│   │   ├── resampleAndAlign
│   │   └── compareCurves
│   │       ├── detEADT
│   │       └── detEADT_tracing
│   ├── surrogateopt
│   ├── SteadyRunner
│   ├── resampleAndAlign
│   └── compareCurves
├── optModelParTime
│   └── (...)
└── resultMgmnt
```

MAINopt Main script for running all functions. Creates a structure P with initial condition of model, runs optimization steps for every age group.

readParamsTable Measurement parameters are averaged for age decades and saved into structure 'params'.

modifiedFixParams Code for modifying fix parameters of the P structure based on mean values from echo measurements.

PRefJa For the first run, a new P structure is generated based on researched parameters from literature and from personalized parameters from the echo data. For the remaining runs, the previous P structure is used as a reference and the personalized parameters are updated according to the age group.

SteadyRunner Script from CircAdapt toolbox [17]. Performs the simulation with the given P structure as many beats, as it requires to find a steady solution.

optBP, optModelParams and optModelParTime Execute the optimization with regard to the blood pressure values, the first set of fitting values and the expanded set of fitting parameters. Within the script, an objective function is defined, the surrogate optimization executed and the resulting model parameter set reviewed and plotted OptModelParTime consists of the same subfunctions as optModelParams, hence they are not listed again. Those subfunctions differing from the ones of the second optimizations are marked by the ending 'Time'.

objFctBP, objFct and objFctTime Objective functions for the optimization. As an input, a set of model parameters is transmitted. The P struct is manipulated using the set of model parameters and a steady solution is computed with the SteadyRunner. The result is evaluated, quantifying the difference to the measurement data.

resampleAndAlign Resample the simulated volume and flow velocity curves and align them with the measurement curve based on valve events, in order to make them comparable.

compareCurves and compareCurvesTime Compare the simulation and measurement curves based on given criteria, i.e. fitting values. Calculate a total error to quantify how good the fitting is.

detEADT and detEADT_tracing Robustly determine the characteristic points on each curve, that are required to calculate the errors of the curve.

surrogateopt Script from the MATLAB Global Optimization Toolbox. Performs optimization as describes in Section 3.5.

resultMgmnt Create a custom folder and move all saved result files (checkpoint files, optimal solution, P structs of each step, figures, etc.) of one age group.

Additional tools

Additionally to the main framework, supplementary code is used for the post-processing of the data. The respective scripts are listed in the following.

plotEchoTracings Plot the volume and flow velocity curves from echocardiography data of all age groups.

plotStds Plot the standard deviations of the averaged tracing curves.

meanDoppler Pre-processing of the Doppler curves: resample and average the MV Doppler curves, resample the LVOT Doppler curves and align them with the MV flow curve. Create a plot to compare the averaged Doppler curve to the flow velocity curve derived from the 2D measurements.

writePatSpecInputFiles Pre-processing of the subject-specific data: CSV files are read, the global coordinates of the curves resampled, smoothed, aligned and plotted together with the Doppler curves for comparison.

plotCurveSet The calculated curves during an optimization are saved in a log-file. All curves are plotted in one figure alongside the echocardiography tracing. The chosen curve according to the fitting criteria is highlighted. The plot allows clicking on curves in order to assess if a better option according to subjective judgment is available. The ID of the manually chosen curve is displayed in the command window and can be used to retrieve the appropriate model parameter set of this curve from the log-file.

showP Simple code to display the relevant model parameters of a P structure.

valLAP Post-processing of the optimized model: comparison of the LA pressure values with norm values from literature. Plot the pressure-volume loop of the optimized model.

compAOpens Post-processing of the optimized model: compare the valve opening areas of optimized model to the values measured by echocardiography or computed from therein measured values.

compStrokeVol Post-processing of the optimized model: Compare the total volume of ejected blood in systole, i.e. the area under the AV flow curve of simulated model and echocardiography tracing.

compMPI Post-processing of the optimized model: compute the MPI of the simulation curves and compare it to the values from the WASE data.

sensitivityAnaFIX Function to identify the sensitivity of fixed parameters on the output and error estimates of the system. A one-at-a-time sensitivity analysis is performed.

sensitivityAna2 Sensitivity analysis for the model parameters. The influence on small changes on each input model parameter on the output values is assessed and presented in a matrix.

curveChar2Array Subsidiary function for the sensitivity analysis: convert the structure array of curve characteristics to a one-dimensional array.

plotFittedParamsBP Assess the changes in model parameters used for the first optimization. Plot the results of the multiple runs alongside the mean value of all sufficiently optimized runs.

plotFittedParams_time_mult Assess the changes in the model parameters for the optimized models of the different age groups. Plot the model parameters as functions of age. Consider different runs, compute the mean value and highlight it alongside the results of separate runs.

B Additional figures and tables

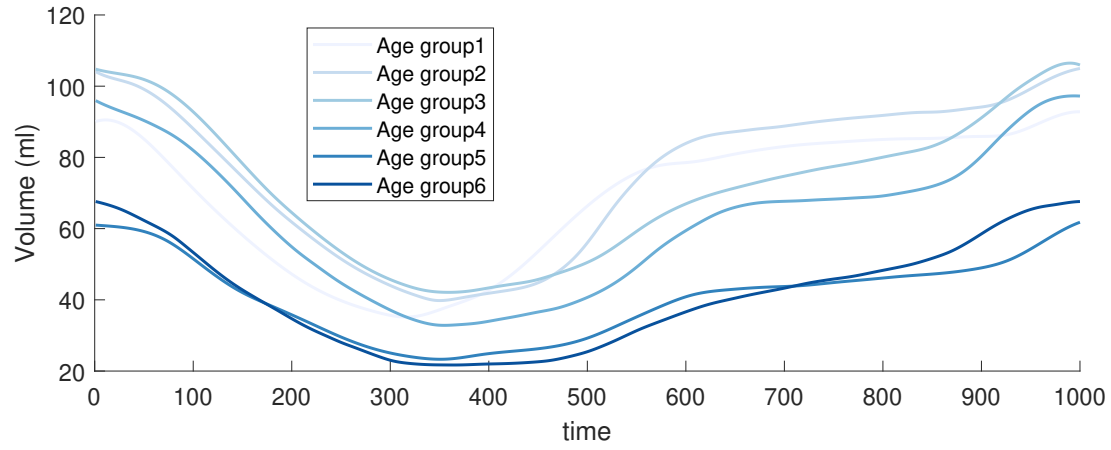

(a) Tracings of the LV volume flow

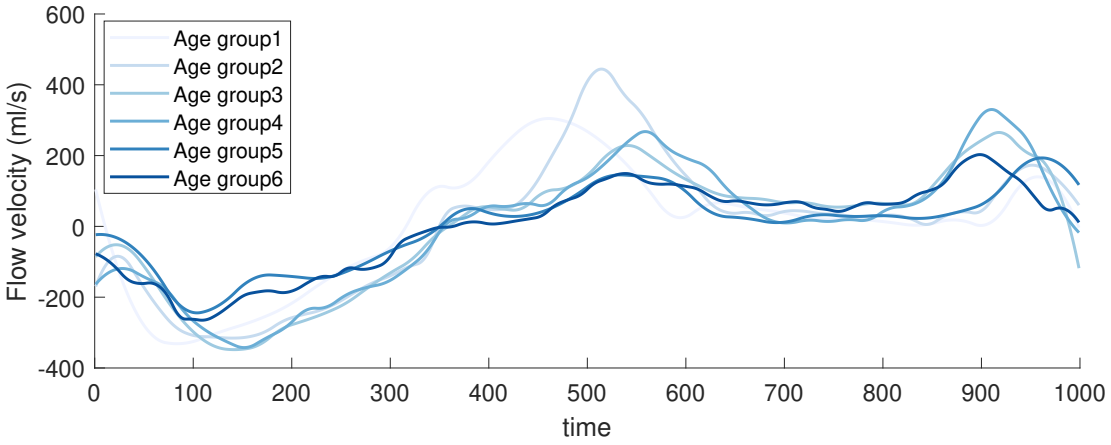

(b) Flow velocity tracings

Figure 23: LV volume and derived flow curves of single subjects from the respective age groups

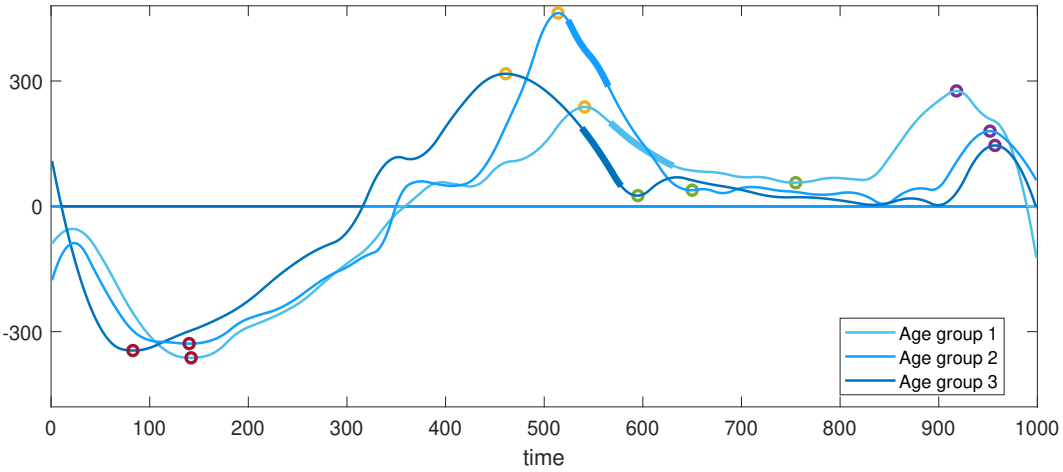

Figure 24: Characteristic points on subject-specific curves

Age Group	Run 1	Run 2	Run 3	Run 4	Run 5
1	0.337	**0.312**	0.480	0.345	0.371
2	0.316	0.382	0.336	**0.309**	0.315
3	0.505	0.393	**0.356**	0.363	0.410
4	**0.331**	0.336	0.378	0.357	0.357
5	0.582	0.545	0.635	**0.524**	0.741
6	**0.595**	0.641	0.652	0.651	0.600

Table 13: Total error of the optimal solution of each run for every age group; best value highlighted yellow and in bold font, values exceeding tolerance highlighted in red

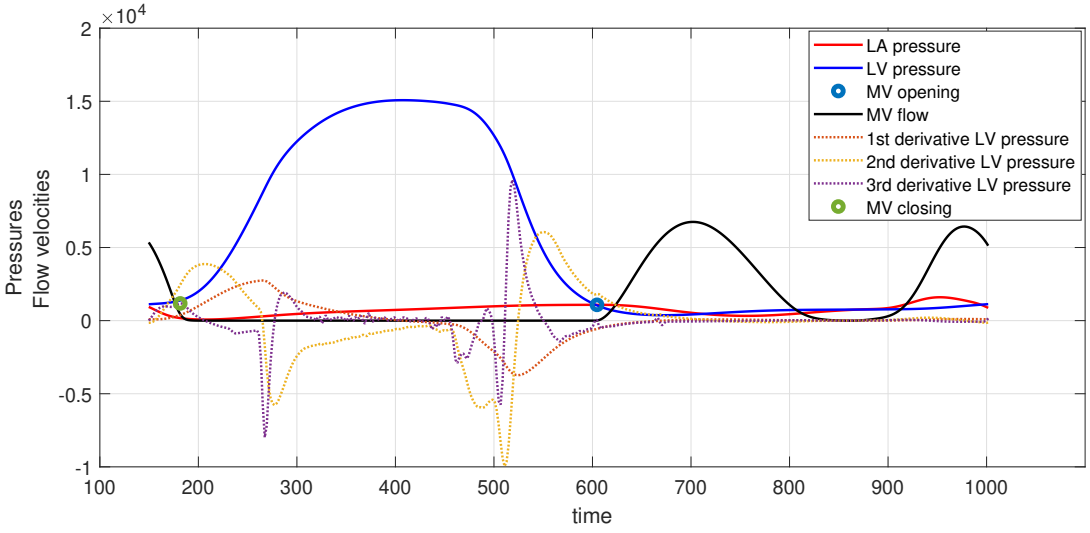

Figure 25: Mitral valve opening and closing events

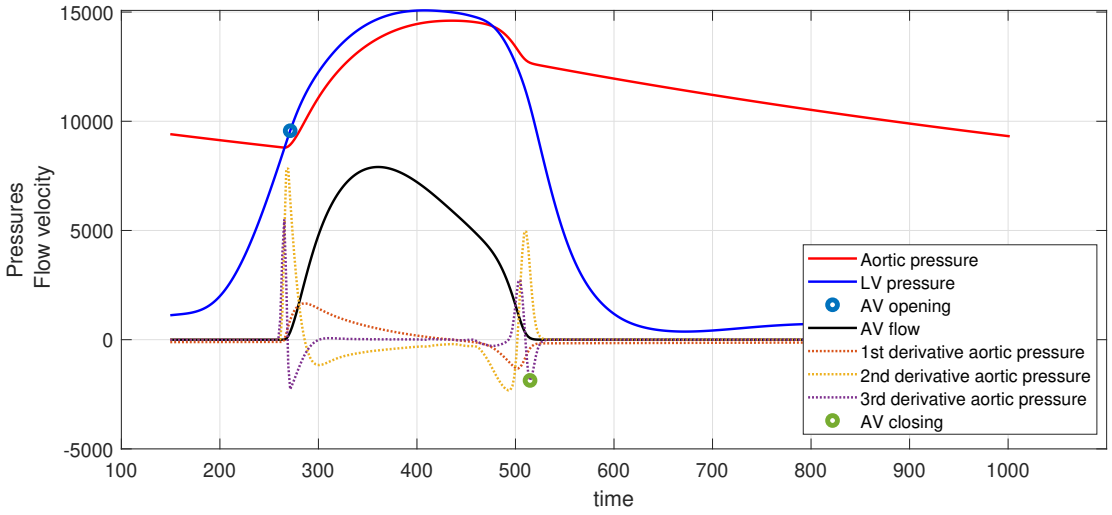

Figure 26: Aortic valve opening and closing events

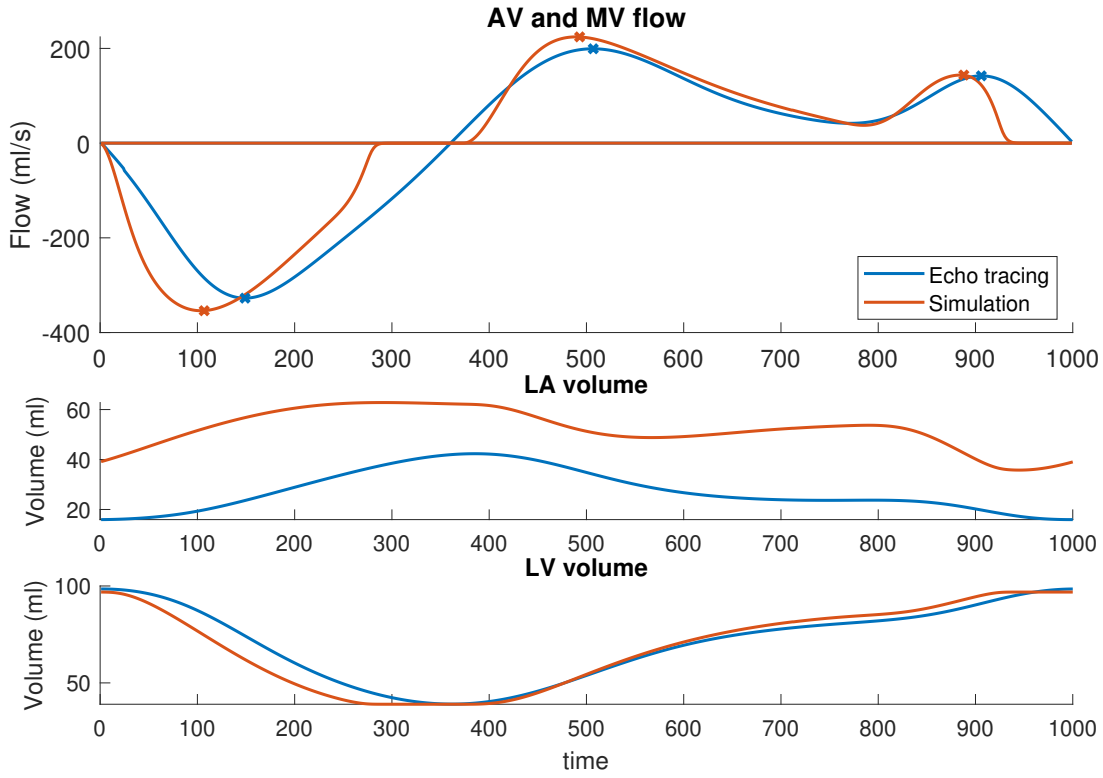

(a) Optimal fit for age group 2

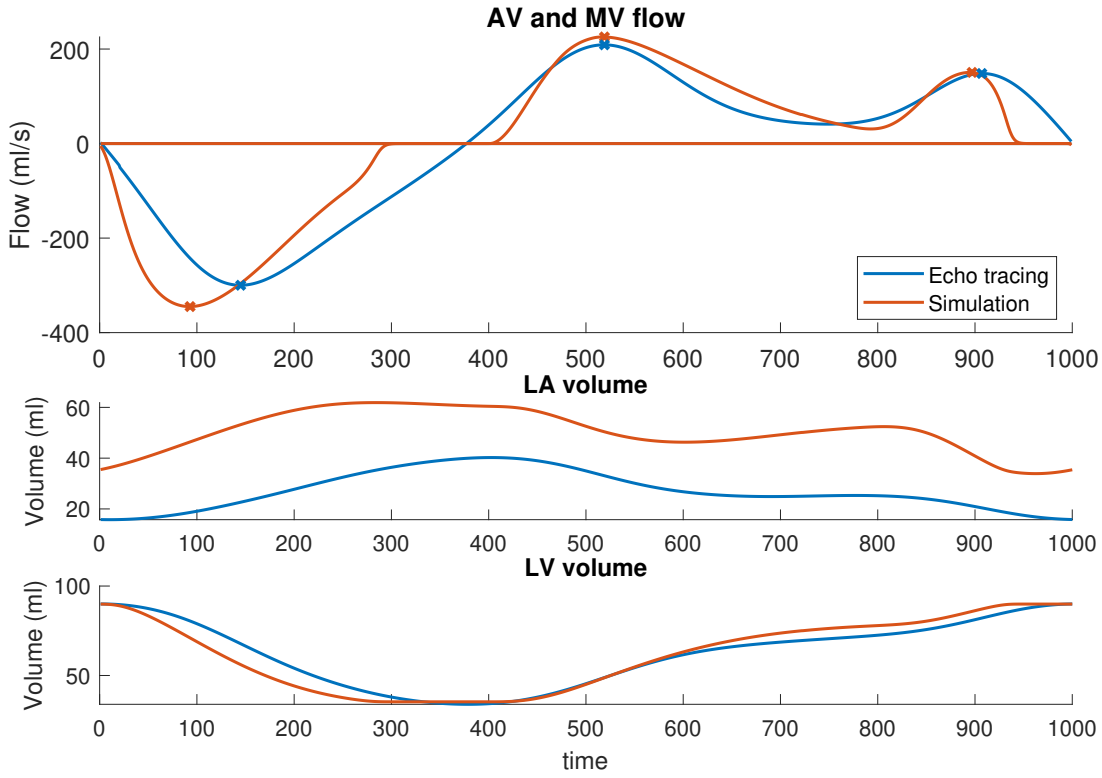

(b) Optimal fit for age group 3

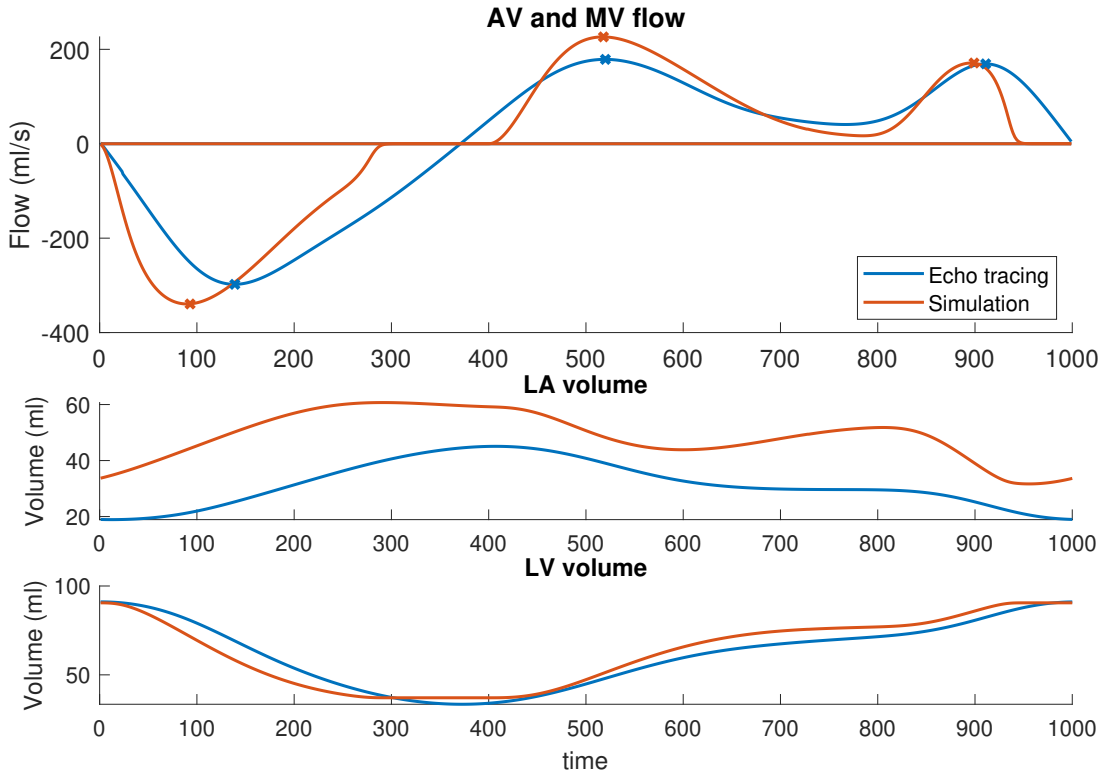

(c) Optimal fit for age group 4

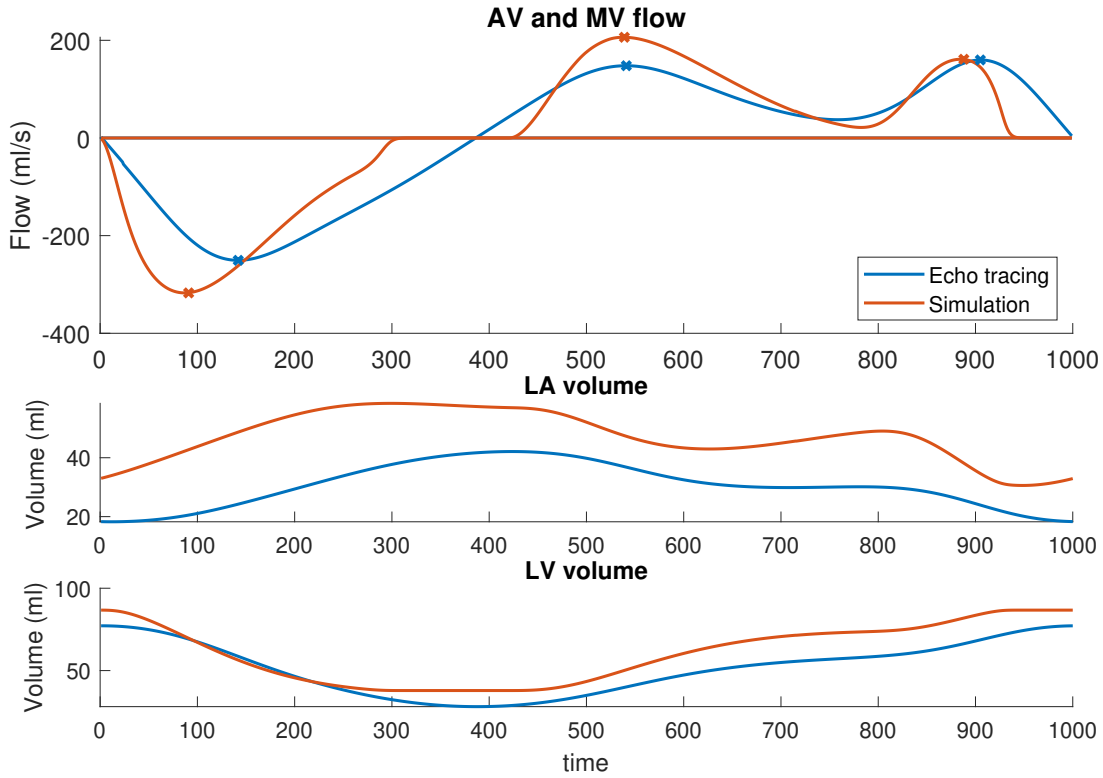

(d) Optimal fit for age group 5

Age Group	Run 1	Run 2	Run 3	Run 4	Run 5
1	**0.339**	0.344	0.346	0.367	0.350
2	**0.474**	0.489	0.484	0.516	0.536
3	0.604	0.603	**0.588**	0.722	0.717
4	0.535	0.577	0.573	**0.512**	0.579
5	**0.969**	0.972	0.980	0.986	0.970
6	0.746	0.747	0.739	0.737	**0.721**

Table 14: Total error of the optimal solution of each run of the subject-specific analysis; best value highlighted yellow and in bold font

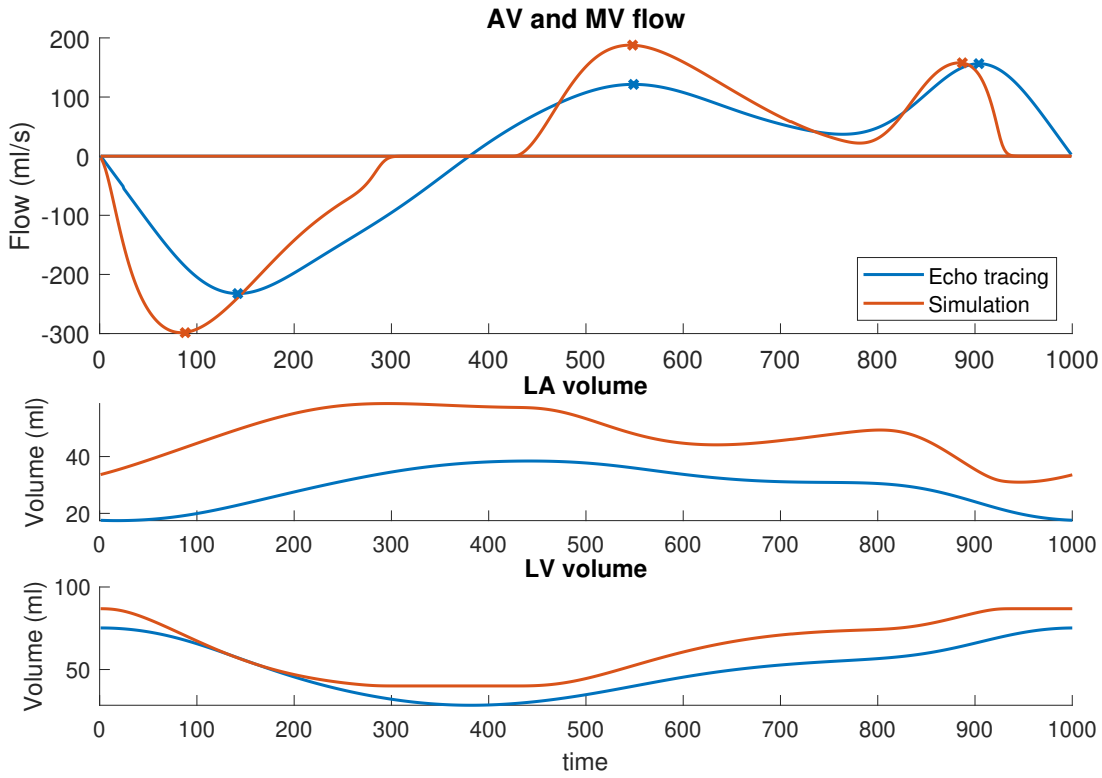

(e) Optimal fit for age group 6

Figure 27: Flow velocity and volume curves of the optimal fit for age groups 2 to 6

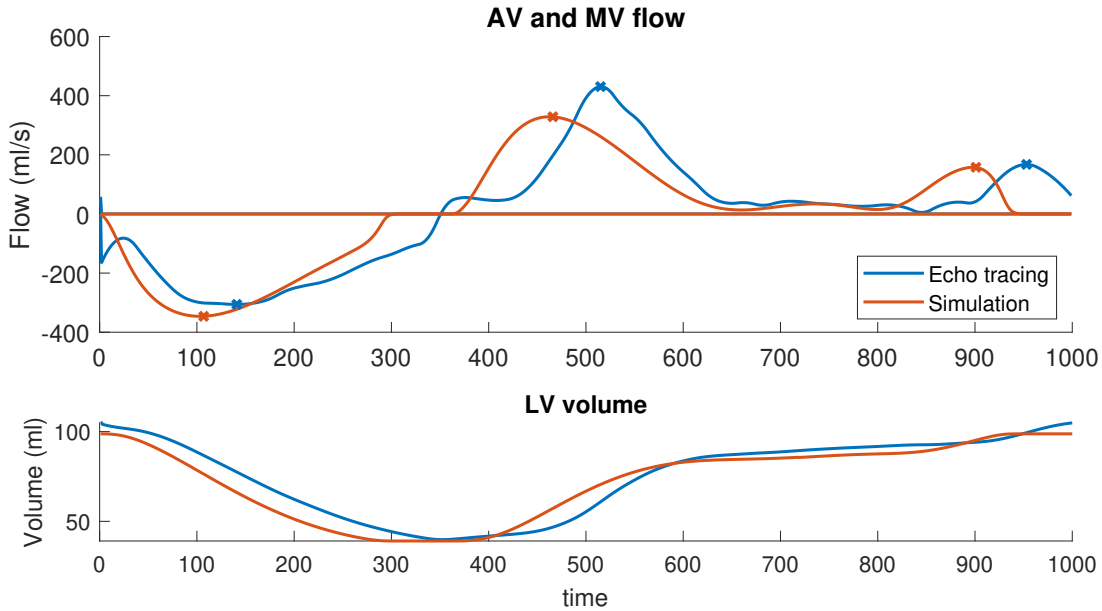

(a) Subject-specific fit for a subject of age group 2

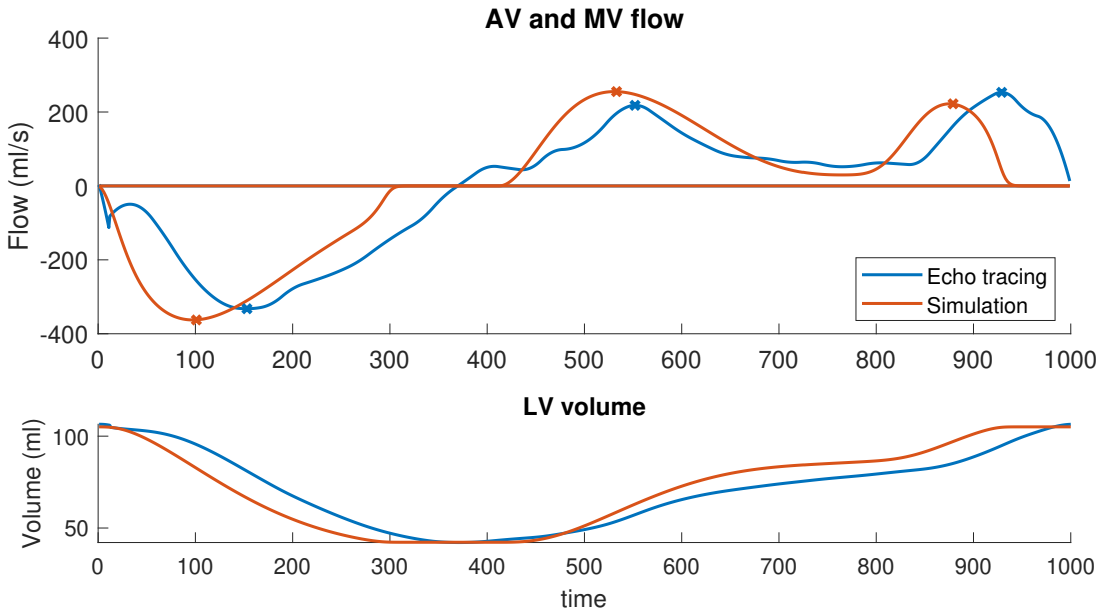

(b) Subject-specific fit for a subject of age group 3

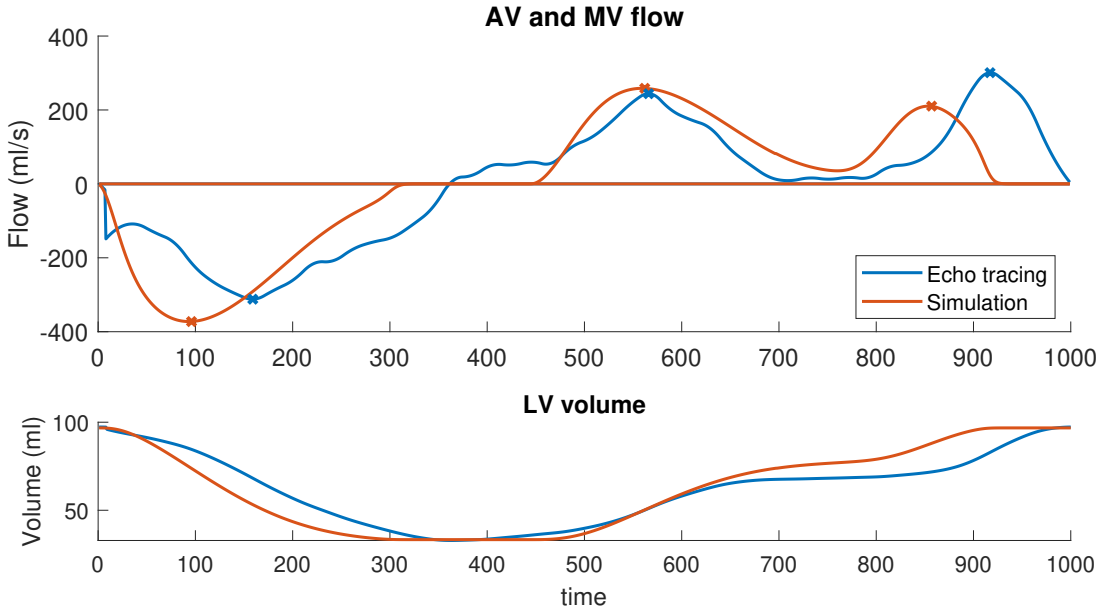

(c) Subject-specific fit for a subject of age group 4

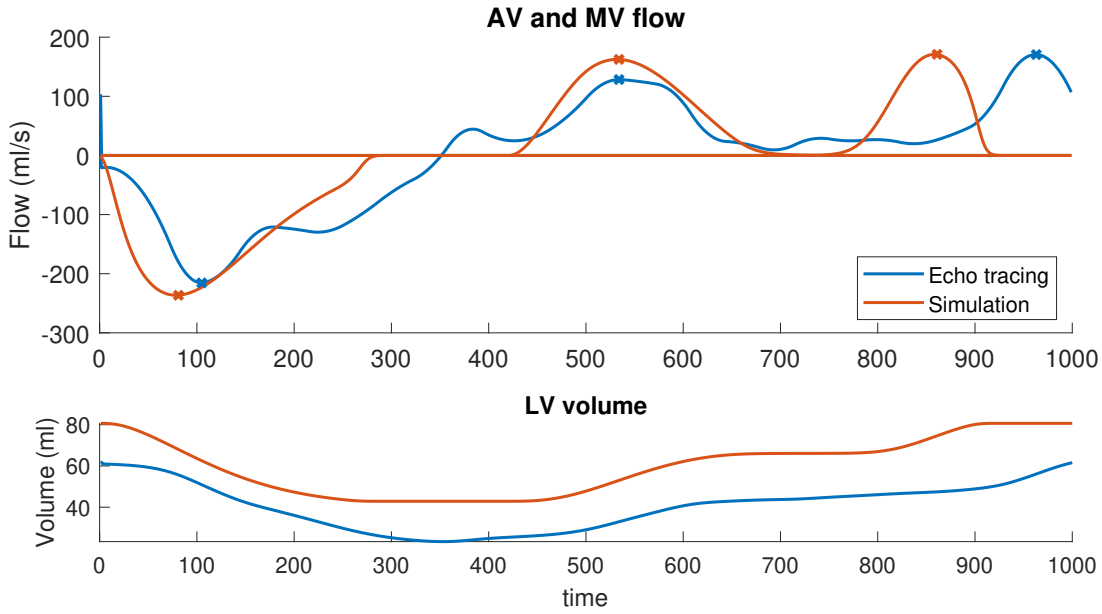

(d) Subject-specific fit for a subject of age group 5

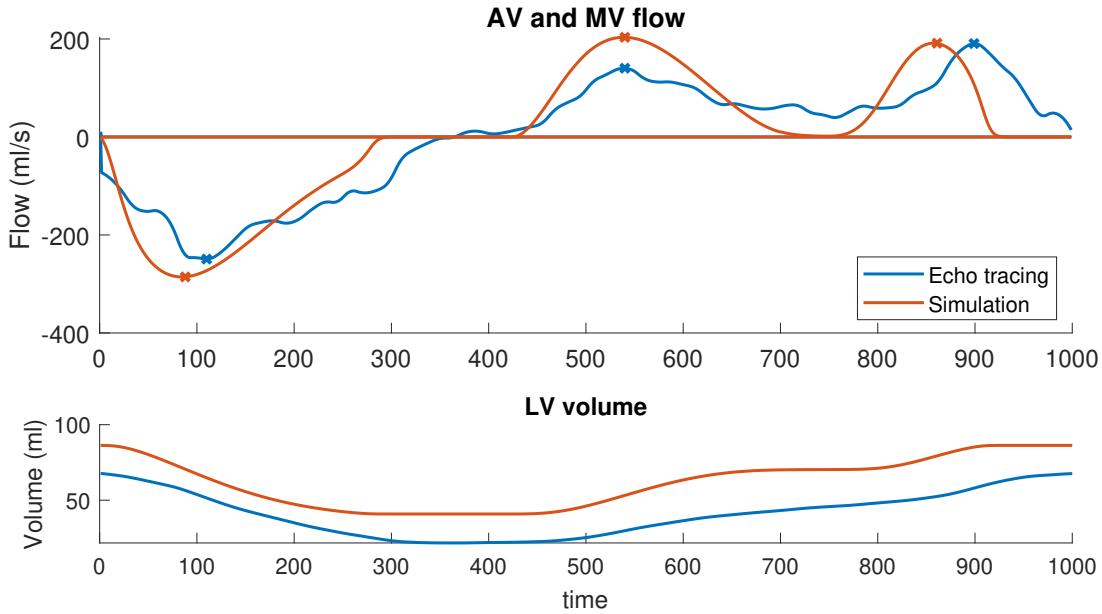

(e) Subject-specific fit for a subject of age group 6

Figure 28: Flow velocity and volume curves of the optimal fit for subjects from age groups 2 to 6

Age Group	$\sigma_{f,pas,LA}$	$\sigma_{f,pas,LV}$	$\sigma_{f,act,LA}$	$\sigma_{f,act,LV}$	$t_{D,LV}$	A_{MV}	A_{AV}
boundaries	[-20 20]	[-20 20]	[-20 20]	[-20 20]	[-20 20]	[-20 20]	[-20 20]
1	-6.1384	-10.2466	-14.0799	-0.19565	18.89075	-2.09618	-11.5409
2	-19.8688	8.216021	1.172554	5.143721	15.51184	-20	-19.3993
3	-19.9975	14.1954	11.10223	19.9986	16.71093	-19.999	-18.4889
4	-20	-17.2279	20	19.77781	19.86526	0.231877	-11.4153
5	-19.9902	-20	20	17.18832	20	-10.9943	5.088194
6	-20	-20	19.99961	11.35229	19.99932	-18.3081	14.86379

Table 15: Optimized model parameters (% from initial value), Optimization 2

Age Group	$t_{R,LA}$	$t_{R,LV}$	$TimeFac$	$d\tau_{av}$	$\sigma_{f,pas,LA}$	$\sigma_{f,pas,LV}$	$\sigma_{f,act,LA}$	$\sigma_{f,act,LV}$	$t_{D,LV}$	A_{MV}	A_{AV}
boundaries	[-20 20]	[-20 20]	[-15 15]	[-10 10]	[-5 5]	[-5 5]	[-5 5]	[-5 5]	[-5 5]	[-5 5]	[-5 5]
1	-1.2871	-15.743	-6.7408	-6.0856	-4.4624	-4.5006	-2.0141	-4.902	-1.0760	4.96674	-0.9373
2	0.58909	-3.0846	-9.4411	-9.7192	-0.1626	-0.0604	1.423	0.93339	1.22645	-3.6546	2.21136
3	-3.0669	-17.304	-5.4042	-9.6594	-2.6205	-0.0879	-0.1691	-0.1329	5	0.62662	-4.2245
4	1.27656	-19.359	-8.6624	-9.5614	-4.9298	3.31022	4.87049	-4.5926	3.65936	-4.9009	-4.9417
5	1.27656	-19.359	-8.6624	-9.5614	-4.9298	3.31022	4.87049	-4.5926	3.65936	-4.9009	-4.9417
6	-5.6565	-19.449	-3.4800	-8.8788	-4.9983	0.63976	3.37773	4.89805	1.84433	0.2960	1.8955

Table 16: Optimized model parameters (% from initial value), Optimization 3

	Run 1	Run 2	Run 3	Run 4	Run 5	Mean value	Std.	Deviation
$t_{R,LA}$	0.4800	0.4721	0.4624	0.4751	0.4747	0.4729	0.0065	1.38
$t_{R,LV}$	0.2013	0.2002	0.2002	0.2000	0.2000	0.2004	0.0005	0.27
$TimeFac$	0.9860	0.9924	1.0419	0.9924	1.0226	1.0071	0.0241	2.39
$d\tau_{av}$	-0.0186	-0.0185	-0.0185	-0.0186	-0.0183	-0.0185	0.0001	-0.64
$\sigma_{f,pas,LA}$	29343.50	28339.05	29126.16	33378.90	28472.01	29731.93	2082.41	7.00
$\sigma_{f,pas,LV}$	8629.47	7980.29	6351.14	7120.92	7173.25	7451.01	875.32	11.75
$\sigma_{f,act,LA}$	25324.63	23690.12	25067.33	26943.93	25641.91	25333.58	1168.36	4.61
$\sigma_{f,act,LV}$	218091.26	223607.73	223214.96	207747.66	222651.83	219062.69	6703.62	3.06
$t_{D,LV}$	0.2220	0.2145	0.1830	0.2162	0.1925	0.2056	0.0169	8.22
A_{MV}	0.000350	0.000382	0.000389	0.000383	0.000349	0.000371	0.000019	5.25
A_{AV}	0.000195	0.000201	0.000199	0.000248	0.000247	0.000218	0.000027	12.39

Table 17: Model parameters of the optimized model of the single subject from age group 1 for the different runs; mean value and standard deviation, as well as the deviation coefficient in percent